# ADVANCED OPTICAL BLADE TIP CLEARANCE MEASUREMENT SYSTEM

PRATT AND WHITNEY AIRCRAFT GROUP, WEST
PALM BEACH, FLA. GOVERNMENT PRODUCTS DIV

JUL 1978

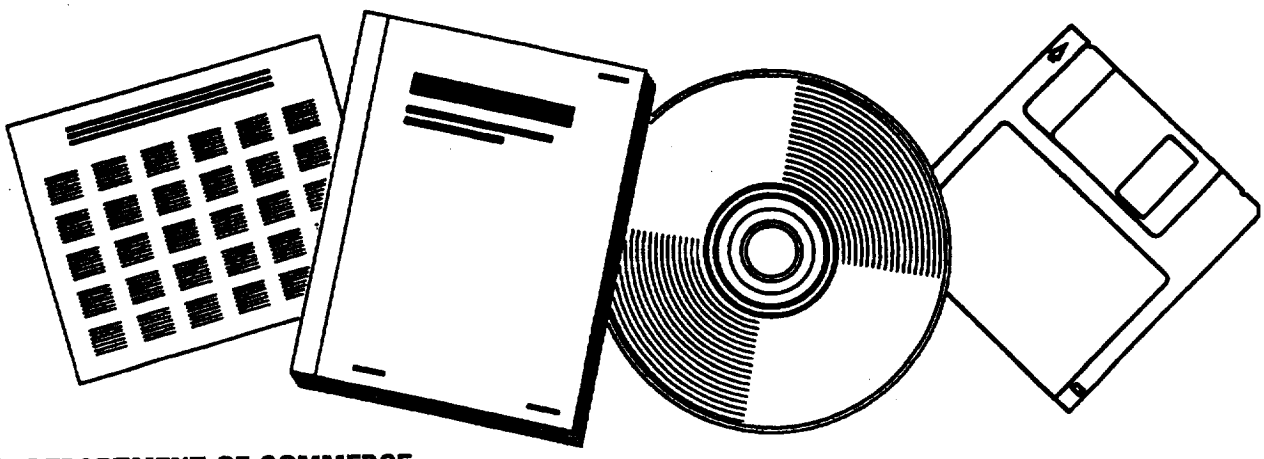

U.S. DEPARTMENT OF COMMERCE
National Technical Information Service

*Tailored to Your Needs!*

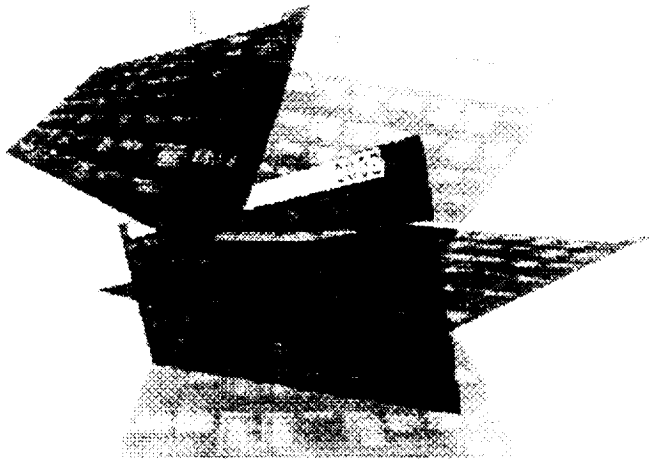

# Selected Research In Microfiche

**SRIM®** is a tailored information service that delivers complete microfiche copies of government publications based on your needs, automatically, within a few weeks of announcement by NTIS.

## SRIM® Saves You Time, Money, and Space!

Automatically, every two weeks, your SRIM® profile is run against all *new* publications received by NTIS and the publications microfiched for your order. Instead of paying approximately $15-30 for each publication, you pay only $2.50 for the microfiche version. Corporate and special libraries love the space-saving convenience of microfiche.

## NTIS offers two options for SRIM® selection criteria:

**Standard SRIM®**–Choose from among 350 pre-chosen subject topics.

**Custom SRIM®**–For a one-time additional fee, an NTIS analyst can help you develop a keyword strategy to design your Custom SRIM® requirements. Custom SRIM® allows your SRIM® selection to be based upon *specific subject keywords*, not just broad subject topics. Call an NTIS subject specialist at (703) 605-6655 to help you create a profile that will retrieve only those technical reports of interest to you.

SRIM® requires an NTIS Deposit Account. The NTIS employee you speak to will help you set up this account if you don't already have one.

For additional information, call the NTIS Subscriptions Department at 1-800-363-2068 or (703) 605-6060. Or visit the NTIS Web site at *http://www.ntis.gov* and select SRIM® from the pull-down menu.

**U.S. DEPARTMENT OF COMMERCE**
**Technology Administration**
**National Technical Information Service**
**Springfield, VA 22161 (703) 605-6000**
**http://www.ntis.gov**

NASA CR-159402
FR-10200A

# ADVANCED OPTICAL BLADE TIP CLEARANCE MEASUREMENT SYSTEM

By
M. J. Ford, R. E. Honeycutt,
R. E. Nordland, and W. W. Robinson

Pratt & Whitney Aircraft Group
Government Products Division
West Palm Beach, Florida 33402

Prepared for
National Aeronautics and
Space Administration
Lewis Research Center

Contract NAS3-20479

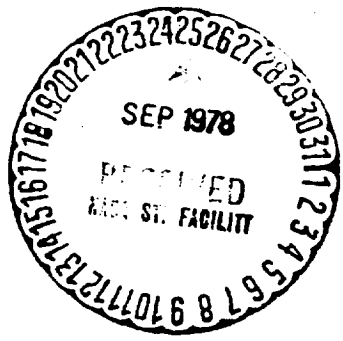

| 1. Report No. | 2. Government Accession No. | 3. Recipient's Catalog No. |
|---|---|---|
| NASA CR-159402 | | |

| 4. Title and Subtitle | 5. Report Date |
|---|---|
| ADVANCED OPTICAL BLADE TIP CLEARANCE MEASUREMENT SYSTEM | July, 1978 |
| | 6. Performing Organization Code |

| 7. Author(s) | 8. Performing Organization Report No. |
|---|---|
| M. J. Ford, R. E. Honeycutt, R. E. Nordlund, W. W. Robinson | FR-10200A |
| | 10. Work Unit No. |

| 9. Performing Organization Name and Address | 11. Contract or Grant No. |
|---|---|
| United Technologies Corporation<br>Pratt & Whitney Aircraft Group<br>Government Products Division<br>P.O. Box 2691, West Palm Beach, FL 33402 | NAS3-20479 |
| | 13. Type of Report and Period Covered |
| 12. Sponsoring Agency Name and Address | Contractor Report |
| National Aeronautics and Space Administration<br>Washington, D. C. 20546 | 14. Sponsoring Agency Code |

15. Supplementary Notes

Project Manager, Dr. John P. Barranger, Instrumentation Development and Application Branch, NASA Lewis Research Center, Cleveland, Ohio

16. Abstract

An advanced electro-optical system was developed to measure single blade tip clearances and average blade tip clearances between a rotor and its gas path seal in an operating gas turbine engine. This system is applicable to fan, compressor, and turbine blade tip clearance measurement requirements, and the system probe is particularly suitable for operation in the extreme turbine environment. A study of optical properties of blade tips was conducted to establish measurement system application limitations. A series of laboratory tests was conducted to determine the measurement system's operational performance characteristics and to demonstrate system capability under simulated operating gas turbine environmental conditions. Operational and environmental performance test data are presented.

| 17. Key Words (Suggested by Author(s)) | | 18. Distribution Statement |
|---|---|---|
| Turbo Machinery | Computerized System | Unclassified - Unlimited |
| Jet Engine | Image Intensifier | STAR Category 07 |
| Blade Clearance | Clearance Measurement | |
| Laser | Engine Diagnostics | |
| Optics | Engine Condition Monitor | |
| Engine Instrumentation | | |

| 19. Security Classif. (of this report) | 20. Security Classif. (of this page) | 21. No. of Pages | 22. Price* |
|---|---|---|---|
| Unclassified | Unclassified | | |

* For sale by the National Technical Information Service, Springfield, Virginia 22161

## TABLE OF CONTENTS

## LIST OF ILLUSTRATIONS

## LIST OF TABLES

## SUMMARY

The objective of this program was to develop an advanced electro-optical system to measure single blade tip clearances and average blade tip clearances between a rotor and its gas path seal in rotating rigs and full scale gas turbine engines. This system is applicable to fan, compressor, and turbine blade tip clearance measurement requirements, and the system probe is particularly suitable for operation in the extreme turbine environment. The program effort included a study of optical properties of blade tips, measurement system design and fabrication, and operational and environmental performance evaluation tests to demonstrate measurement system capability.

The study of optical properties of blade tips investigated the optical properties of six typical gas turbine engine blades which had been subjected to an engine operating environment. The purpose of the study was to use the resulting optical properties data to determine the measurement system application limitations in terms of available blade tip reflected laser energy and distribution. The data were applied in defining the measurement system design criteria.

The measurement system consists of an optical subsystem, an electronic subsystem, and a computing and graphic terminal. The optical subsystem provides the basic blade tip clearance measurement by using an established correlation between blade tip clearance and the location of a reflected laser spot on a linear photodiode array. The electronic subsystem provides the scan, gate, and process functions required for single and average blade tip clearance measurements. The computing and graphic display terminal provides optical and electronic subsystem control and clearance data presentation.

Laboratory tests were conducted to determine the measurement system's operational performance characteristics and to demonstrate system capability under simulated operating gas turbine environmental conditions. The operational performance evaluation tests included a static calibration and a series of simulated rotating blade row tests. Results of the evaluation tests are presented, and these results confirm the measurement system operational performance characteristics. The environmental tests subjected the measurement system probe to vibration, temperature, and pressure environments typically encountered in an operating gas turbine engine. Results of these tests indicate no degradation in measurement system performance.

## INTRODUCTION

Blade tip to shroud clearance in an operating gas turbine engine is a critical parameter. Excess clearance allows a portion of the engine gas to flow over the blade tip without performing work, and insufficient blade tip clearance can jeopardize engine integrity. Previously, it has been possible to measure average blade tip clearance over several rotor revolutions, but the type of system (Refs. 1 and 2) used did not have adequate response for transient or single blade tip clearance measurement. It is necessary that any system used for research and development be capable of measuring and displaying single as well as average blade clearances. A practical means of measuring single blade tip clearance did not exist.

The objective of this program was to develop an advanced fast time response system to measure single blade tip clearances and average blade tip clearances in rotating rigs and full scale engines. A series of laboratory tests was conducted to determine the measurement system's operational performance characteristics and to demonstrate performance under simulated engine test conditions. Evaluation of these test results demonstrate that the measurement system performance meets overall program goals.

The block diagram in Figure 1 depicts the major functional components of the system.

A rangefinder triangulation principle is used to detect blade tip clearance by means of an optical probe assembly attached to the operating engine gas path seal. A helium-neon laser beam is directed through lenses and fiber optic coupling to the probe where it is focused in the region of the blade tip. The focused laser spot on the blade tip is imaged back through the probe, a coherent fiber optic coupling, and lenses to a gated image intensifier.

The image intensifier amplifies the low intensity reflected laser spot and transfers it onto a linear photodiode array. The spot's linear position on the array, which represents the blade tip clearance, is converted to a video signal.

A blade passing pulse train, detected by sensing a portion of the imaged laser spot prior to its reaching the image intensifier, provides blade counting and synchronization information.

A Tektronix Model 4051 Computing and Graphic Display Terminal is programmed to provide Optical and Electronic Subsystem control and clearance data presentation online in near real time. The Electronic Subsystem interfaces between the 4051 and the Optical Subsystem.

Test variables (e.g., AVERAGE or SINGLE BLADE measurement modes, number of rotor blades, clearance limits) are entered into the 4051 by the system operator via the 4051's keyboard. The 4051 then activates the proper software programs and instructs the Electronic Subsystem to set the hardware in accordance with the preprogrammed test variable requirements. Communication between the 4051 and the electronic hardware is accomplished via a General Purpose Interface Bus.

Manually operated controls are provided on the Electronic Subsystem front panel for remote adjustment of optical filters and lenses to optimize the linear photodiode array video output. An image intensifier automatic gain control compensates for limited intensity variations.

In operation, the Electronic Subsystem processes the linear photodiode array output and identifies the diode site corresponding to the blade tip clearance by picking the video signal peak. The clearance information is presented to the 4051. The 4051 is programmed to convert diode site information into clearance data in thousandths of an inch (mils).

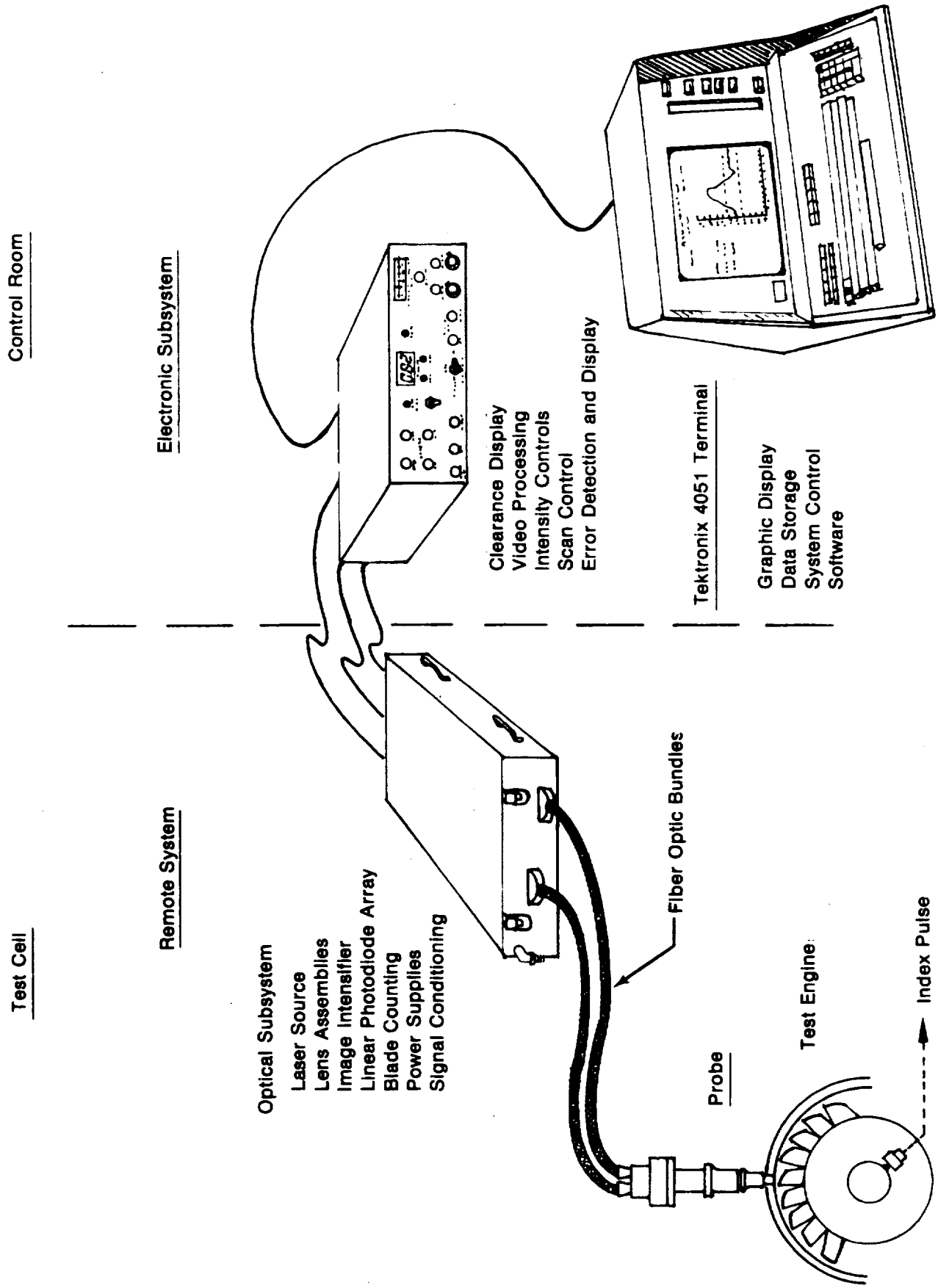


*Figure 1. System Major Components*

In the AVERAGE mode, the image intensifier is gated on continuously to yield an optical average of all blades on the rotor, providing a reading each revolution.

In the SINGLE BLADE mode, the image intensifier is gated on to view only one blade at a time as requested by the 4051. Each blade on the rotor is viewed in turn to yield data for the entire stage. A NASA provided index pulse and the blade passing pulse train are used to synchronize the gating process. A NASA provided synthesized blade passing pulse train may also be used.

Programs in the 4051 are used to format the clearance data for presentation on the graphic terminal screen. AVERAGE data are presented in a plot of "Clearance versus Scan." (a time history of average clearance). SINGLE BLADE Mode-1 data are presented in a plot of "Clearance versus Blade Number," and SINGLE BLADE Mode-2 data are presented in a plot of single blade "Clearance versus Scan" (a time history).

This system is innovative in that it combines specific optical, electro-optical, electronic and computer/graphic elements to measure and display average and single blade tip clearances in rotating machinery over a wide range of rotational speed and with a variety of blade materials and configurations.

The program was conducted in four major phases including:

- Optical Properties of Blade Tips Study
- Measurement System Detail Design
- Operational Performance Evaluation
- Environmental Performance Evaluation

This Final Report addresses specifically these major program phases.

## DISCUSSION

# I. OPTICAL PROPERTIES OF BLADE TIPS STUDY AND DISCUSSION OF RESULTS

## A. STUDY OBJECTIVE

The blade tip clearance probe utilized in the Advanced Optical Blade Tip Clearance Measurement System must function under a variety of engine running conditions and at various engine station locations. This broad spectrum of application will subject the probe laser input to a wide range of intensity distribution after interaction with the target blade tips of the fan, compressor, or turbine sections. It would, therefore, be useful to investigate the laser energy distribution resulting from interaction with a "representative" sample of engine blades from each of these sections. The purpose of this Optical Properties of Blade Tips Study was to make such an investigation and to utilize the resulting data to help determine the application limitations of the blade tip clearance probe.

## B. SUMMARY OF STUDY RESULTS

The following conclusions were drawn from the study of the optical properties of six typical gas turbine engine blades which had been subjected to an engine operating environment and from predicted performance characteristics of the measurement system.

- The range of the laser intensity detected from the test blades can be accommodated by the measurement system.
- While a primarily specular (mirror-like) surface is desirable, the degree of diffusivity (scattering) observed will not seriously impact the measurement system performance.
- The acquired signal level is not highly sensitive to probe rotation about the blade axis.
- Best performance of the blade tip clearance probe is obtained when the viewing angle is equal to the angle of laser radiation incidence. This is the scheme utilized in previous systems and the system developed under this NASA contract.

The study was limited primarily to measuring the scattered/reflected intensity distribution in the plane containing the incident laser beam and the nominal reflected beam within the reflected beam quadrant, for various angle of incidence and blade rotation positions.

The optical characteristics of the selected fan, compressor, and turbine blades, which were subjected to an engine operating environment, were defined by determining the distribution of 6328Å laser radiation scattered from the blade tips. A helium-neon laser beam, focused through a lens, was the radiation source. The scattered light was collected by a fiber optic bundle which simulates the approximate magnitude of a typical blade tip clearance probe acceptance cone. The collected radiation was coupled to a photomultiplier tube and read out on a digital picoammeter.

The polar intensity distribution of the 6328Å laser radiation was plotted as a function of the intensity received by the detector, relative to the input laser intensity. A total of six blades were studied: two fan blades, two compressor blades, and two turbine blades.

Results of this study substantiated the basic blade tip clearance probe design concept and provided an understanding of the range of attenuation to the input laser energy produced by interaction with the various blade tips.

## C. SCOPE OF STUDY

From a purely technical standpoint, the total hemispherical distribution of the laser radiation after interaction with the blade tip should be defined for many angles of incidence from 0° to 90°. In addition, many measurements from the same blade for different spot positions on the blade tip should be averaged to remove effects due to variations in blade tip condition. The variations are caused by localized wear patterns such as those due to machining or blade rubbing and will introduce diffraction and interference intensity distribution effects. The coherent nature of the laser radiation itself introduces another nonuniformity in the form of a speckle pattern. Any blade has a wide range of intensity distribution patterns that are position sensitive with respect to the location of the incident focused laser spot on the blade tip.

For this study, certain limitations and measurement constraints had to be established in order to efficiently acquire a useful set of data for several fan, compressor, and turbine blades.

The scope of this study was, therefore, set by the following guidelines:

1. Two blades from each of the three engine sections would be studied.

2. The blades would be selected to be as representative of the most diffuse tip surface (that is, those with highest scattering characteristics), or greatest engine operating exposure, as would be possible with available sources of used blades.

3. The area of the blade surface to be studied would be the central region, as this is the area typically seen by the blade tip clearance probe.

4. The blade would be traversed in its direction of rotation, with an average signal level being recorded.

5. To test for effects due to blade tip condition, such as blade rub patterns, the blade would be rotated so that the incident beam aligned with the direction of blade rotation (0°), as well as normal to the direction of blade rotation (90°).

6. Only three angles of incidence would be utilized: 15°, 30°, and 45° with respect to the blade tip normal. The angles selected were those which cover practical probe configurations.

7. Data from the scattered radiation would be acquired only in the quadrant containing the nominal reflected beam. The data points would be at 5° intervals within ±15° of the nominal angle of reflection, and at 15° intervals at other angles within the stated quadrant and only in the plane containing the incident and nominal reflected beams.

8. Two additional data points would be acquired at ±15° from the nominal angle of reflection in the plane normal to the plane stated above and which also contains the blade tip laser spot.

The size of the spot incident upon the blade tip is of the same magnitude as some of the surface variations, and therefore, small variations in the spot position can introduce a large variation in the detected signal. Traversing the blade tip will tend to minimize this variation, but even this average can be expected to vary over the width of the blade tip. However, this variation will not unduly impact the blade tip clearance probe performance.

## D. STUDY METHOD

The Optical Properties of Blade Tips Study test arrangement is shown in Figure 2. A helium-neon laser source was reflected from mirror $M_1$ to mirror $M_2$ which directed the laser beam toward the test blade and defined the angle of incidence, $\theta_i$. This incident laser beam was focused to approximately a .13 mm diameter spot on the blade tip by the lens L. Mirrors $M_1$ and $M_2$ as well as lens L were adjustable so that the angle of incidence to the blade tip could be conveniently changed.

The test blade itself was mounted on a base with five degrees of freedom: X-Y translation, Z rotation, and X-Y tilt. The X-Y tilt was required to align the blade tip normal to the vertical axis of the optical table.

The scattered radiation was collected by a 3 mm diameter fiber optic bundle placed 50 mm from the blade tip. This resulted in an acceptance cone of $2.8 \times 10^{-3}$ steradians. This was selected as a conservative approximation to the probe acceptance angle of approximately $8.0 \times 10^{-3}$ steradians. This difference is of little consequence since the reflected signal values can be easily scaled within the small range of variation.

The fiber optic bundle was mounted so as to allow free rotation within the quadrant containing the nominal angle of reflection. Movement of the bundle tip in the plane normal to the plane containing the incident and nominal reflected beam and passing through the blade tip was accomplished by repositioning the fiber optic mounting structure.

The radiation collected by the fiber optic bundle was transferred to a photomultiplier tube which was read out on a digital picoammeter.

The photomultiplier was calibrated relative to the output intensity ($I_o$) of the laser source. The data can therefore be converted to intensity received by multiplying the laser intensity by the intensity ratio ($I/I_o$) given in the data plots.

For each value of $\theta_i$, (15°, 30°, and 45°) the fiber optic bundle was set at the nominal angle of reflection and at 5° intervals for ±15° about the nominal angle of reflection, as well as each 15° for the other positions within the nominal reflected beam quadrant ($\alpha$).

Data were also taken for ±15° from the nominal angle of reflections in the plane normal to the above plane and which contained the blade tip ($\pm\beta$).

Both sets of data were taken for each of two blade rotation angles, 0° and 90°, with respect to the direction of blade rotation ($\phi$).

For each data point, the blade tip was translated in its normal direction of rotation with the resulting intensity variations averaged, keeping only two significant digits.

## E. STUDY TEST DATA

The acquired data were plotted on 3 cycle logarithmic polar graph paper. A typical plot is presented in Figure 3. The data points for the plane containing the incident and nominal reflected beams ($\alpha$) are shown circled with solid lines connecting each point. The data points for the plane normal to the plane just described and containing the nominal reflected beam ($\beta$) are shown within triangles and connected by dashed lines. The logarithmic scale is the dimensionless ratio of the detected intensity, I, to the output laser intensity, $I_o$, and this intensity ratio is plotted as a function of angle of observation.

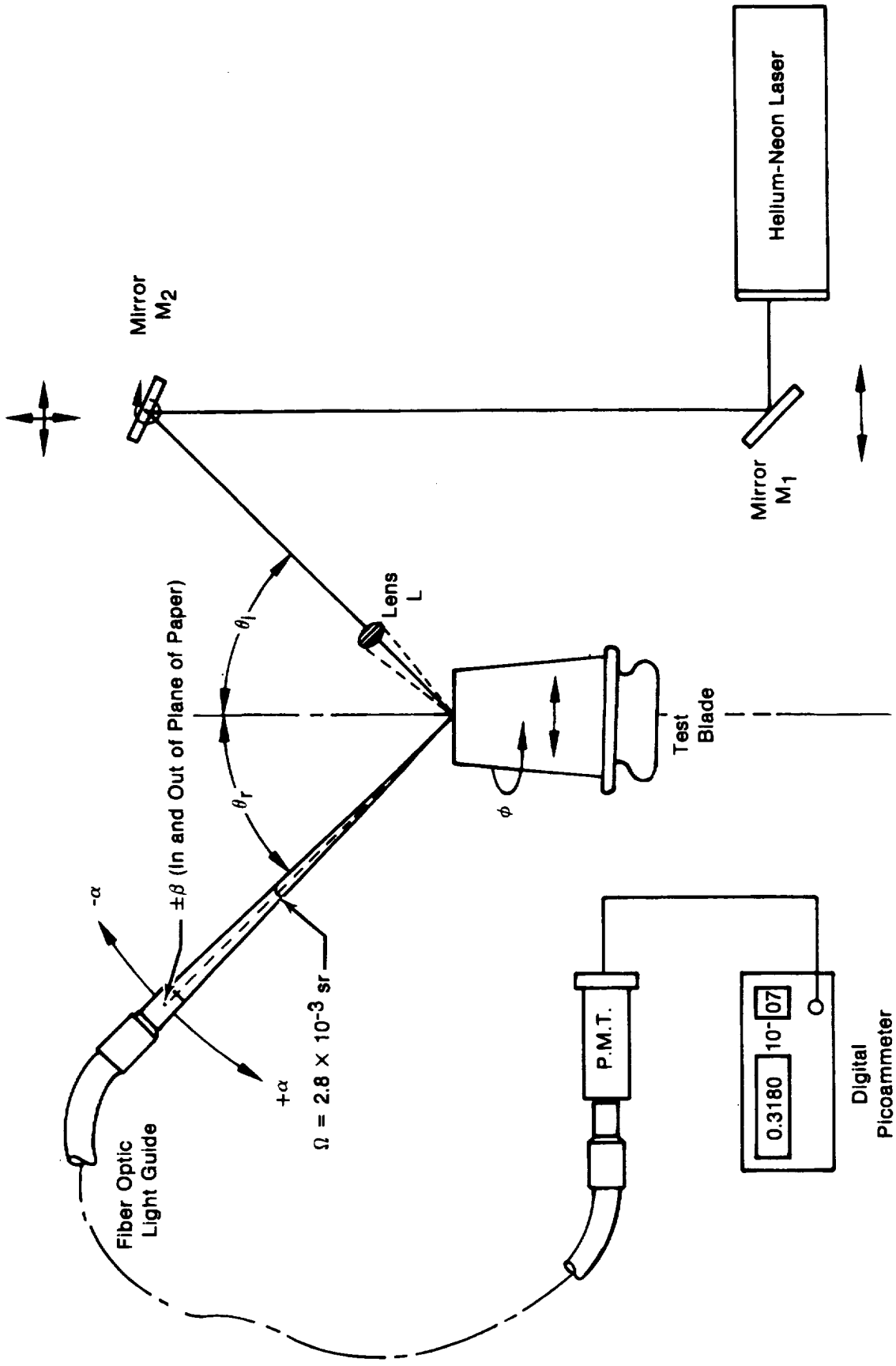


*Figure 2. Optical Properties of Blade Tips Study Setup*

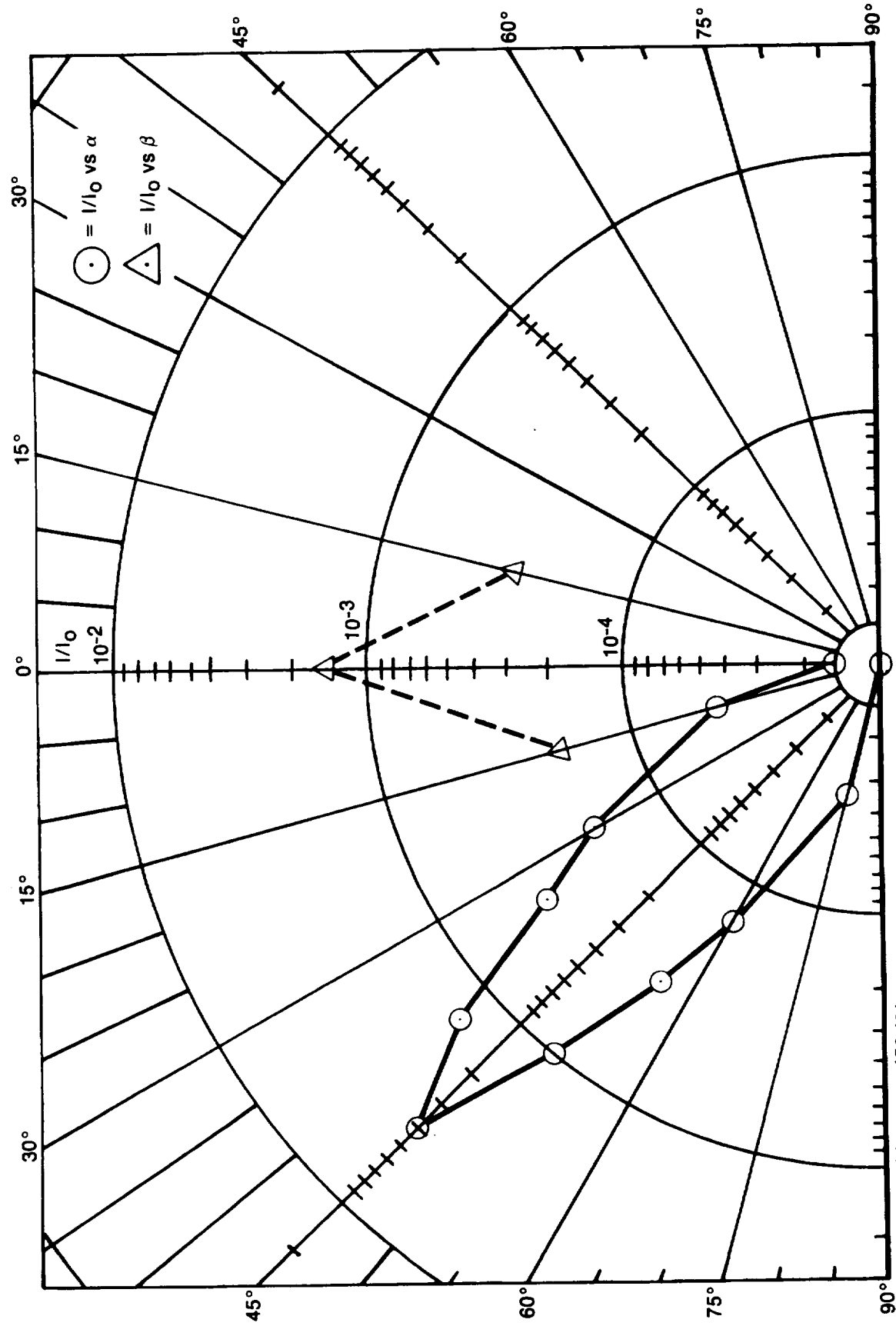


*Figure 3. Blade Number 1 Intensity Ratio*

Six plots were generated for each blade studied and correspond to the three angles of incidence ($\theta_i$ = 15°, 30°, 45°) at each of the two angles of blade rotation ($\phi$ = 0° and 90°).

## F. DISCUSSION OF RESULTS

In considering the results of this Optical Properties of Blade Tips Study, it will be instructive to begin with a general inspection of the qualitative data. The shape of the scattered radiation indicates that, for the most part, the pattern is diffuse as demonstrated by the broad appearance of the radiation lobes. The specular component is, however, manifest in the peak response at, or within, 5° of the nominal angle of reflection. The slight variation of this peak position can be explained by small misalignments of the blade tip normal with the optical table vertical, as well as by the local scattering pattern.

Two exceptions to the generally diffuse behavior were seen in the data for Blade #1, First Stage Fan blade, and Blade #4, Twelfth Stage Compressor blade. Both of these blades show narrow, peaked lobes, with those of Blade #1 being more specular. This would indicate that the area on the blade tip in the region of the focused laser spot was uniform providing a primarily specular surface, which is a desirable characteristic.

Quantitatively the data generally support the observations just made concerning the specular/diffuse characteristics of the data. That is, the more diffuse surface producing a broad lobe would spread the incident radiation over a large area; thus, resulting in a lower peak intensity.

Figure 4 is a logarithmic plot of the nominal reflected angle intensity ratio for each blade tip. Points for the same blade are connected to each of the six incident/rotational configurations of the blade. From this plot it is first apparent that the intensity ratio for the six blades ranges from approximately $4 \times 10^{-3}$ to about $1 \times 10^{-4}$. This range can be accommodated by the measurement system.

It can also be seen from this plot that the blades demonstrating more specular properties possess generally higher values of $I/I_o$. Those blades with more diffuse patterns, as well as more absorbing surfaces, fall to lower values.

While the data do not show strong rotational effects, there was observed a distinctive diffraction pattern that was dependent on the rotational position of the blade tip. In particular, when the blade was rotated so that the wear pattern was at right angles to the incident beam ($\phi$ = 90°), there was a bright laser radiation pattern in the plane containing the incident and nominal reflected beams. This dispersion effect was caused by the grooved pattern on the blade tip. When the blade tip was rotated, the radiation pattern rotated as well, so that when the tip had been rotated 90° to $\phi$ = 0°, the pattern had also rotated 90°. This pattern falls beyond the field of view of the probe and has no significant impact on the measurement system performance.

The coherent laser radiation also produced a granular speckle pattern over the entire scattering hemisphere. This speckle pattern resulted in a rapidly varying signal level as the fiber optic tip was slowly moved. This caused difficulty in establishing the representative signal level, as well as in reproducing the signal level at a given point. This effect was apparent when attempting to take data at the $\pm\beta$ angles and appeared as intensity variations in the $\alpha$ and $\beta$ angle data points. The measurement system, however, will see the average of these effects with no significant impact on performance.

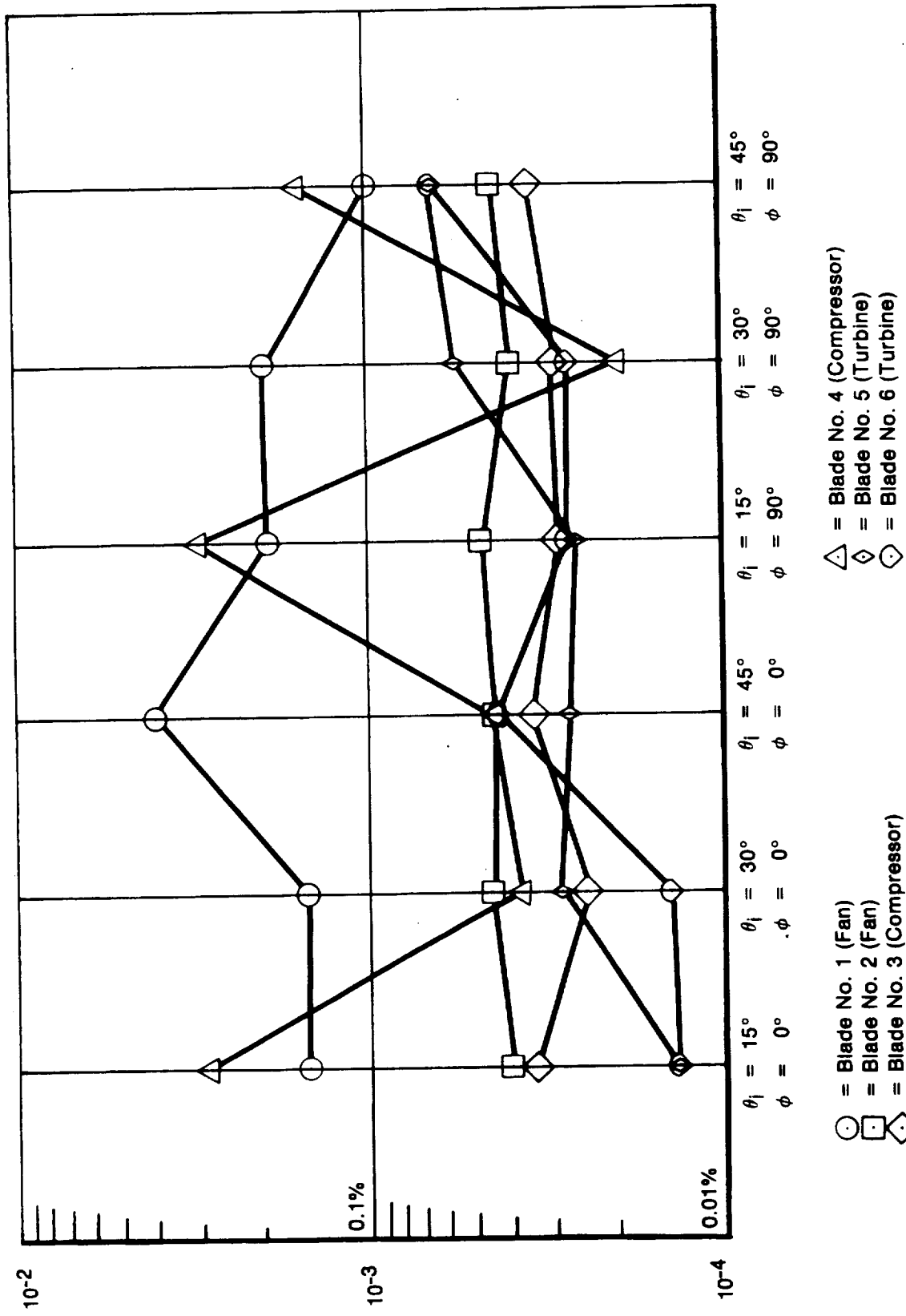


*Figure 4. Nominal Reflected Angle Intensity Distribution*

## G. STUDY CONCLUSIONS

This study demonstrated two significant system operational principles:

1. The validity of the blade tip clearance probe viewing configuration being based on sensing the specular component of the scattered radiation pattern.

2. The range of the detected intensity being approximately from $4 \times 10^{-3}$ to $1 \times 10^{-4}$ of the incident laser energy after interaction with the blade tip, which can be accommodated by the measurement system.

These two principles were utilized in assessing the throughput characteristics of the Advanced Optical Blade Tip Clearance Measurement System.

In addition, the following system application information was acquired:

1. Usefulness of the probe system in the fan, compressor, and turbine areas is dependent, but not critically, on the specular nature of the blade tips. An increase in the diffuse character of the blade tip, within the range seen by this study, will not seriously impact the measurement system performance.

2. There is little difference in the signal level received by the probe for a tip rotational position of 0° or 90° with respect to the direction of blade rotation.

In general, the blade tips studied show no characteristics which would detract from the validity of the Advanced Optical Blade Tip Clearance Measurement System design concept, either in operation or application.

## II. SYSTEM DESIGN REQUIREMENTS SUMMARY

**A.** The Advanced Optical Blade Tip Clearance Measurement System primary operational performance design goals were as follows:

- Tip Clearance Measurement Range — 0 to 0.120 inches (0. to 3.05 mm)
- Measurement Accuracy — ±0.002 inches (±0.0508 mm)
- Measurement Resolution — ±0.001 inches (±0.0254 mm)
- Capability of Static Calibration
- Measurement of Average and Single Blade Clearance Measurement on a 120 Blade Rotor at the following conditions:

| | |
|---|---|
| Rotor Speed | - 600 RPM to 60,000 RPM |
| Blade Tip Speed | - 61.0 m/sec (200 ft/sec) to 609.6 m/sec (2,000 ft/sec) |
| Blade Tip Thickness | - 0.79 mm (0.031 inches) minimum |

- Computer Compatible Signal Input/Output Format
- Input to Designate Selected Blade for Single Blade Clearance
- Display Blade Clearances in Bar Chart or Similar Form

B. The Advanced Optical Blade Tip Clearance Measurement System environmental performance design goals were as follows:

- Measurement system probe to be capable of operation without degradation in a typical gas turbine environment where probe adjacent wall temperatures reach 1311 K (1900°F).
- Measurement system probe to be capable of operation without degradation in a typical gas turbine environment where gas path operating pressures reach 30 atmospheres.
- Measurement system probe to be capable of operation without degradation in a typical gas turbine environment where vibration levels encountered are as high as 12.7 mm/sec in the 50 Hz to 2500 Hz frequency range.

Environmental performance design goals were applied only to the probe since the other components are not subjected to the severe gas turbine environment.

## III. SYSTEM DESIGN CONCEPT SUMMARY

The Advanced Optical Blade Tip Clearance Measurement System basically consists of an Optical Subsystem, an Electronic Subsystem, and a Tektronix Model 4051 Computing and Graphic Display Terminal. Figure 5 illustrates the system configuration.

A rangefinder triangulation principle is used to detect blade tip clearance by means of an optical probe assembly attached to the operating engine gas path seal. The optical probe is designed to meet the environmental performance requirements. A helium-neon laser beam is directed through lenses and fiber optic coupling to the probe where it is focused onto the blade tip. The blade tip reflects the focused laser spot back through the probe, a coherent fiber optic coupling, and lenses to the gated Image Intensifier.

The Image Intensifier amplifies the low intensity reflected laser spot and transfers it onto the Linear Photodiode Array (LPA). The spot's linear position on the array, which represents the blade tip clearance, is converted to a video signal.

The blade passing pulse train, detected by sensing a portion of the reflected laser spot ahead of the Image Intensifier, provides blade counting and synchronization information.

A Tektronix Model 4051 Computing and Graphic Display Terminal is utilized for system control and clearance data presentation. The Electronic Subsystem interfaces the 4051 and the Optical Subsystem.

Test variables (e.g., AVERAGE or SINGLE BLADE measurement modes, number of rotor blades, clearance limits) are entered into the 4051 by the system operator via the 4051's keyboard. The 4051 then activates the proper software programs and instructs the Electronic Subsystem to set the hardware in accordance with the preprogrammed test variable requirements. Communication between the 4051 and the electronic hardware is accomplished via a General Purpose Interface Bus (GPIB).

Manually operated controls are provided on the Electronic Subsystem front panel for remote adjustment of optical filters and lenses to optimize the LPA video output at steady state engine test conditions. An image intensifier automatic gain control compensates for limited intensity variations.

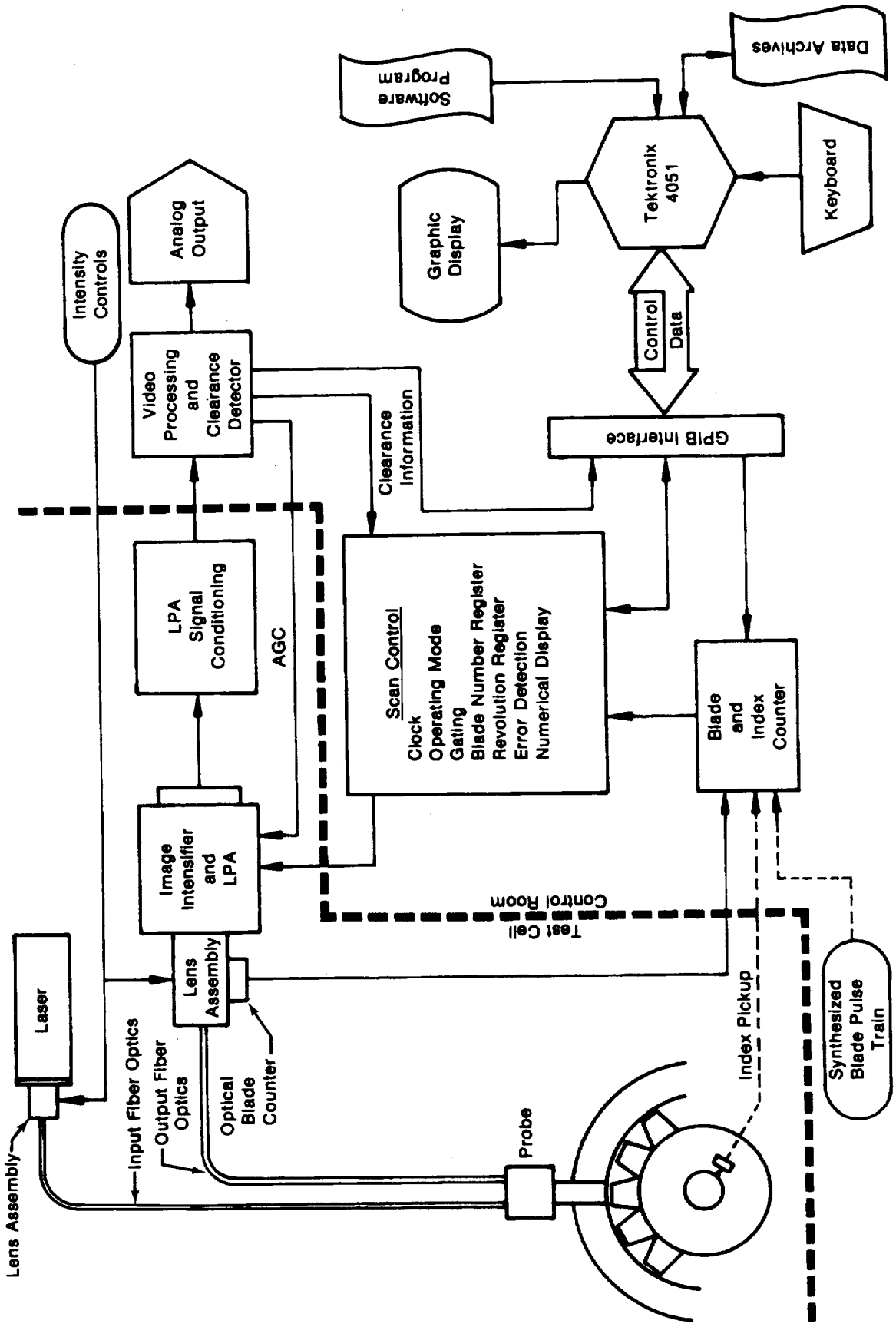


*Figure 5. System Configuration*

During tests, the Electronic Subsystem processes the LPA output and identifies the diode site corresponding to the blade tip clearance by picking the video signal peak. This clearance information is presented to the 4051 in thousandths of an inch (mils) for plot presentation.

In the AVERAGE Mode the Image Intensifier is gated on continuously to yield an optical average of all blades on the rotor.

In the SINGLE BLADE Mode the Image Intensifier is gated on to view only the blade requested by the 4051. A NASA provided index pulse and the blade passing pulse train are used to synchronize the gating process. A NASA provided synthesized blade passing pulse train may also be used.

Programs in the 4051 are used to format the clearance data for presentation on the graphic terminal screen. AVERAGE Mode data are presented in a plot of "Clearance versus Scan" (a time history of average clearance). SINGLE BLADE Mode-1 data are presented in a plot of "Clearance versus Blade Number," and SINGLE BLADE Mode-2 data are presented in a plot of "Clearance versus Scan" (a time history of a selected single blade clearance).

## IV. OPTICAL SUBSYSTEM DESIGN

The Optical Subsystem of the Advanced Optical Blade Tip Clearance Measurement System is described in this section with respect to design requirement, component function, and optical performance. Reference should be made to Figure 6, Remote System Chassis Layout, where applicable.

The Optical Subsystem includes the probe assembly that is attached directly to the operating engine gas path seal. This probe is coupled to a laser and detector in the remote system by means of flexible fiber optic bundles. In operation, input to the probe is generated by a helium-neon laser whose output intensity is first regulated by a neutral density filter wheel and then focused to a small spot by a microscope objective lens onto the tip of the probe input fiber optic bundle. This flexible fiber optic bundle transmits the spot image energy to the engine mounted probe head assembly.

The input laser spot image is transferred by the probe optics onto the tip of the target engine blade. By utilizing the rangefinder triangulation principle, the blade tip gap is determined by the reflected image of the input spot through the probe to the tip of the probe output fiber optic bundle. This information is relayed through this fiber optic bundle to its output head which is carefully positioned by the X-Y translation stage at the prime focus of a relay lens assembly.

The relay lens assembly objective lens receives 70% of the output spot radiation, collimates it, and filters the laser signal at 6328Å ±10Å to the Image Intensifier lens which in turn forms the image of the spot position on the Image Intensifier face plate. The gated Image Intensifier amplifies and transmits the spot signal to a LPA which forms the output video signal.

The relay lens assembly concave mirror receives approximately 15% of the probe output spot energy which is transferred to a photomultiplier tube by way of a fiber optic light guide. This photomultiplier tube then generates an electronic pulse train which is used for blade passing detection and counting.

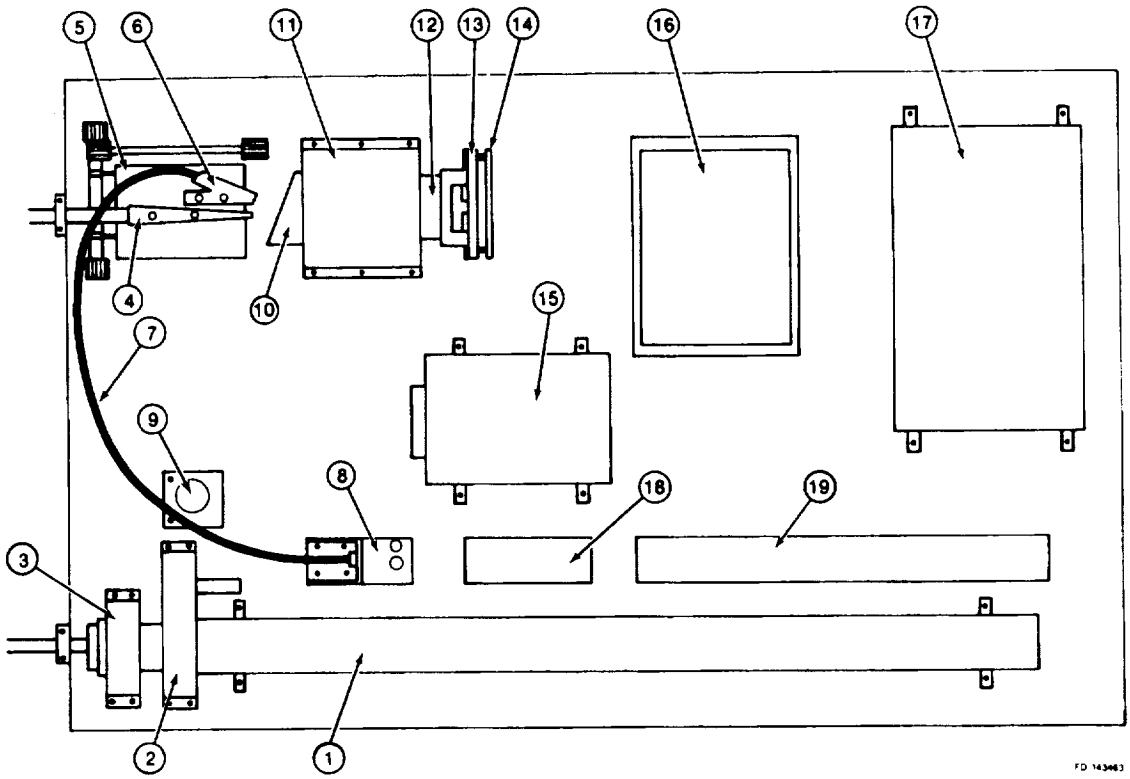


*Figure 6. Remote System Chassis Layout*

| Item | Description |
|---|---|
| 1 | Laser, Hughes Model 3235 H-C, 10 mW He-Ne |
| 2 | Neutral Density Filter Wheel/Drive Assembly |
| 3 | Objective Lens Translator Assembly |
| 4 | Probe Output Head |
| 5 | X-Y Positioning Mount |
| 6 | Blade Passing Detector Head |
| 7 | Blade Passing Fiber Optic Light Guide |
| 8 | Blade Passing Photomultiplier Tube Housing |
| 9 | Blade Passing Photomultiplier Tube Power Supply |
| 10 | Blade Passing Detector Concave Annular Mirror |
| 11 | Relay Lens/Image Intensifier Lens Housing |
| 12 | Image Intensifier Tube and Adapter |
| 13 | Photodiode Array Circuit Board Mounting Bracket |
| 14 | Photodiode Array Circuit Board |
| 15 | Image Intensifier Tube Power Supply |
| 16 | Circuit Board Rack |
| 17 | Laser Power Supply, Hughes Model 3535H |
| 18 | Power Supply |
| 19 | Power Supply |

The probe head assembly design and its associated input/output schemes were based on proven concepts used successfully in current probe systems at Pratt & Whitney Aircraft. However, the Image Intensifier/LPA device utilizes technology which has unproven reliability and performance in this application. Since the Image Intensifier device is the most critical component of the system, great care was exercised in its selection. Because specifications for pulsed (gated) operation of the selected device were not available from the vendor, a careful analysis was performed based on the device's operational principles. It was concluded that the risks inherent in the device were acceptable for the development of this Advanced Optical Blade Tip Clearance Measurement System with a reasonable confidence level for successful application.

**Helium-Neon Laser Source**

The helium-neon laser radiation source (6328Å) is a Hughes Model 3035H 10 mW Laser System. The Laser System includes a Model 3235H-C 10 mW Laser Head and a Model 3535H Power Supply.

The Laser Head has the following primary characteristics:

Minimum Output Power ($TEM_{00}$, CW) = 10 mW @ 6328Å
Beam Diameter @ $1/e^2$ = 1.37 mm
Beam Divergence = 0.6 mrad
Polarization = Random.

The laser tube is enclosed in a rectangular housing which is mounted securely to the Remote System Chassis.

The laser tube is provided with an on-off mechanical beam shutter near the beam exit, which is useful during laboratory setup and calibration.

The selection of the Hughes Model 3035H 10 mW Laser System was primarily a result of demonstrated reliability of the Hughes product line. However, power/cost trade-offs and inherent vendor product integrity were also employed in the selection. From these considerations, the Hughes system surfaced as the most attractive choice.

**Neutral-Density Filter Wheel**

The neutral-density filter wheel is used to control the laser radiation intensity at the blade tip. This control adjusts for the variation in the optical properties of different engine blade types, and the variation in energy received by the Image Intensifier at different engine speeds and system operating modes. The primary purpose of the filter wheel is to set the incident beam intensity at a preselected and established value to provide the intensity needed for the SINGLE BLADE Mode and AVERAGE BLADE Mode for the blade type being investigated. To accomplish this task, the drive motor is automatically indexed to the appropriate filter wheel location when the system mode is selected. The attenuation can be further controlled manually by stepping the filter around its nominal position. The wheel position is monitored by observing the filter wheel position meter on the Electronic Subsystem front panel, where 0 is minimum attenuation and 100 is maximum attenuation.

To prevent damage to the Image Intensifier, the filter wheel can also be positioned at maximum attenuation to block out the laser beam at low engine speed. This feature is in addition to the automatic LOW RPM protection for rotor speeds below 600 RPM.

The filter wheel is also used during setup and calibration of the probe system to prevent damage to the Image Intensifier.

To protect the filter wheel from damage and contamination, it is contained in a housing with entrance and exit holes for the laser beam. The housing is hard coupled to both the Remote System Chassis and the laser housing. The drive motor is hard coupled to the filter wheel housing.

### Objective Lens Translator Assembly

The objective lens translator assembly couples the laser beam to the probe input fiber optic bundle. The assembly consists of a 20-power microscope objective lens to focus the laser beam to a spot of approximately 12 $\mu$m diameter on the end of the fiber optic bundle.

The objective lens translator assembly is mounted in a housing which consists of four parts: The objective lens translator assembly mount, coupling disc, alignment disc, and positioning disc. The coupling disc mates directly to the objective lens translator assembly. It has a close sliding fit with the alignment disc. This arrangement allows accurate location of the alignment disc within the coupling disc without any perceptible play. The positioning disc is actually the tip of the laser input fiber optic bundle. It attaches to the alignment disc and is used to locate the focused laser spot at an optimum area of the coherent fiber array for peak transfer of the laser energy through the fibers. Once aligned, the assembly can be separated at the alignment and coupling discs and then reattached without loss of spot position location on the fiber optic bundle face.

The objective lens translator assembly is hard coupled to both the filter wheel housing and the translator housing. The translator housing is hard coupled to the Remote System Chassis.

### Laser Input Fiber Optic Bundle

The fiber optic bundle which transfers the focused laser spot to the blade tip clearance probe head is a 1.27 mm $\times$ 1.27 mm array of coherent multifibers with 10 $\mu$m fiber elements. The length of the bundle is 2.74 meters.

By utilizing a coherent array of 10 $\mu$m fiber elements, efficient transfer of the focused laser spot energy through the fiber bundle is realized. Since the fiber elements are arranged in a coherent, close packed structure, the spot movement will only shift the spot energy from the initial target fiber area to an adjacent fiber area.

The bundle is sheathed in a flexible, braided stainless steel conduit which is sealed against oil and moisture. This significantly ruggedizes and protects the bundle from rough handling in the test cell environment.

### Probe Head Assembly

The probe head assembly transfers and focuses the input laser spot image to the target blade tip. It then views the radial movement of the blade tip by utilizing the rangefinder triangulation principle, and reimages the spot's position onto the output fiber optic ribbon. The probe head assembly consists of two primary components:

- The probe body, which houses the viewing prism and mates directly to the gas path seal.
- The interface housing, which contains the objective lens and the mating connections for the input and output fiber optics, as well as for the dry nitrogen purge line.

The probe body is designed to bayonet fit directly to the gas path seal whose clearance with the rotating blade tips is to be measured. This direct coupling concept is fundamental to the successful application of the laser blade tip clearance device since the probe tip must move with the gas path seal to provide a stable and meaningful frame of reference. In addition, the distance from the bayonet mount to the gas path seal should be as short as possible to reduce the errors induced by thermal growth. To this end, the bayonet mount is located at the tip of the probe body.

The entire probe head assembly must be capable of free radial movement to account for differential case growth and also provide a seal with the case structure to prevent case cooling air and/or main stream gas flow leakage. This task is accomplished with a piston ring type seal.

Once fitted to the gas path seal, the probe is prevented from rotating by means of a rotation lock key. The key is bolted into place against the flat machined from the rotation lock flange on the probe body. This key, while preventing rotation and subsequent loosening of the bayonet fit, does not constrain movement of the probe along its axis resulting from thermal growth of the engine/probe system.

Probe cooling is accomplished with a dry nitrogen purge at a flow rate of 10 grams per second. The gaseous nitrogen enters the probe through a #4 Aeroquip fitting welded to the side of the interface housing. The gas flows between the inner wall of the probe body and the interface housing extension which accepts the objective lens. It enters the lower portion of the probe body in front of the objective lens through holes in the lens mount and finally exits through the prism viewing slot after flowing around the prism itself. The chamber containing the fiber optic input/output tips and the rear lens surface is not purged since it is a sealed chamber. The chamber is cooled by the flow of gaseous nitrogen around the extension which holds the objective lens.

The optical components contained within the probe assembly consist of the objective lens and the sapphire viewing prism. The viewing prism is seated at the bottom of the probe tip. It is spaced away from the viewing slot by a .5 mm counterbore which allows the nitrogen purge flow to pass across the prism face and exit through the slot; thereby keeping the prism face clean. The prism is retained against the counterbore lip by a thin wall sleeve. The prism and sleeve are kept from rotating by an anti-rotation pin through an axial slot in the upper sleeve wall.

The objective lens is contained within the lens mount which has a close sliding fit with the tip of the interface housing extension. When assembled, the lens mount is spring loaded into place by a spring spacer between it and the prism retainer. This arrangement allows the interface housing chamber to be sealed and still allows the lens to be removed for cleaning or replacement.

The objective lens aperture is divided in half by a light baffle within the interface housing extension. One half of the lens is used for focusing the laser input radiation onto the blade tip, while the other half is utilized for refocusing the laser spot on the output fiber optic ribbon. This technique has the advantage of eliminating backscatter of input laser radiation from the lens surface and chamber walls, thereby greatly improving the signal-to-noise ratio. It, however, also has the disadvantage of reducing the effective collecting aperture of the objective lens. In trading off these considerations, it was realized that the greatly enhanced S/N ratio at the output ribbon more than compensated for the apparent decrease of intensity.

The signal-to-noise ratio of the probe is further enhanced by sand blasting and blackening the interior wall surfaces of the probe. This is particularly important for the prism retainer walls which are roughened and blackened to improve absorption of reflections from the prism faces and other stray radiation sources.

The fiber optic input and output tips are coupled to the rear of the interface housing. They are bolted into place after being focused by the use of focus positioning shims. Once the input and output bundles have been precisely spaced, they can be removed and replaced without affecting probe alignment or calibration.

A summary of the probe optical design parameters derived for this system is given in Table 1.

The optical system parameters satisfy two primary constraints:

- The prism width, W, as determined by the probe tip envelope, and
- The probe range, R, as determined by the prism to probe tip spacing ($R_1$) and the maximum probe tip to blade tip clearance to be measured ($R_0$).

The system variables are:

- The prism height, L
- The prism angle, $\alpha$
- The input bundle incident angle, $\theta_1$, and
- The objective lens focal length, f.

The basic probe optical system is shown in Figure 7 with the detail and symbol definition of the prism ray geometry shown in Figure 8. All symbols and relationships involved in the calculation equations can be defined by reference to these two figures.

The calculation of the probe optical design parameters has been accomplished by a series of iteration processes consisting of three groups of calculations:

- determination of the input angle, $\theta_1$, with the resulting definition of prism configuration (L and $\alpha$)
- determination of the objective lens focal length, f, and resulting spacing of the input and output bundles and prism with respect to the objective lens $\ell'$ (in) and $\ell$ (focus)
- determination of the angular location of the output bundle with respect to the probe axis, $\theta_2$ (focus), and the spot travel range on the face of the output bundle, D.

The boundary conditions which determine the interaction of the laser radiation with the sapphire viewing prism are given as:

$$n \sin u = n' \sin u' \text{ (Snell's Law)}, \tag{1}$$

Where u is the angle with respect to the boundary normal in the medium with an index of refraction n, and u' is the angle with respect to the boundary normal in the medium with the higher index of refraction n'.

$$n = 1.000 \quad \text{(air @ 6328Å)} \tag{2}$$

$$n' = 1.766 \quad \text{(sapphire @ 6328Å)} \tag{3}$$

$$\tan \phi'_2 = Y/L \quad (E_R \text{ to strike apex}), \tag{4}$$

and

$$\tan \phi_2 = Y/R \quad \text{(defines probe range)}. \tag{5}$$

*Table 1. Probe Optical Design Parameters Summary*

| | |
|---|---|
| Laser Input Angle, $\theta_1$ | 7.0° |
| Output Angle, $\theta_2$ (out) | 5.1° |
| Total Probe Range, R | .190" (4.83 mm) |
| Effective Probe Range, $R_e$ | .120" (3.05 mm) |
| Objective Lens Focal Length, f | 25.4 mm (1.00") |
| Laser Input to Lens Spacing, $\overline{IO}$ = f (in) | 49.7 mm (1.96") |
| Lens to Output Ribbon Spacing, $\overline{OF'}$ = f' (focus) | 48.0mm (1.89") |
| Lens to Prism Spacing, $\overline{OP}$ = $L_{apex}$ | 35.0 mm (1.38") |
| Output Spot Range, D | 3.17 mm (.125") |
| Prism Height, L | 9.76 mm (.384") |
| Effective Prism Aperture, W | 10.16 mm (.400") |
| Prism Thickness, t | 5.08 mm (.200") |

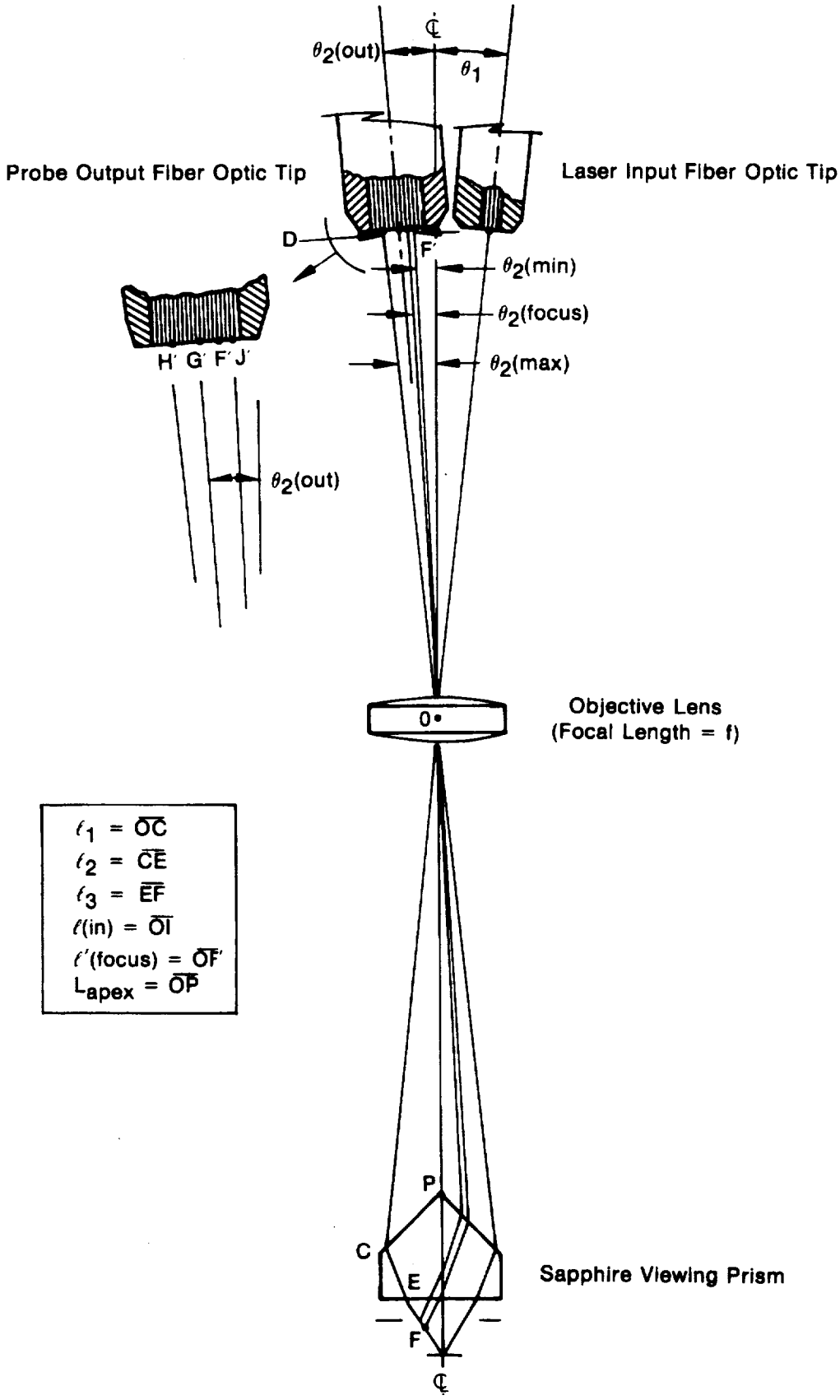


*Figure 7. Basic Probe Optical System*

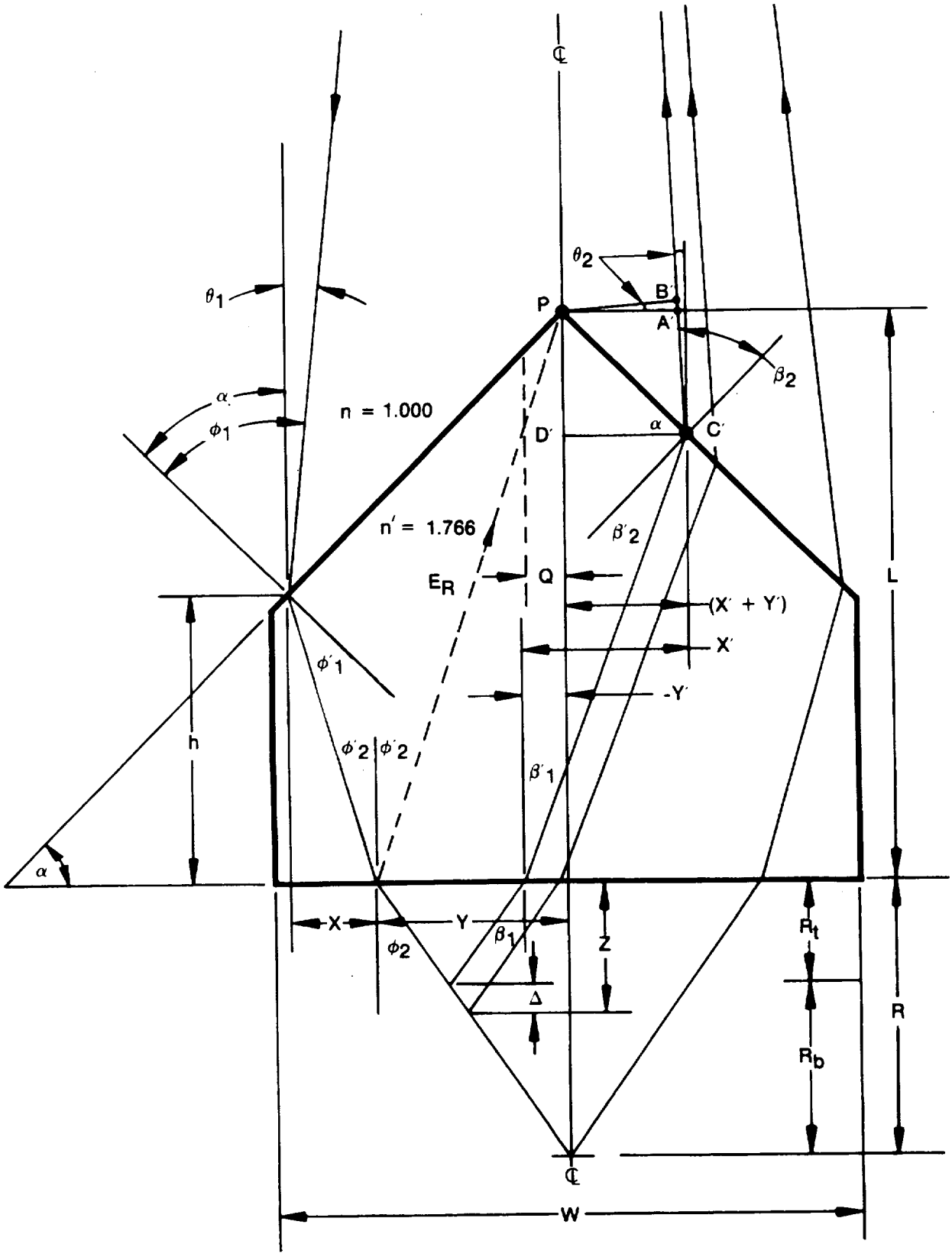


*Figure 8. Prism Ray Geometry*

Referring to Figure 8 for symbol definition, we find the following relationships result from application of the above boundary conditions:

$$L = \frac{R \tan \phi_2}{\tan \phi'_2} \qquad \text{(prism height)}, \tag{6}$$

$$\phi_1 = \alpha + \theta_1 \tag{7}$$

$$\phi'_1 = \sin^{-1} \left( \frac{\sin \phi_1}{n'} \right), \tag{8}$$

$$\phi'_2 = \alpha - \phi'_1, \tag{9}$$

or $$\phi'_2 = \alpha - \sin^{-1} \left[ \frac{\sin (\alpha + \theta_1)}{n'} \right]. \tag{10}$$

and $$\phi_2 = \sin^{-1} (n' \sin \phi'_2). \tag{11}$$

From Figure 8 it can also be seen that

$$X = h \tan \phi'_2, \tag{12}$$

and

$$\tan \alpha = \frac{L - h}{(X + Y)}. \tag{13}$$

From which

$$X = \frac{L \tan \phi'_2 - Y \tan \alpha \tan \phi'_2}{1 + \tan \alpha \tan \phi'_2}. \tag{14}$$

Recalling equation (4),

$$Y = L \tan \phi'_2, \tag{15}$$

so

$$X = \frac{L (\tan \phi'_2 - \tan \alpha \tan^2 \phi'_2)}{1 + \tan \alpha \tan \phi'_2}. \tag{16}$$

The iteration procedure to establish the laser input angle, $\theta_1$, the prism height, L, and the prism angle, $\alpha$, is as follows:

Step 1: Select $\theta_1$ candidate values (fiber optic bundle input angle)

Step 2: Select R (total probe range)

Step 3: Select $\alpha$ (prism angle)

Step 4: Select W (probe envelope diameter)

Step 5: Find $\phi'_2$ from equation (10)

Step 6: Find $\phi_2$ from equation (11)

Step 7: Find L (prism height) from equation (6)

Step 8: Find Y from equation (15)

Step 9: Find X from equation (16)

Step 10: Calculate X + Y and check to see if

$$Q < (X + Y) < \frac{W}{2}, \tag{17}$$

where W is the probe envelope diameter and Q is minimum acceptable radial distance from the probe axis to the point where the input ray first strikes the prism. The value of Q is arbitrarily selected to fit the design application. For this case, Q was selected to be W/10.

- If condition (17) is true, then $\theta_1$, $\alpha$ and L are established by their current values.
- If $Q \geq (X + Y)$, then the input beam strikes the prism too close to the probe axis. For this application, the value of the prism angle, $\alpha$, is held constant at 45° and $\theta_1$ is increased by 0.1°. Return to Step 5 and continue.
- If $(X + Y) \geq W/2$, then, with $\alpha$ held constant at 45°, $\theta_1$ is decreased by 0.1° and the procedure continued at Step 5.

With the prism configuration and the input angle defined, the objective lens characteristics and positioning requirements are now to be found.

From Figure 7 it is seen

$$\ell_1 = \frac{X + Y}{\sin \theta_1}, \tag{18}$$

and

$$\ell_2 = \frac{X}{\sin \phi'_2}, \tag{19}$$

which must be corrected for effective optical path length in the prism, that is, the equivalent air thickness, to yield

$$\ell^*_2 = \eta' \ell_2 \tag{20}$$

The distance $\ell_3$ is the distance from the point the input laser radiation exits the viewing prism to the laser nominal focus point. This point will be located at the distance Z from the prism base along the probe axis. Since a well defined spot size is most important at some distance near zero clearance, $R_1$, the nominal focus will be set at

$$Z = R_1 + \Delta, \tag{21}$$

where $\Delta$ is an offset to some clearance value greater than zero selected by the application requirements to provide increased accuracy near the rub condition where measurements are most critical. Therefore:

$$\ell_3 = \frac{Z}{\cos \phi_2}. \tag{22}$$

Substituting from equation (11)

$$\ell_3 = \frac{Z}{\cos [\sin^{-1}(n' \sin \phi_2')]}. \tag{23}$$

The total optical path length is given by

$$\ell_p = \ell_1 + \ell_2^* + \ell_3. \tag{24}$$

The thin lens equation now gives

$$\ell(\text{in}) = \left(\frac{1}{f} - \frac{1}{\ell_p}\right)^{-1} \tag{25}$$

as the lens to input fiber optic bundle distance for a lens of focal length f.

By utilizing the above information, the distance from the objective lens to the prism apex along the system centerline can be found:

$$L_1 = \ell_1 \cos \theta_1 \tag{26}$$

$$L_2 = \ell_2 \cos \phi_2' \tag{27}$$

$$L_{apex} = L_1 + L_2 - L \qquad \text{(system invariant)} \tag{28}$$

We have now established the distance from the objective lens of focal length f to the prism apex, $L_{apex}$, and the resulting distances from the input fiber optic bundle to the lens, $\ell(\text{in})$, and the lens to the focused laser input spot, $\ell_p$. However, in recalling from condition (17) that the condition $X + Y < W/2$ can be satisfied for a family of input angles, $\theta_1$, we will wish to utilize an input angle, $\theta_1$, which gives a close to unity magnification, M, of the laser spot size at the nominal focus. That is,

$$M = \frac{\ell_p}{\ell(\text{in})} \approx 1 . \tag{29}$$

The candidate $\theta_1$ values should be selected on this basis to preserve spot definition and position.

The positions of the output spot images on the fiber optic ribbon for the effective range, R, of the probe must now be found. Since at maximum range the light path is symmetric to the probe axis, the maximum spot position on the ribbon will be at

$$\theta_2 \text{ (max)} = \theta_1 \tag{30}$$

relative to the objective lens axis. The ray for minimum clearance $\theta_2$(min), must, however, be traced through the system. The location of the output fiber optic bundle will be determined by the ray through the nominal focal point given by equation (21), $\theta_2$ (focus). The output rays are all constrained by the requirement that they must pass through the center of the objective lens defined by equation (25). This condition is met with due consideration of the value for $L_{apex}$ given by equation (28), which is an invariant for both input and output rays.

By again referencing Figure 7 and Figure 8, it is seen that for the generalized return ray to pass through the center of the lens,

$$\overline{PA'} = L_{apex} \tan \theta_2, \tag{31}$$

also

$$\overline{PB'} = \overline{PA'} \cos \theta_2, \tag{32}$$

$$\overline{PC'} = \frac{\overline{PB'}}{\cos (\alpha + \theta_2)},$$

and

$$X' - (-Y') = (X' + Y') = \overline{PC'} \cos\alpha = \overline{D'C'}.$$

In combining these equations it is found that

$$(X' + Y') = L_{apex} \cos \alpha \left[ \frac{\sin \theta_2}{\cos (\alpha + \theta_2)} \right]. \tag{34}$$

The refraction at point C′ requires

$$\beta_2' = \sin^{-1} \left[ \frac{\sin (\alpha + \theta_2)}{n'} \right], \tag{35}$$

where

$$\beta_2 = \alpha + \theta_2.$$

Also

$$\beta_1' = \alpha - \beta_2',$$

therefore

$$\beta_1 = \sin^{-1} [n' \sin (\alpha - \beta_2')]. \tag{36}$$

We can find X′ from the following analysis:

$$\overline{PD'} = (X' + Y') \tan \alpha \tag{37}$$

$$X' = (L - \overline{PD'}) (\tan \beta_1') \tag{38}$$

or,

$$X' = [L - (X' + Y') \tan \alpha] \tan (\alpha - \beta_2'), \tag{39}$$

and

$$Y' = (X' + Y') - X'. \tag{40}$$

The distance Z from the prism face to the point on the input laser radiation beam whose output value $\theta_2$ is being found, can be determined by reference to the following generalized diagram.

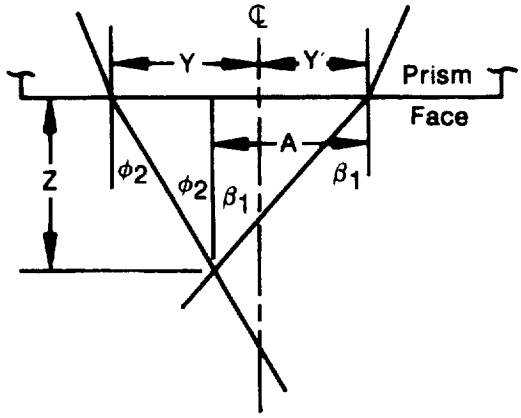


It is seen that

$$\tan \beta_1 = \frac{A}{Z} , \tag{41}$$

and

$$\tan \phi_2 = \frac{(Y + Y') - A}{Z} . \tag{42}$$

(Y' may be negative)

By eliminating A from these equations, it is found that

$$Z = \frac{Y + Y'}{\tan \phi_2 + \tan \beta_1} , \tag{43}$$

where Y and $\phi_2$ are the values derived from the laser input as given by equations (15) and (11), respectively. The values for Y' and $\beta_1$ are those from equations (40) and (36), respectively. The value for Z determined by equation (43) is to be compared to the actual value of Z for the point whose value of $\theta_2$ is being found.

Therefore, the procedure for establishing $\theta_2$ for an output point Z can be summarized in the following steps:

Step 1: Calculate $L_{apex}$ from equation (28).

Step 2: Select an initial value for $\theta_2$ to be $0<\theta_2<\theta_1$ for the given point at Z.

Step 3: Calculate $(X' + Y')$ from equation (34).

Step 4: Calculate $\beta_2'$ from equation (35).

Step 5: Calculate $X'$ from equation (39).

Step 6: Calculate $Y'$ from equation (40).

Step 7: Calculate $\beta_1$ from equation (36).

Step 8: Find Z from equation (43).

Step 9: Compare value of Z from Step 8 to value of Z required for establishing $\theta_2$. If these values are equal within, say, $\pm 0.025$ mm, then the value for $\theta_2$ has been established. If the values of Z are unequal, then go back to Step 2 after scaling a new value for $\theta_2$ by

$$\theta_2 = \theta_A + \left[ \frac{Z_A - Z}{Z_A - Z_B} \; (\theta_B - \theta_A) \right] \quad \text{for } \theta_B > \theta_A \tag{44}$$

The above procedure should be followed to establish $\theta_2$ (min) and $\theta_2$ (focus) for $Z = R_t$ and $Z = R_t + \Delta$, respectively. With these two quantities, the distance from the focus point to the objective lens $\ell_2'$ and the distance from the objective lens to the output fiber optic ribbon $\ell'$ (focus) are calculated. The calculations are accomplished by using the corresponding relationships defined by equations (18) through (25), with calculations based on equations (26), (27), and (28) serving as a validity check through the invariant $L_{apex}$.

The angle of the output fiber optic ribbon with respect to the lens axis is now found from

$$\theta_2(\text{out}) = \left[ \frac{\theta_2(\text{max}) - \theta_2(\text{min})}{2} \right] + \theta_2(\text{min}) \tag{45}$$

The value for $\ell'(\text{out})$, the distance of the output fiber optic ribbon from the objective on the $\theta_2(\text{out})$ angle line, is used as the proper position for the output image plane and is found from

$$\overline{F'G'} = \ell'(\text{focus}) \sin [\theta_2(\text{out}) - \theta_2(\text{focus})] \tag{46}$$

$$\ell'(\text{out}) = \frac{\overline{F'G'}}{\tan [\theta_2(\text{out}) - \theta_2(\text{focus})]} \tag{47}$$

The spot range is next found from

$$\overline{G'J'} = \ell'(\text{out}) \tan [\theta_2(\text{out}) - \theta_2(\text{min})] \tag{48}$$

$$D = 2\,\overline{G'J'} \tag{49}$$

Final trade-off for selecting the appropriate candidate $\theta_1$ is based upon the spot range being at or near unit magnification of the true blade tip measurement range. That is

$$D \sim R_b \tag{50}$$

One additional consideration must now be made. We recall the calculated values for $\phi_2 = \beta_1(\text{max})$ and $\beta_1(\text{min})$ from equations (11) and (36), respectively. In the Optical Properties of Blade Tips

Study, it was shown that, for the most part and considering realistic variations, the detected signal strength of the scattered radiation from the blade tip does not fall off significantly in the region ±5° around the nominal angle of reflection. The operation of the probe is, therefore, not appreciably affected if

$$|\phi_2 - \beta_1(\min)| < 5° \tag{51}$$

This constraint must be considered before final optical design data are accepted.

A summary of results based on the preceding discussion for this Advanced Optical Blade Tip Clearance Measurement System appears in Table 2 and in Table 3. Three values of the total probe range, R, were selected. The probe range variations reflect mechanical design changes in the prism face to probe tip distance, while the measurement range of the probe is maintained at 0.120". The prism angle, $\alpha$, and the maximum inside diameter of the probe envelope, W, were kept constant at 45° and 10.16 mm, respectively. Also established as a constant for the system was the objective lens focal length, f, which was set at 25.4 mm.

After proceeding with the calculations developed from equations (1) through (28), the first trade-off decision was centered around equation (29) which states that the laser spot magnification at its nominal focal point should be approximately unity. In studying Table 2 it is seen that the two input angles, 6.5° and 7.0°, with total ranges of 0.170" and 0.190", respectively, have values of M close to unity. These, therefore, became our candidate values and the parameters generated from them were utilized for subsequent calculations and analysis.

We then continued the procedures outlined by equations (30) through (49) and arrived at the next trade-off consideration dictated by equation (50) for the spot range to be approximately equal to the real measurement range of blade tip clearance. It is seen from the data in Table 3 that a 7.0° laser input angle with a total range of 0.190" provided the best approach to $D \sim R_{th}$.

The final consideration assured that, for minimum clearance, the angle of incidence of the laser radiation on the blade tip was equal to the nominal angle of reflection to within ±5°. As can be seen the parameters selected meet this condition.

It should be noted here that the focus offset, $\Delta$, was selected to be 0.508 mm. This choice was based on the assumption that the most critical blade tip clearance region would occur within twice this value, an assumption which has been validated by past experience with typical engine clearances.

### Probe Output Fiber Optic Bundle

The fiber optic bundle linking the probe output image plane with the input image plane of the Image Intensifier relay lens assembly is a 1.27 mm by 5.08 mm coherent array of 10 $\mu$m fiber elements. The length of the bundle is approximately 2.75 meters.

The bundle is sheathed in a flexible, braided stainless steel conduit which is sealed against oil and moisture. This significantly ruggedizes and protects the bundle from rough handling in the test cell environment.

### X-Y Positioning Mount

The X-Y positioning mount provides a mounting base for the probe output head and the blade passing detector head while allowing accurate focus positioning with respect to the relay lens assembly. The translation stage is hard coupled to the Remote System Chassis. Once the probe output and blade passing detector heads have been positioned, the translation slides are secured by set screws.

*Table 2. Preliminary Design Trade-Off Study Parameters*

| $\theta_1$ | 6.000° | 6.500 | 7.000 | 7.500 | 6.000 | 6.500 | 7.000 | 7.500 | 6.000 | 6.500 | 7.000 | 7.500 |
|---|---|---|---|---|---|---|---|---|---|---|---|---|
| $\alpha$ | 45.000° | 45.000 | 45.000 | 45.000 | 45.000 | 45.000 | 45.000 | 45.000 | 45.000 | 45.000 | 45.000 | 45.000 |
| $\phi_1$ | 18.892° | 18.695 | 18.499 | 18.305 | 18.892 | 18.695 | 18.499 | 18.305 | 18.892 | 18.695 | 18.499 | 18.305 |
| $\phi_2$ | 34.877° | 34.475 | 34.079 | 33.688 | 34.877 | 34.475 | 34.079 | 33.688 | 34.877 | 34.475 | 34.079 | 33.688 |
| R | 4.318 mm | 4.318 | 4.318 | 4.318 | 4.572 | 4.572 | 4.572 | 4.572 | 4.826 | 4.826 | 4.826 | 4.826 |
| L | 8.794 mm | 8.762 | 8.731 | 8.701 | 9.312 | 9.278 | 9.245 | 9.213 | 9.829 | 9.793 | 9.758 | 9.724 |
| Y | 3.010 mm | 2.965 | 2.921 | 2.878 | 3.187 | 3.139 | 3.093 | 3.048 | 3.364 | 3.314 | 3.265 | 3.217 |
| X | 1.475 mm | 1.466 | 1.457 | 1.447 | 1.562 | 1.552 | 1.542 | 1.532 | 1.648 | 1.638 | 1.628 | 1.618 |
| X + Y | 4.485 mm | 4.431 | 4.378 | 4.326 | 4.748 | 4.691 | 4.635 | 4.580 | 5.012 | 4.952 | 4.893 | 4.835 |
| W/2 | 5.080 mm | 5.080 | 5.080 | 5.080 | 5.080 | 5.080 | 5.080 | 5.080 | 5.080 | 5.080 | 5.080 | 5.080 |
| Z | 1.778 mm | 1.778 | 1.778 | 1.778 | 2.032 | 2.032 | 2.032 | 2.032 | 2.286 | 2.286 | 2.286 | 2.286 |
| f | 25.400 mm | 25.400 | 25.400 | 25.400 | 25.400 | 25.400 | 25.400 | 25.400 | 25.400 | 25.400 | 25.400 | 25.400 |
| $l_p$ | 53.115 mm | 49.371 | 46.175 | 43.416 | 56.421 | 52.456 | 49.071 | 46.149 | 59.728 | 55.542 | 51.968 | 48.883 |
| $l$(in) | 48.678 mm | 52.314 | 56.455 | 61.211 | 46.197 | 49.245 | 52.655 | 56.493 | 44.194 | 46.804 | 49.684 | 52.874 |
| $L_{apex}$ | 38.184 mm | 34.457 | 31.276 | 28.532 | 40.430 | 36.483 | 33.115 | 30.210 | 42.676 | 38.510 | 34.955 | 31.888 |
| M | 1.091 mm | 0.944 | 0.818 | 0.709 | 1.221 | 1.065 | 0.932 | 0.817 | 1.351 | 1.187 | 1.046 | 0.925 |

*Table 3. Final Probe Design Trade-off Study Parameters*

| | R = .170" (4.318 mm) | | | R = .190" (4.826 mm) | | |
|---|---|---|---|---|---|---|
| | $\theta_2$(max) | $\theta_2$(focus) | $\theta_2$(min) | $\theta_2$(max) | $\theta_2$(focus) | $\theta_2$(min) |
| $\theta_1$ | 6.500° | 6.500 | 6.500 | 7.000 | 7.000 | 7.000 |
| $L_{apex}$ | 34.457 mm | 34.457 | 34.457 | 34.955 | 34.955 | 34.955 |
| $\theta_2$ | 6.500° | 3.216 | 2.483 | 7.000 | 3.907 | 3.221 |
| X'+Y' | 4.431 mm | 2.051 | 1.562 | 4.893 | 2.562 | 2.084 |
| $\beta_2$ | 26.305° | 24.976 | 24.669 | 26.501 | 25.262 | 24.978 |
| X' | 1.466 mm | 2.446 | 2.668 | 1.628 | 2.582 | 2.796 |
| Y' | 2.965 mm | −0.394 | −1.106 | 3.265 | −0.020 | −0.712 |
| $\beta_1$ | 34.475° | 37.208 | 37.850 | 34.079 | 36.614 | 37.204 |
| Z | 4.318 mm | 1.778 | 1.270 | 4.826 | 2.286 | 1.778 |
| $\phi_2$ | 52.618 mm | 51.407 | 51.224 | 55.037 | 53.950 | 53.744 |
| F'(focus) | — | 50.207 mm | — | — | 47.997 | — |
| $\theta_2$(out) | — | 4.492° | — | — | 5.111 | — |
| D | — | 3.521 mm | — | — | 3.167 | — |
| $R_o$ | — | 3.048 mm | — | — | 3.048 | — |
| $\lvert \phi_2 - \beta_1 \rvert$ (min) | — | 3.375° | — | — | 3.125° | — |

**Relay Lens Assembly**

The relay lens assembly serves three primary functions:

- To receive and collimate the laser spot image radiation received from the probe output fiber optic bundle.
- To isolate the 6328Å radiation from unwanted background radiation.
- To collect peripheral radiation from the probe output head which is not collected by the objective lens and utilize that energy to produce a blade passing pulse train.

The above functions are accomplished by the optical elements contained in a single assembly that is coupled directly to the Image Intensifier lens.

**Blade Passing Detection System**

The requirement to generate a blade passing pulse train is achieved through utilization of a concave annular mirror. The objective lens of the relay lens assembly views the probe output spot image through a hole in the center of the concave mirror equal to the objective lens diameter. Therefore, the objective lens receives approximately 70% of the fiber optic bundle output intensity distribution while the annular mirror segment will receive the peripheral radiation from the bundle which would otherwise be lost. The radiation collected by the mirror is focused onto the tip of a fiber optic light guide positioned beside the probe output head. The light guide is of sufficient diameter for the spot to always be detected throughout the probe spot range. Once the radiation is detected by the light guide tip, it is transmitted to a photomultiplier tube (PMT) where the pulse train signal is generated. Laboratory measurements demonstrated that this scheme receives 15 to 20% of the total energy available from the probe output tip. This, together with the radiation received by the objective lens, showed this scheme to utilize about 85% of the total radiation emitted by the probe output tip.

The photomultiplier housing contains the PMT. The PMT output is conditioned and processed by the Electronic Subsystem.

### Image Intensifier Lens

The collimated and filtered signal radiation from the relay lens assembly is reimaged onto the Image Intensifier faceplate by a motorized iris f/1.3 lens. The lens is hard coupled to both the relay lens assembly and the Image Intensifier device.

The lens contains a motorized iris to maintain a minimum spot image size on the Image Intensifier faceplate and ultimately the Reticon diode array.

During conditions of sufficient signal radiation the iris is set at the position to obtain minimum spot size as determined by the Reticon video output. If the primary system throughput controls (laser filter wheel and Image Intensifier gain control) require augmentation, the iris can be opened or closed to provide the necessary signal level.

### Image Intensifier/LPA

The Image Intensifier device used in this system is a "Second Generation" Proximity Focused Microchannel Plate Image Intensifier optically coupled to a Reticon RL 256C/17 LPA (256 elements with one mil center to center diode spacing). The Image Intensifier uses a gateable, remotely programmable power supply.

The entire image intensification process is performed internally with no external electronics other than the gateable power supply. The tube consists of an input window with an S20 photocathode deposited on the inside surface, a microchannel plate, and an output phosphor screen coupled directly to a Reticon photodiode array by way of a fiber optic faceplate. The tube envelope is 40 mm in diameter and 30 mm long.

The Image Intensifier tube operation is described by the following discussion: The optical signal energy enters the input window where it strikes the photocathode. At the photocathode, photoelectrons are produced and subsequently accelerated toward the microchannel plate by an electric field potential. At the microchannel plate, secondary electrons are produced and multiplied through each microchannel element by the applied potential across the plate. This is the primary gain mechanism of the device. The multiplied secondary electrons exiting each microchannel element are again accelerated by an applied potential and strike the phosphor screen where the electron energy is converted back to photon energy. This conversion process results in additional gain as a function of the applied voltage between the microchannel plate and the phosphor. These photons generated by the phosphor are then guided by the output fiber optic faceplate to the LPA. The signal spot size is preserved throughout the amplification process by the proximity focusing technique of the tube. That is, the photon/electron/photon flow through the device remains collimated due to the close proximity of each surface and the strength of the accelerating potential between the surfaces.

The output of the device is, however, limited by a saturation effect within the microchannel plate. This limit is defined by ITT in terms of a maximum allowable input flux density (lumen/cm$^2$) for a continuous (steady state) signal source. To determine tube/detector compatibility for this measurement system application, a comparison of the pulsed input conditions to the specified continuous input limitations was needed.

The estimated total spot energy seen by the Image Intensifier per 1.3 microsecond duration pulse (worst case blade passing duty cycle) is approximately $1.3 \times 10^{-15}$ joules. This quantity of energy is quite low and corresponds to only $4.20 \times 10^{+3}$ photons per pulse. Since the ITT specifications can be given only with respect to continuous photometric radiation flux input, the above pulse quantity must be converted into an equivalent continuous radiation input level for comparison.

When this is done, in photometric units, the flux density of the pulse spot corresponds to an equivalent continuous input level of $1.4 \times 10^{-8}$ lumen/cm$^2$. Thus, it is clearly seen that our equivalent continuous input level exceeds the ITT specification by a factor of 2600, even though it is equally clear that the input per pulse is quite low. This dilemma is deepened by the fact that the Image Intensifier device's specified luminous gain is sufficient to amplify this low level pulse to a detectable signal at the Reticon array.

The compatibility question was resolved by careful and detailed analysis of the operational principles of the microchannel plate device, and consideration of published reports from investigators who have experience with gated and/or pulsed operation.

Based on this analysis, it was concluded that operation of the ITT device in the pulsed and/or gated mode would produce, with a reasonable confidence level, a detectable signal at the Reticon diode array. The above analysis indicated that the technical risks inherent in utilizing the ITT device were acceptable and the probability for success of the system was favorable.

## V. ELECTRONIC SUBSYSTEM DESIGN

The Electronic Subsystem controls the components of the Optical Subsystem and processes the data from the Linear Photodiode Array (LPA). It also interfaces to the Tektronix 4051 computer to receive commands and transmit tip clearance data.

The system operating mode is determined by the operator through keyboard commands to the system software resident in the 4051. The system software transforms the operator's requests into the appropriate command sequences for transmission to the Electronic Subsystem. The command sequences are made up of variables (e.g., SINGLE BLADE Mode, BLADE NUMBER) which, when received by the Electronic Subsystem, cause the desired operating mode to be selected. The LPA scan control logic executes the command by controlling the Optical Subsystem in the desired mode. The 4051 software then asks for tip clearance data with another command sequence. In addition to the tip clearance data, an error line has been provided to signal the 4051 if the data are invalid, due to a detected hardware error condition.

The Optical Subsystem control circuits operate in one of two basic modes, AVERAGE or SINGLE BLADE. In the AVERAGE Mode, the Image Intensifier is gated on continuously and the LPA optically averages the clearance of all blades. In the SINGLE BLADE Mode, the Image Intensifier is gated on to view only the requested blade. In the SINGLE BLADE Mode, more than one revolution of the requested blade may be optically averaged by the LPA to provide a higher signal level.

To optimize the LPA output, the video signal is automatically increased or decreased by controlling the gain of the Image Intensifier with an automatic gain control (AGC). A coarse laser light level control is manually adjusted via a servo operated variable neutral density filter. The LPA video output is converted to a digital (diode site) clearance number for transmission to the 4051 and display on the front panel.

### Software Commands Supported by Electronic Subsystem

AVERAGE/SINGLE BLADE Mode selection determines whether the optics will average all the blades each revolution or look at one blade at a time.

NUMBER OF REVOLUTIONS, in the range of 1 to 255, determines how many rotor revolutions will be optically averaged and processed (SINGLE BLADE Mode only).

MINIMUM CLEARANCE ALARM is activated by the 4051 when the software has detected a measured clearance at or less than a preselected minimum.

MAXIMUM CLEARANCE ALARM is activated by the 4051 when the software has detected a measured clearance at or greater than a preselected maximum.

BLADE NUMBER, in the range of 1 to 120, determines the specific blade(s) to be processed (SINGLE BLADE Mode only).

### Hardware Operating Modes

AVERAGE Mode turns on the Image Intensifier gate continuously and the LPA is scanned every revolution. An updated clearance number is available to be presented to the Tektronix 4051 Graphics Terminal each revolution. The maximum rate at which the 4051 can input data is one byte every 1.48 milliseconds. This corresponds to a rotor speed of slightly greater than 40,000 RPM. For higher rotor speeds, the 4051 will accept data every other revolution.

SINGLE BLADE Mode gates the Image Intensifier on to view only the requested blade. The LPA is scanned every "N" revolutions of the rotor to provide an optical average of a single blade for "N" revolutions ($1 \leq N \leq 255$). After each scan of the LPA an updated clearance number is presented to the 4051. SINGLE BLADE data can be presented as clearance of any preselected blade versus scan (a time history) or clearance versus blade number.

### Circuit Descriptions

The General Purpose Interface Bus (GPIB) is a communication system which uses a byte-serial, bit-parallel means to transfer digital data among a group of instruments and other system components. Up to 15 devices may be interconnected by one continuous bus not exceeding 20 meters in length. The signal lines and their timing and control conventions are defined in the GPIB specifications, reference IEEE STD 488-1975.

There are only three types of devices connected to the GPIB; talkers, listeners, and controllers. The 4051 is the only controller in this system. It assigns other devices as listeners and talkers.

A listener is a device which receives commands or data from a talker in a predefined format. The Electronic Subsystem has two listen addresses. One has been assigned to receive 4 BYTES in sequence: NUMBER OF REVOLUTIONS, AVERAGE Mode/SINGLE BLADE Mode, MINIMUM CLEARANCE ALARM, and MAXIMUM CLEARANCE ALARM. The other has been assigned to receive a single byte, BLADE NUMBER.

A talker is a device which sends data to a listener via the GPIB. An address has been assigned to activate the Electronic Subsystem talker to send clearance data over the GPIB to the 4051 which functions as a listener, at that time.

The talkers, listeners and controller communicate by means of the GPIB "handshake."

#### *GPIB Transceiver Logic*

The GPIB receiver logic performs two functions. It terminates all GPIB lines with a resistive network and inverts from the negative logic on the GPIB to positive logic required in the Electronic Subsystem. These positive true signals are used by other GPIB interface logic in the Electronic Subsystem to receive data, decode addresses and perform the required handshake sequence.

The drivers convert from positive logic in the Electronic Subsystem to negative logic on the GPIB. The drive signals are the tip clearance number, data errors, and GPIB handshake.

### *Address Decoder/Listener Handshake Logic*

The listener handshake logic performs the required sequencing to accomplish the transfer of data through the GPIB to the 4051. The listener handshake logic is enabled during address transfers and whenever the Electronic Subsystem is in the listen mode.

The listen address decoder detects the occurrence of addresses on the GPIB as listed below. These addresses are assigned to the Electronic Subsystem to allow communication with the 4051.

- A LISTEN address which receives the command sequence NUMBER OF REVOLUTIONS, AVERAGE Mode/SINGLE BLADE Mode, MINIMUM CLEARANCE ALARM, MAXIMUM CLEARANCE ALARM.

- A LISTEN address which receives only one data byte, BLADE NUMBER.

Since the LPA scanner is running asynchronously with the software, circuitry was provided to synchronize the talker logic to ensure that the clearance data transmitted correspond to the current mode of operation. The talker logic performs the required sequencing to transmit the clearance data to the 4051 in response to the 4051's command as indicated below.

- A TALK address which causes the interface to sequentially transmit CLEARANCE DATA bytes to the 4051 while the 4051 reads and stores them.

### *Index, BPP Conditioning Logic*

This logic time shifts the index pulse to coincide with the blade passing pulse (BPP). This insures that the blade following the index pulse will always be blade number one.

### *Clock and Cal Logic*

The clock provides 500 kHz which is used for scanning the LPA, 200 Hz which is used for simulation of index pulses, and 400 Hz for simulation of blade passing pulses. These simulation pulses provide signals representing a 2-bladed rotor at approximately 12,000 RPM during calibration.

### *LPA Scan Control Logic*

This circuitry uses the BLADE NUMBER, NUMBER OF REVOLUTIONS, and AVERAGE Mode/SINGLE BLADE Mode flags to initiate the LPA scan and to gate the Image Intensifier. To provide accumulated light to the LPA a 340 $\mu$sec delay is provided to take advantage of the decaying phosphorescence of the Image Intensifier.

In AVERAGE Mode, the Image Intensifier is gated on continuously and the LPA is scanned once for each rotor revolution.

In SINGLE BLADE Mode, two options are available:

- The clearance of each blade, in turn, is measured until data from all blades are obtained. In this option, the Image Intensifier is gated on only during the passage of the blade being measured.

- The clearance of one blade is measured continuously and the LPA is scanned once for each revolution.

### *LPA Site Counter and Clearance Register Logic*

This logic, in conjunction with the peak detector, determines the LPA diode site corresponding to the first video peak representing minimum clearance of the blade being measured and updates the clearance register.

### *Display Logic*

The display logic provides clearance data, blade number and number of revolutions to the numerical display on the Electronic Subsystem front panel. A three digit display has been provided to display the data selected. Leading zero blanking has been utilized for the first two digits; i.e., when either of the first two digits is zero, then their indication is blanked. A display test pushbutton has been provided to allow verification of all segments of the display.

### *PMT Gate Logic*

The PMT gate logic prevents the photomultiplier tube from operating in the calibrate mode and when rotor speed is below 600 RPM. This is done to protect the photomultiplier tube from excessive light.

### *D/A Converter*

The digital to analog converter provides clearance data in analog form for general use external to the system.

### *Video Gate Control*

The video gate control switches the LPA video signal to the peak detector circuitry. Its purpose is to eliminate data past the first peak which represents minimum clearance.

### *Filter Position Control*

The purpose of this circuit is to generate two manually adjustable, but automatically switched, setpoints for the neutral density filter wheel positions. Two different setpoints are required for the two modes of operation, AVERAGE MODE and SINGLE BLADE MODE since the AVERAGE MODE requires considerably less laser light than does the SINGLE BLADE MODE.

### *Peak Detector*

The peak detector detects the first peak above the preset threshold level in the video output of the LPA. The threshold level control eliminates low level noise. The peak detector compares each new LPA diode output with the previous one. When three successive diode sites have lower outputs than the previous one, the first peak has been identified. Switching transients are ignored by delay sampling of each LPA diode site. The LPA diode site at which the peak occurs is translated into a clearance number by means of the LPA diode site counter circuitry. The amplitude of the first video peak is used to establish AGC voltage to optimize the LPA output. This MAX/MIN VIDEO detector monitors the amplitude of the first video peak to determine if the data are valid. If the peak is near the noise level or saturation level an error signal is generated.

PEAK DETECTOR CIRCUIT FUNCTIONS

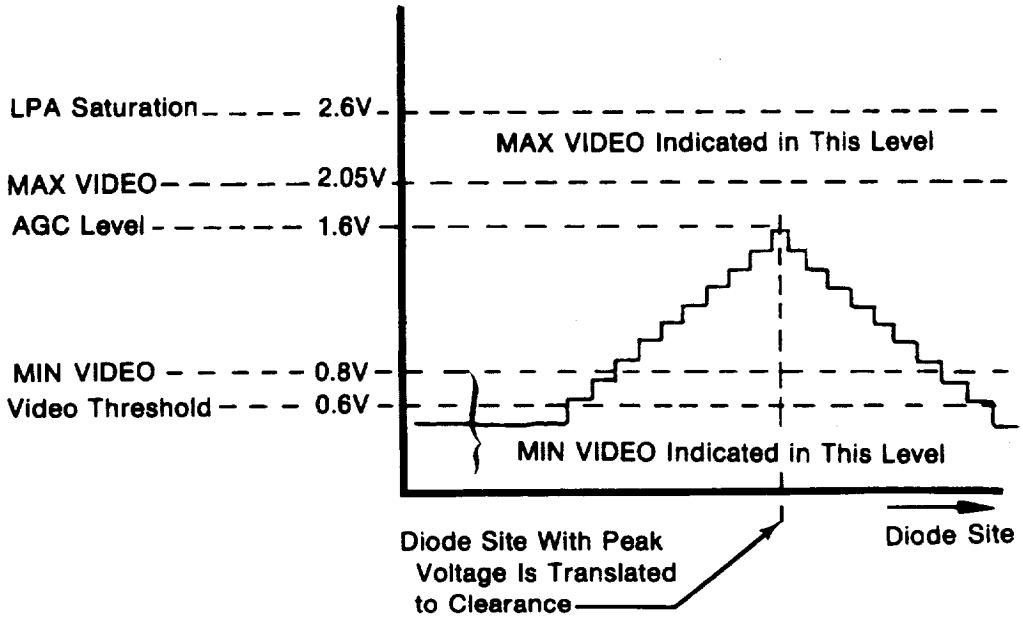


Where

*LPA Saturation* (2.6V) is saturation voltage of the LPA.

*MAX VIDEO* (2.05V) is the maximum acceptable LPA peak voltage. An error signal is generated if the peak voltage exceeds this level.

*AGC Level* (1.6V) is the optimum LPA peak voltage operating level.

*MIN VIDEO* (0.8V) is the minimum acceptable LPA peak voltage. An error signal is generated if the LPA peak voltage is less than this level.

*Video Threshold* (0.6V) is the minimum LPA peak voltage level which the AGC circuit can "lock-on" to.

***Front Panel Controls and Indicators (Figure 9)***

AVERAGE MODE indicator illuminates when the system is in AVERAGE Mode, in which the LPA optically averages the clearance of all blades on the rotor.

SINGLE BLADE MODE indicator illuminates when the system is in SINGLE BLADE Mode, in which the LPA optically averages the clearance for the preselected blade for 1 to 255 revolutions of the rotor.

MAX CLEARANCE LIMIT indicator is controlled, through software, by the 4051 and illuminates when the software has detected a clearance at or greater than the preselected maximum value.

MIN CLEARANCE LIMIT indicator is controlled, through software, by the 4051 and illuminates when the software has detected a clearance at or less than the preselected minimum value.

DISPLAY normally indicates the latest clearance data.

BLADE NUMBER switch, when depressed, provides the display an indication of blade number.

NUMBER REVS switch, when depressed, provides the display an indication of number of revolutions.

LED TEST switch, when depressed, forces the display to indicate 888 which illuminates all segments for verification of their operation.

HOLD switch, when depressed, prevents further updating of the display register allowing the operator to read a sample of rapidly varying clearance readings.

OPERATE/CALIBRATE switch selects the sources of the blade passing pulse train and the index pulse train. In the OPERATE position, the sources of the signals are derived from the rotor under test. In the CALIBRATE position, an internal oscillator generates these signals, simulating a two-bladed rotor at approximately 12,000 RPM. This position is used for a static calibration of the system, with the probe attached to a calibration fixture.

IMAGE INTENSIFIER LENS CONTROL is a three-position momentary switch which allows remote manual operation of the Image Intensifier lens motorized iris. The switch is normally in the OFF position, but can INCREASE or DECREASE lens aperture when activated.

DATA ERROR lights illuminate and flag the 4051 when an error has occurred.

- MIN VIDEO indicator illuminates when the LPA output is near the noise level or undetectable.
- MAX VIDEO indicator illuminates when the LPA output is at or near saturation. The Image Intensifier gain is also set to minimum when this occurs.
- BLADE NUMBER indicator illuminates when the selected blade number is greater than the number of rotor blades, as determined by the ratio of the blade passing frequency to the index frequency.
- LOW RPM indicator illuminates when the frequency of the index pulse train drops below 10 Hz (600 RPM).
- VIDEO MALF indicator illuminates when the Optical Subsystem has detected an error condition; (i.e., MIN VIDEO, MAX VIDEO).

ATTENUATOR POSITION meter indicates the position of the neutral density filter wheel which is used to attenuate the laser beam from 0 to 100%.

FILTER POSITION ERROR indicator illuminates when the neutral density filter wheel is not at the desired position as determined by the setting of the AVERAGE MODE or SINGLE BLADE MODE filter position controls.

AVERAGE MODE, a 10-turn dial with a range from 0 to 100%, is used to set the desired position of the neutral density filter wheel when the system is in the AVERAGE Mode.

SINGLE BLADE MODE, a 10-turn dial with a range from 0 to 100%, is used to set the desired position of the neutral density filter wheel when the system is in the SINGLE BLADE mode.

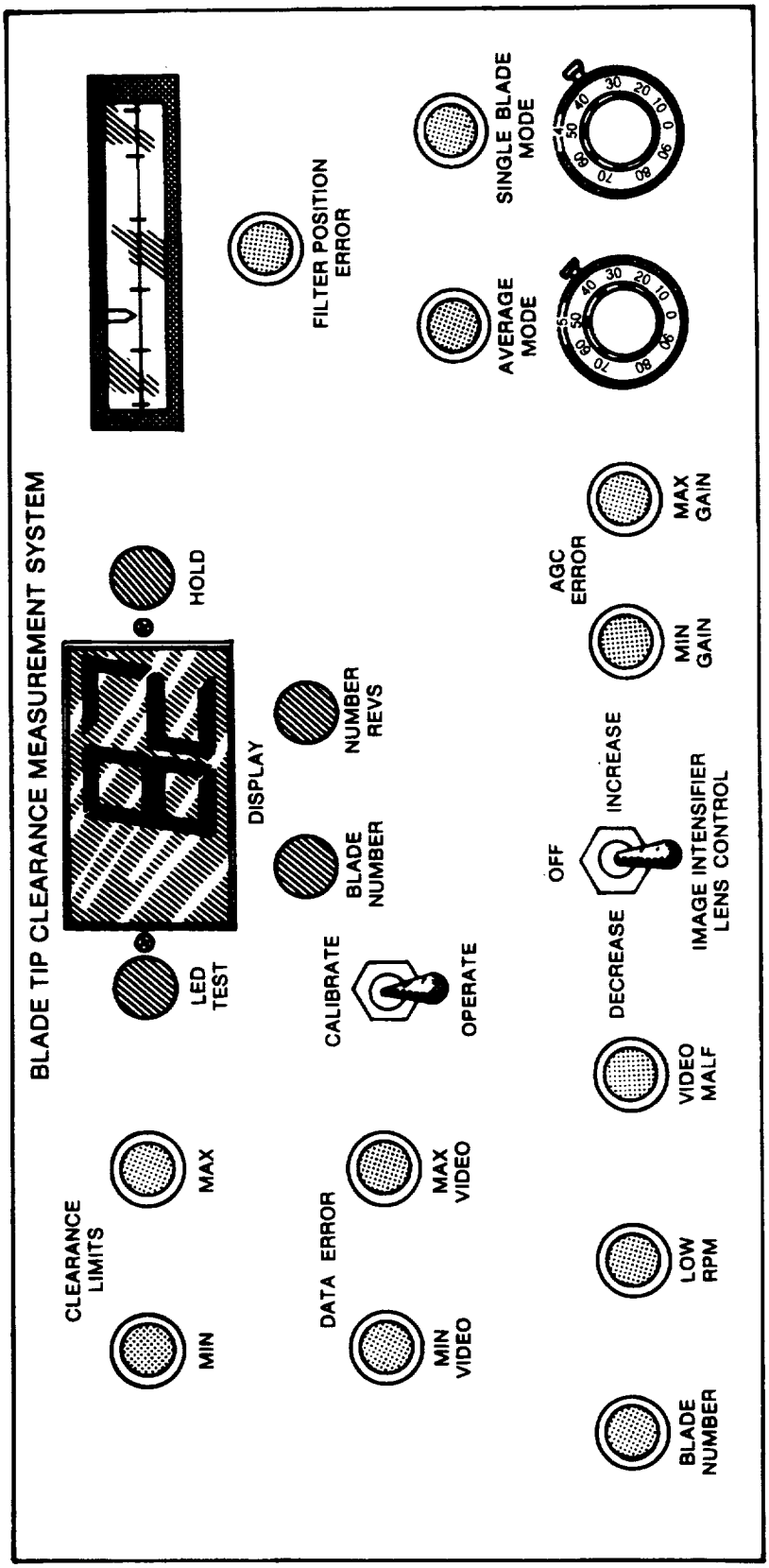


*Figure 9. Electronic Subsystem Front Panel*

MIN GAIN indicator illuminates when the Image Intensifier AGC has driven the gain of the Image Intensifier to the minimum value. This AGC error indicates an adjustment of the neutral density filter wheel position or Image Intensifier lens motorized iris is required to further attenuate the optical signal to the LPA.

MAX GAIN indicator illuminates when the AGC has driven the gain of the Image Intensifier to the maximum value. This AGC error indicates an adjustment of the neutral density filter wheel position or Image Intensifier lens motorized iris is required to increase the optical signal to the LPA.

## VI. SYSTEM SOFTWARE

The Tektronix model 4051 Computing and Graphic Display Terminal controls the Electronic Subsystem and provides clearance data presentation. Specific test conditions are accepted by programs resident in the 4051's core memory from operator keyboard entries. Upon execution, the programs issue control instructions and receive blade tip clearance (in mils) in return via the GPIB.

The program operates in three modes:

- AVERAGE Mode
- SINGLE BLADE Mode
    - SINGLE BLADE Mode-1 (Sequence of blades)
    - SINGLE BLADE Mode-2 (Scan of one blade)

Optically averaged clearance of all blades or individual blade clearances are plotted (in mils) on the 4051's Graphic Display.

In AVERAGE Mode, data are presented on the graphic terminal screen in a plot of "Clearance versus Scan" (a time history). In the SINGLE BLADE Mode-1 data are presented in a plot of "Clearance versus Blade Number," and SINGLE BLADE Mode-2 data are presented in a plot of "Clearance versus Scan," (a time history of a selected single blade clearance). Plot formats are illustrated by Figures 10, 11, and 12.

Each test is initiated by pressing a "user" key and test variables are entered by the operator via the Tektronix 4051 keyboard. The 4051 then activates the appropriate software programs and instructs the Electronic Subsystem to operate according to the test variable input requirements.

In addition, the program

- Provides ZOOM capability for expanded plots, Figure 13.
- Provides operator option to record and identify data on the cassette tape.
- Provides for data storage file retrieval.
- Provides keyboard manual abort capability.

A flow diagram of the system software follows.

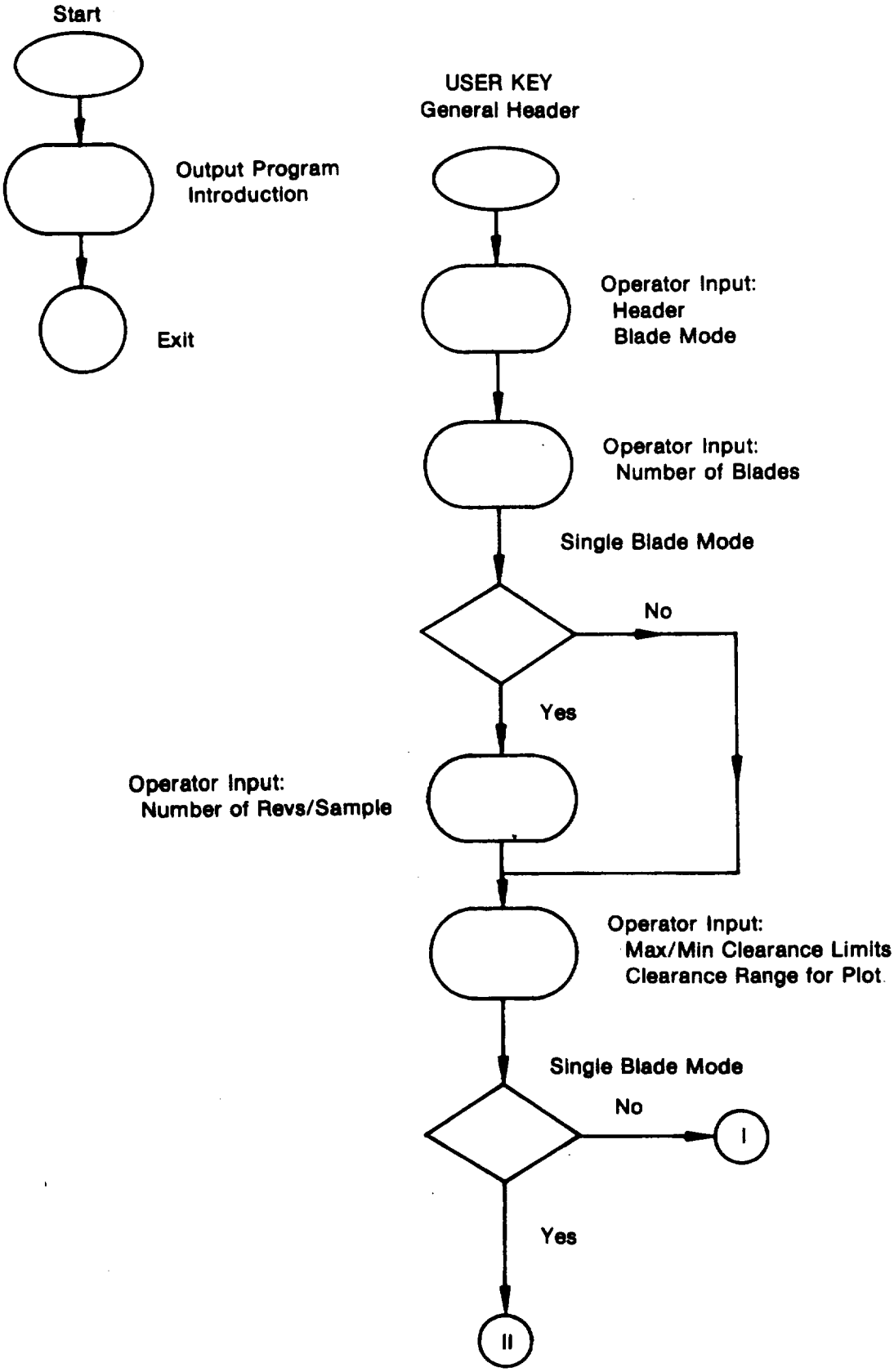
Start
Output Program Introduction
Exit
USER KEY
General Header
Operator Input:
Header
Blade Mode
Operator Input:
Number of Blades
Single Blade Mode
No
Yes
Operator Input:
Number of Revs/Sample
Operator Input:
Max/Min Clearance Limits
Clearance Range for Plot
Single Blade Mode
No
I
Yes
II

FD 143467

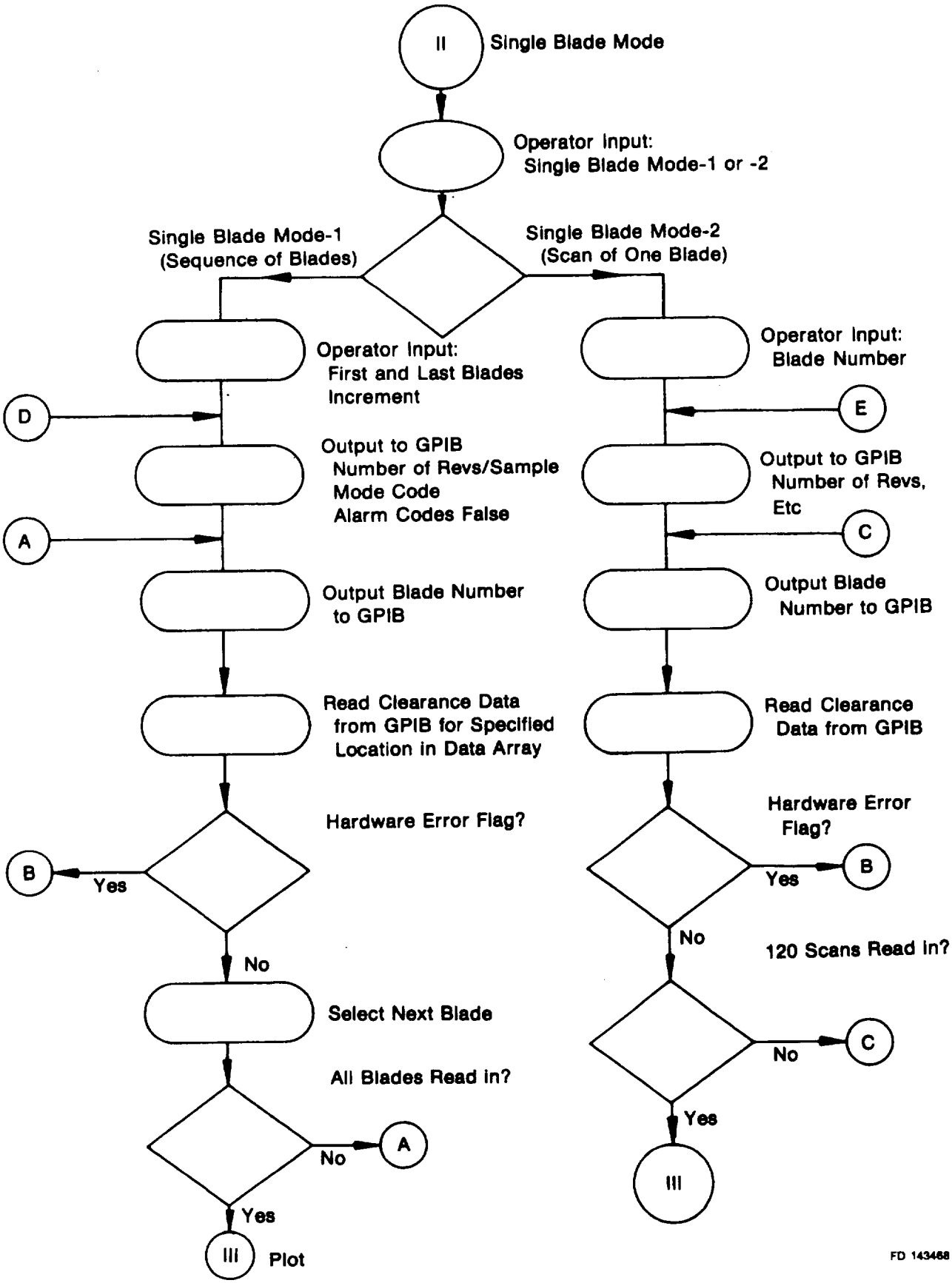
II
Single Blade Mode
Operator Input:
Single Blade Mode-1 or -2
Single Blade Mode-1
(Sequence of Blades)
Single Blade Mode-2
(Scan of One Blade)
Operator Input:
First and Last Blades
Increment
Operator Input:
Blade Number
D
E
Output to GPIB
Number of Revs/Sample
Mode Code
Alarm Codes False
Output to GPIB
Number of Revs,
Etc
A
C
Output Blade Number
to GPIB
Output Blade
Number to GPIB
Read Clearance Data
from GPIB for Specified
Location in Data Array
Read Clearance
Data from GPIB
Hardware Error Flag?
Hardware Error
Flag?
B
Yes
Yes
B
No
120 Scans Read In?
No
Select Next Blade
No
C
All Blades Read In?
Yes
No
A
III
Yes
III
Plot
FD 143468

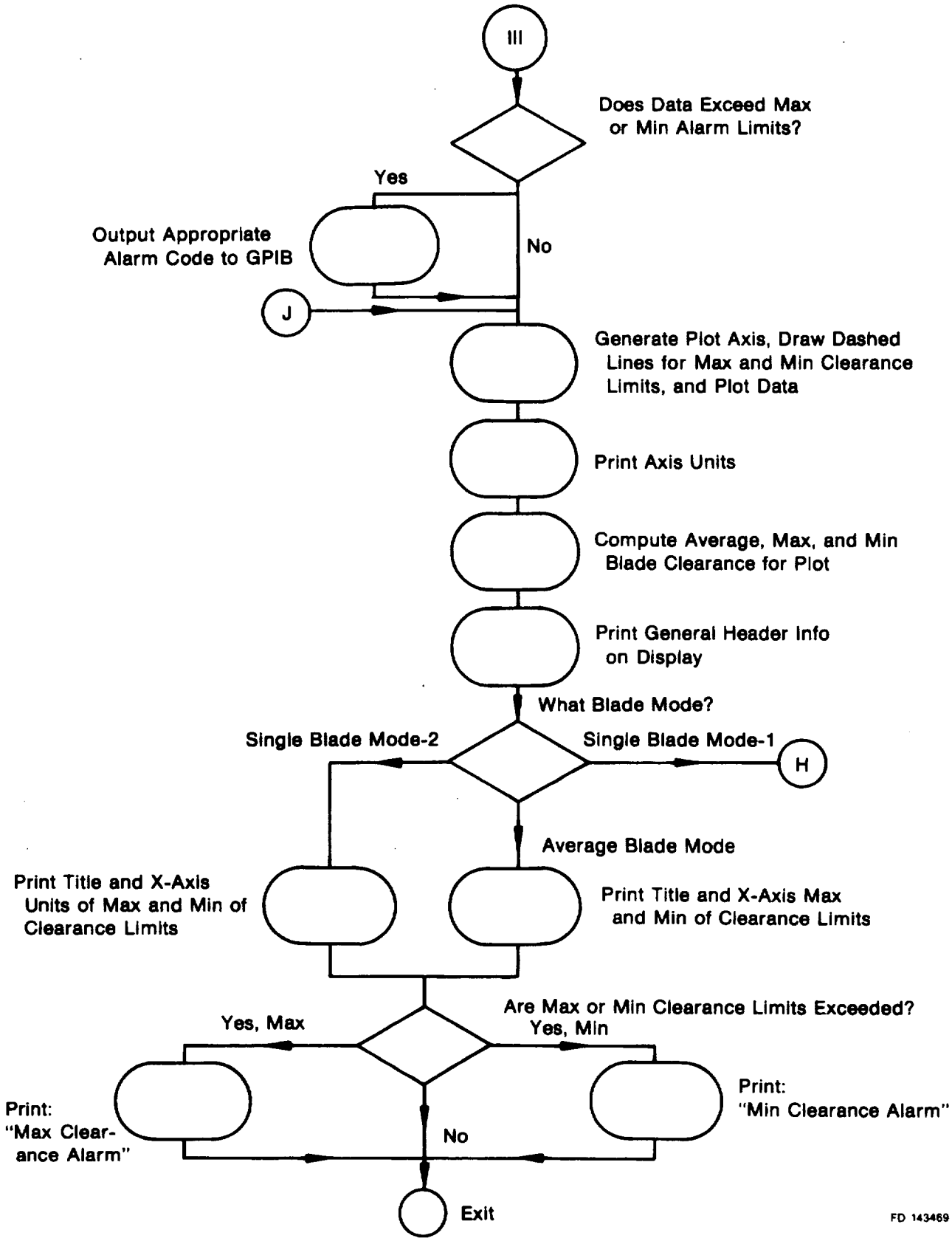
III
Does Data Exceed Max or Min Alarm Limits?
Yes
No
Output Appropriate Alarm Code to GPIB
J
Generate Plot Axis, Draw Dashed Lines for Max and Min Clearance Limits, and Plot Data
Print Axis Units
Compute Average, Max, and Min Blade Clearance for Plot
Print General Header Info on Display
What Blade Mode?
Single Blade Mode-2
Single Blade Mode-1
H
Average Blade Mode
Print Title and X-Axis Units of Max and Min of Clearance Limits
Print Title and X-Axis Max and Min of Clearance Limits
Are Max or Min Clearance Limits Exceeded?
Yes, Max
Yes, Min
Print: "Max Clear-ance Alarm"
Print: "Min Clearance Alarm"
No
Exit
FD 143469

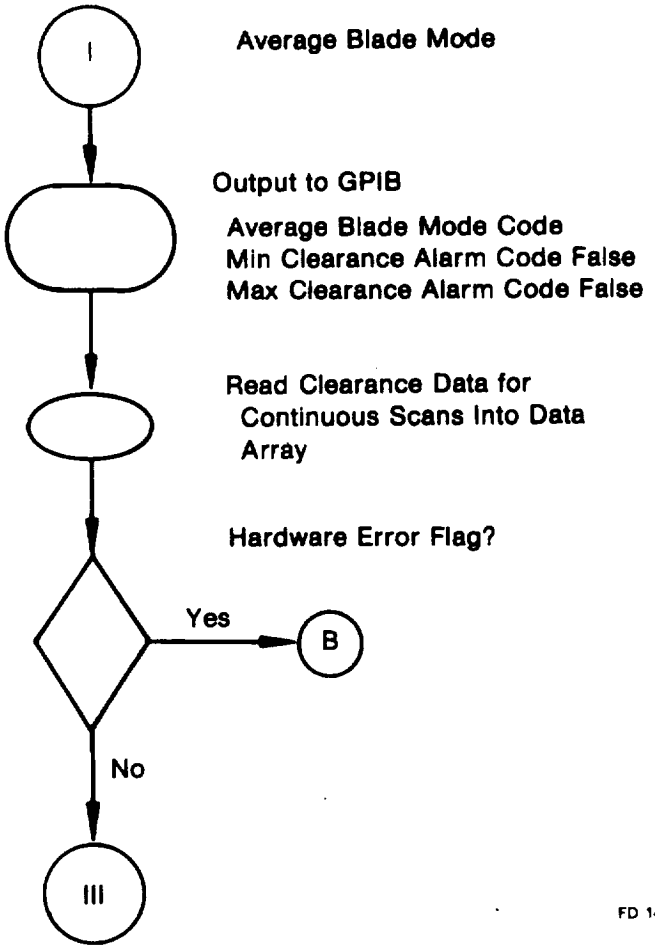
I
Average Blade Mode
Output to GPIB
Average Blade Mode Code
Min Clearance Alarm Code False
Max Clearance Alarm Code False
Read Clearance Data for
Continuous Scans Into Data
Array
Hardware Error Flag?
Yes
B
No
III
FD 143470

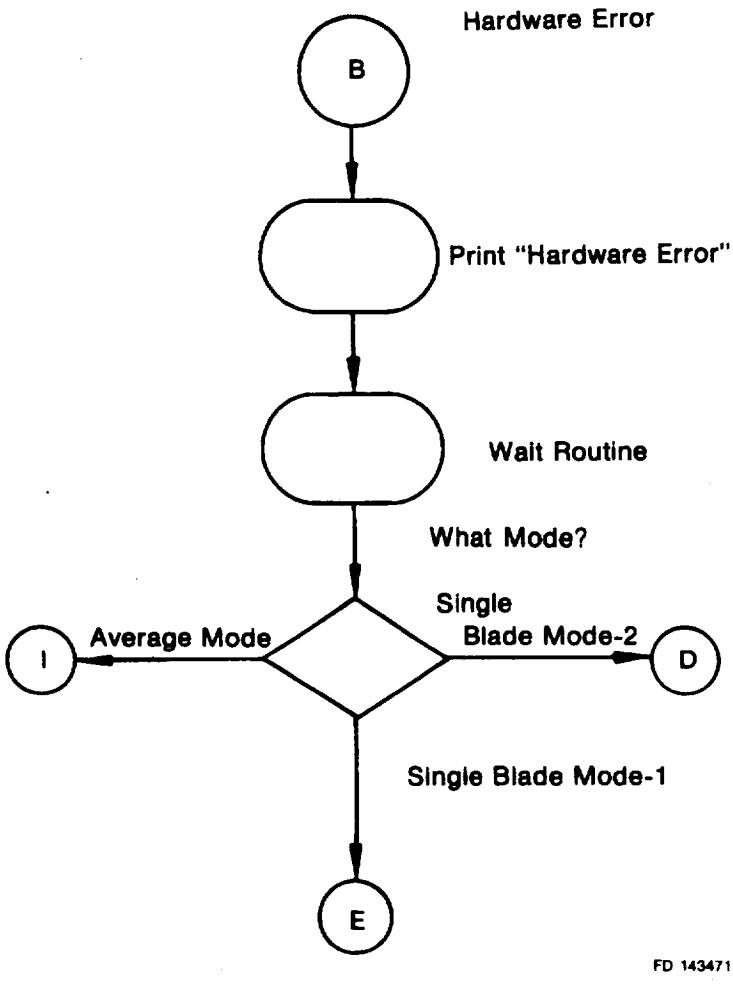
Hardware Error
B
Print "Hardware Error"
Wait Routine
What Mode?
Single
Blade Mode-2
Average Mode
I
D
Single Blade Mode-1
E
FD 143471

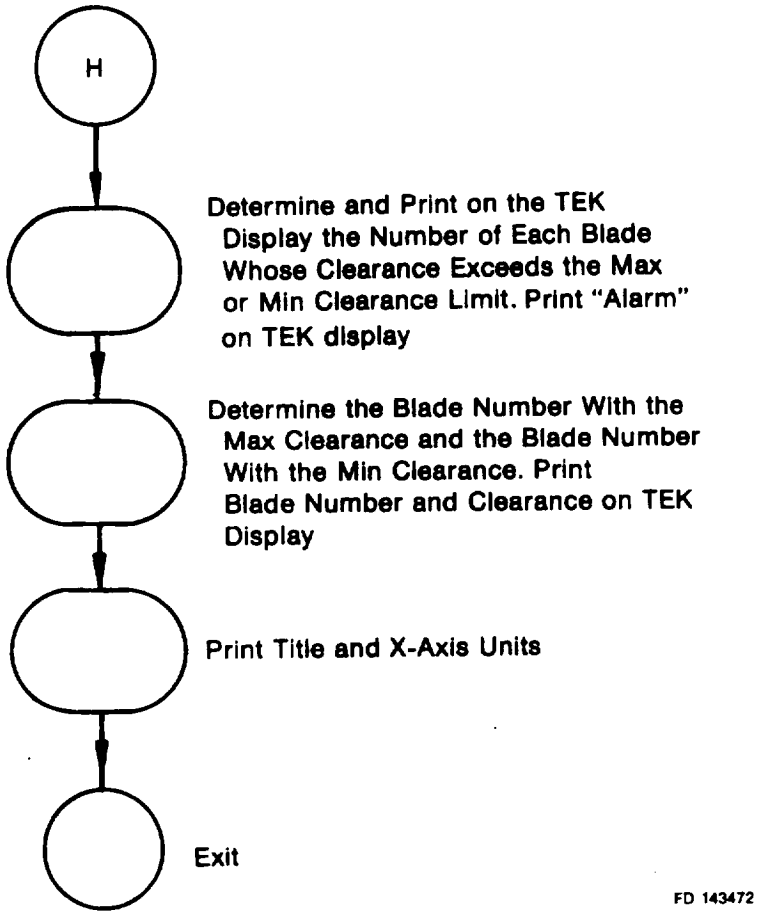
H
Determine and Print on the TEK Display the Number of Each Blade Whose Clearance Exceeds the Max or Min Clearance Limit. Print "Alarm" on TEK display
Determine the Blade Number With the Max Clearance and the Blade Number With the Min Clearance. Print Blade Number and Clearance on TEK Display
Print Title and X-Axis Units
Exit
FD 143472

USER KEY
Repeat Previous Measurement
for Single Blade Mode-1

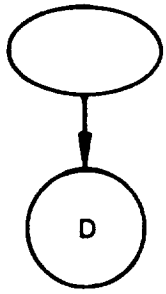


USER KEY
Repeat Previous Measurement
for Average Blade Mode

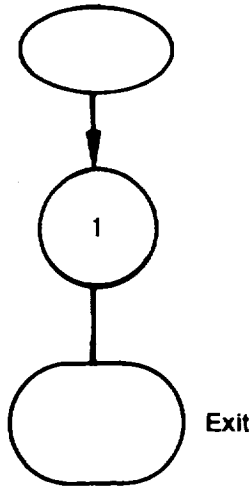


FD 143473

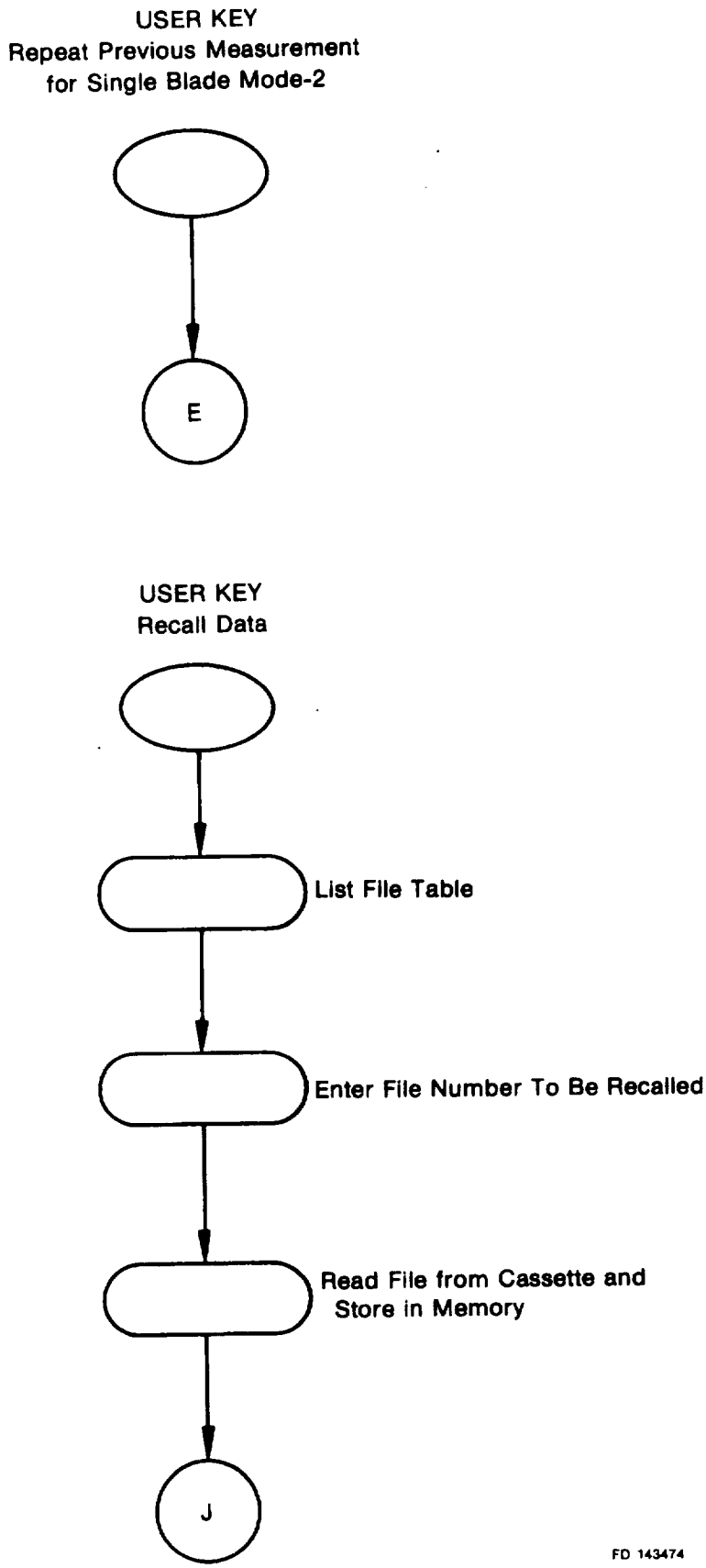
USER KEY
Repeat Previous Measurement
for Single Blade Mode-2
E
USER KEY
Recall Data
List File Table
Enter File Number To Be Recalled
Read File from Cassette and
Store in Memory
J
FD 143474

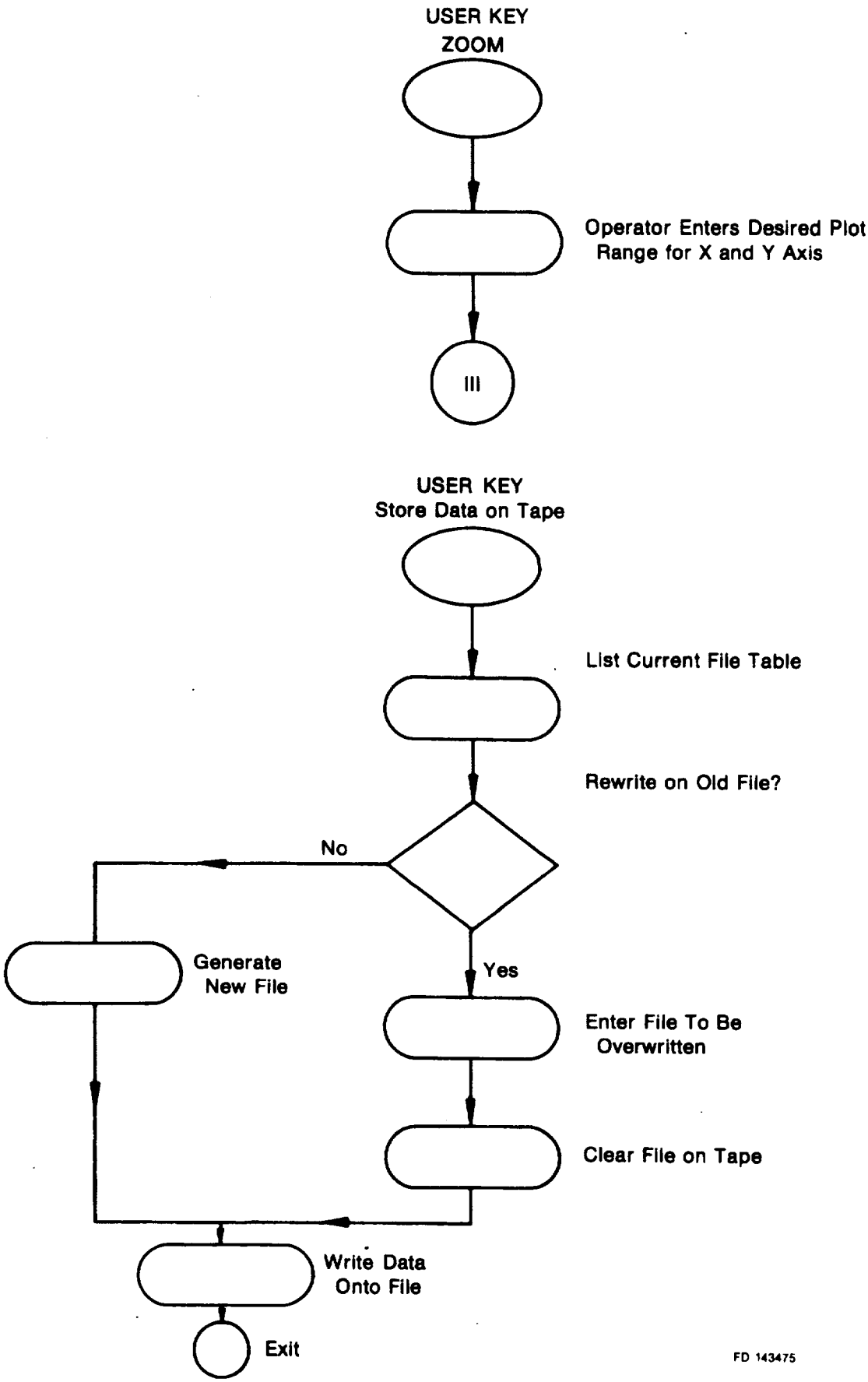
USER KEY
ZOOM
Operator Enters Desired Plot Range for X and Y Axis
III
USER KEY
Store Data on Tape
List Current File Table
Rewrite on Old File?
No
Yes
Generate New File
Enter File To Be Overwritten
Clear File on Tape
Write Data Onto File
Exit
FD 143475

USER KEY
Manual Clearance Alarm

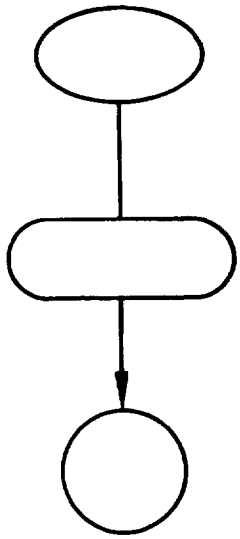

Output:
Number of Rev's/Samples
Single Blade Mode
Min Clearance Alarm True
Max Clearance Alarm True

Exit

FD 143476

USER KEY
Turn Image Intensifier Off

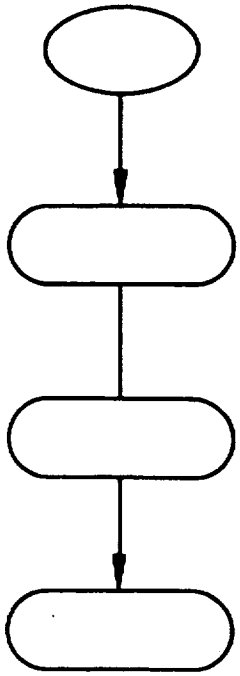

Output: Blade Number 255

Output:
Number of Rev's/Samples
Single Blade Mode
Min Clearance Alarm Code False
Max Clearance Alarm Code False

Exit

FD 143477

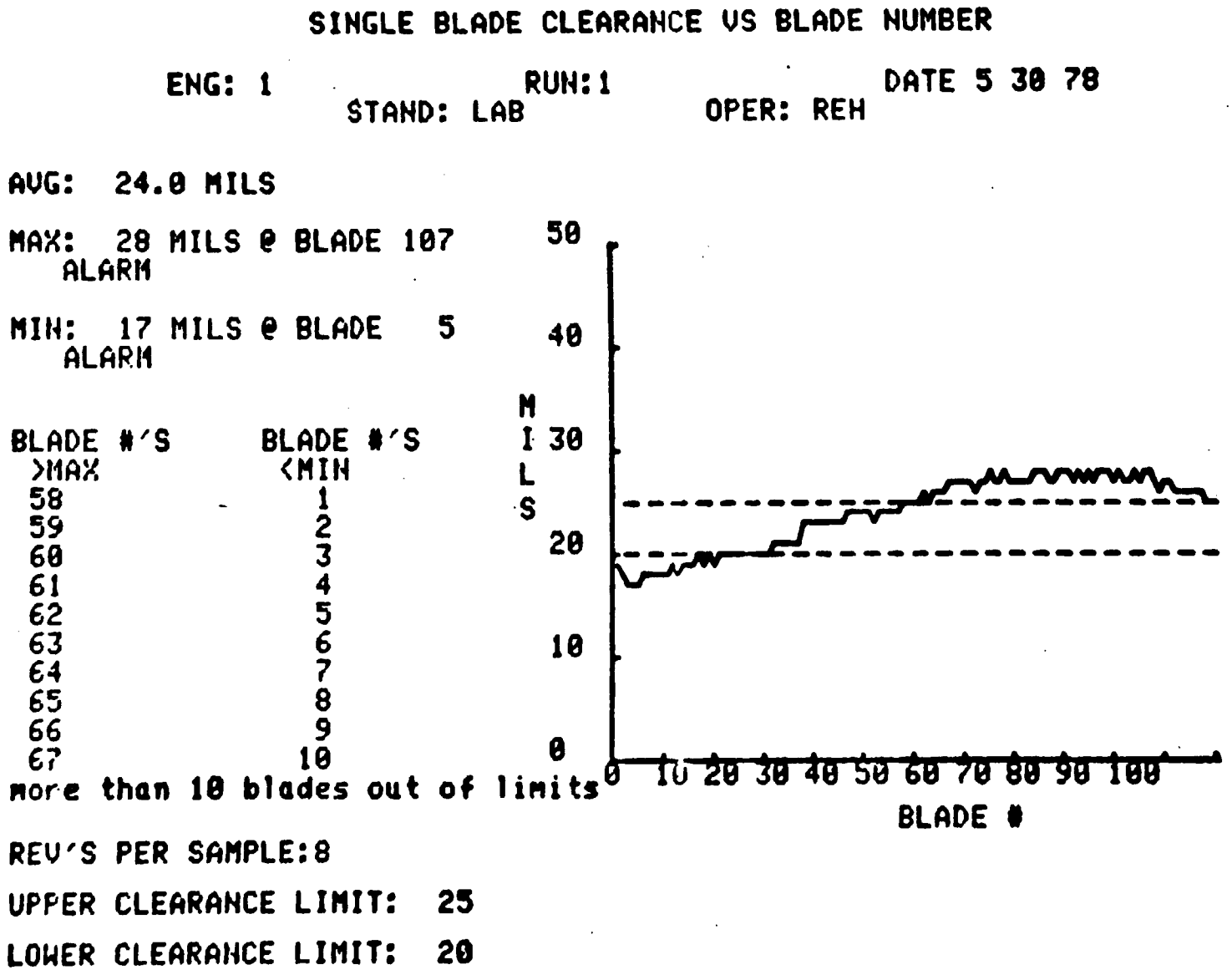


*Figure 10. Example Plot, Single Blade Mode-1*

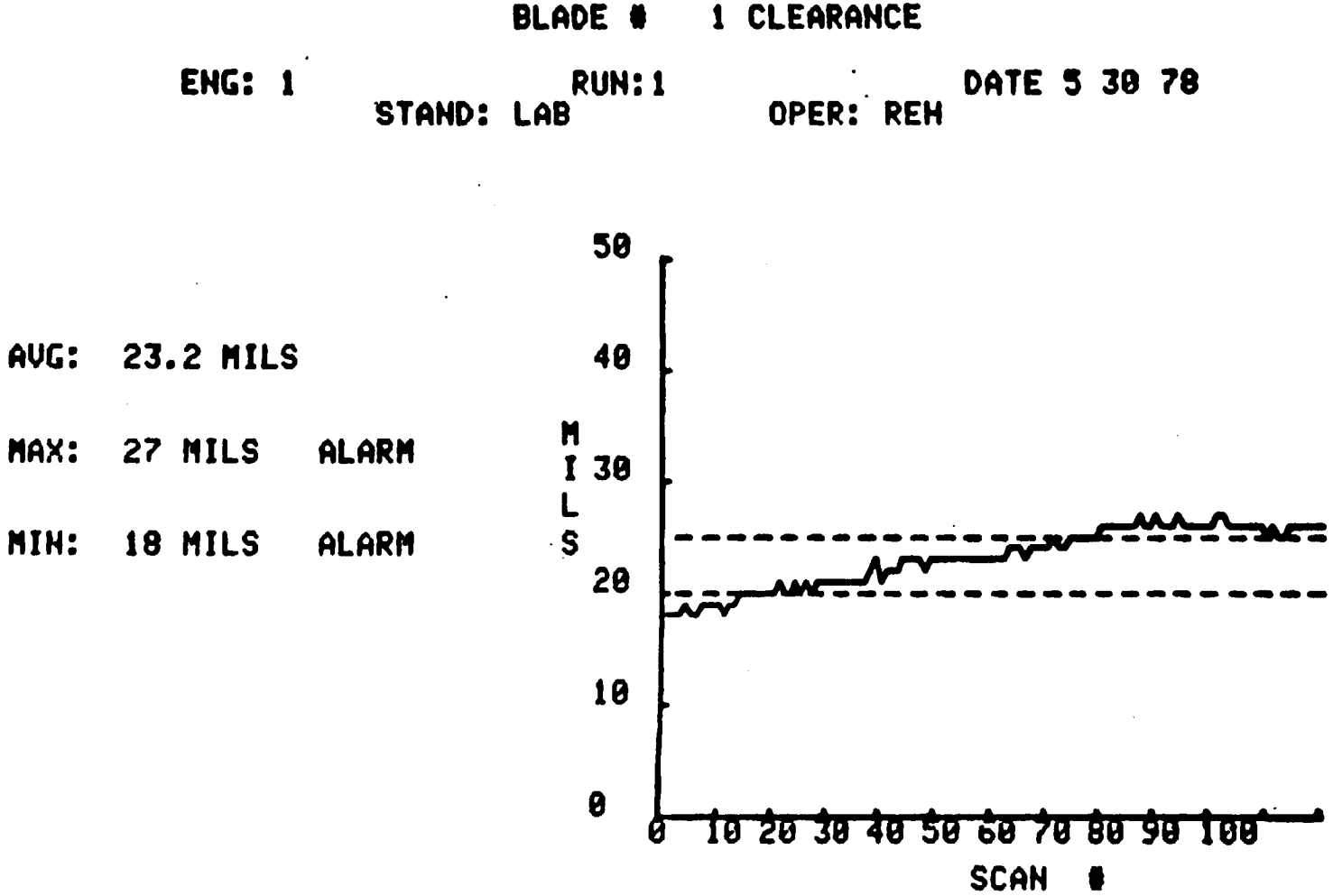


*Figure 11. Example Plot, Single Blade Mode-2*

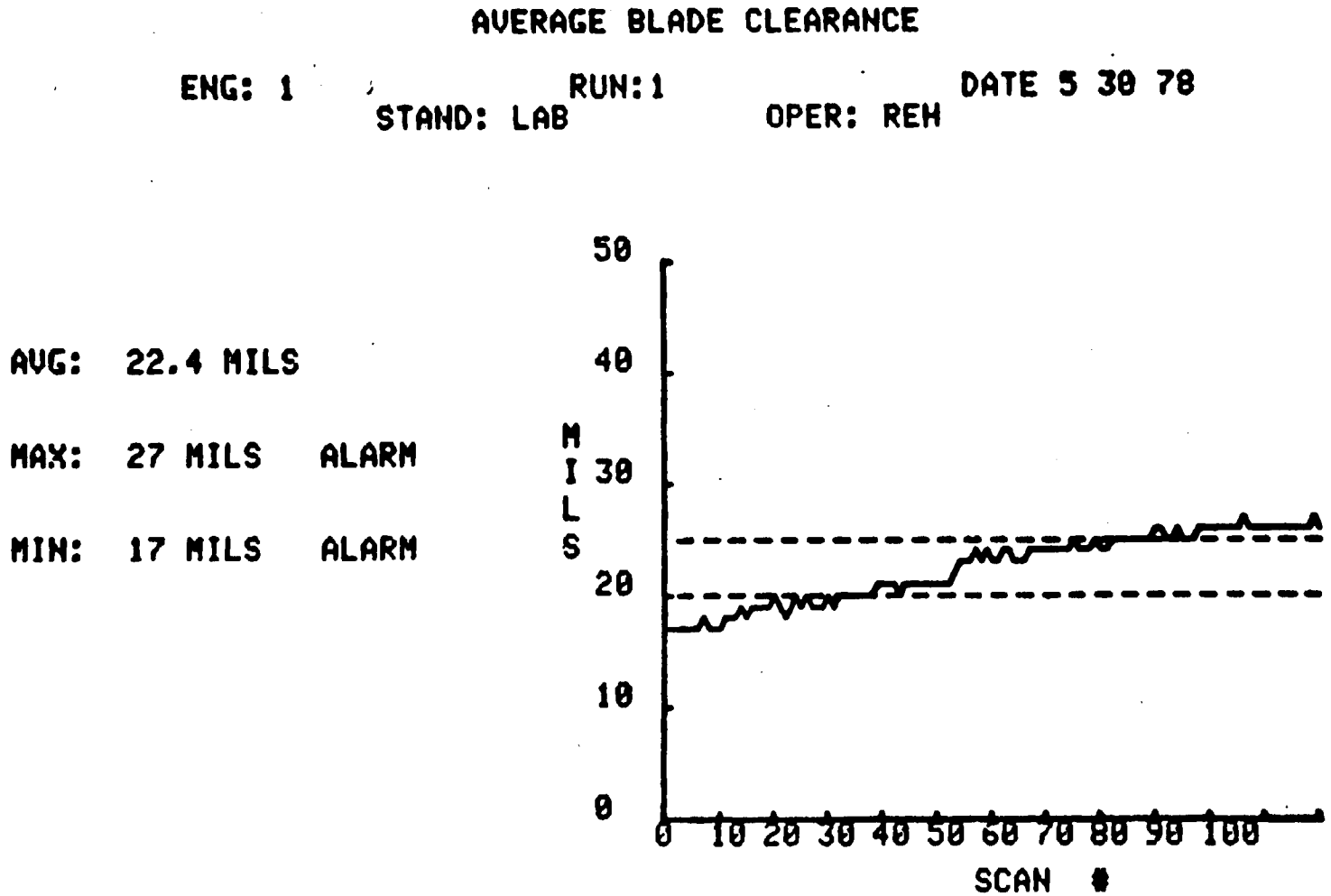


*Figure 12. Example Plot, Average Blade Mode*

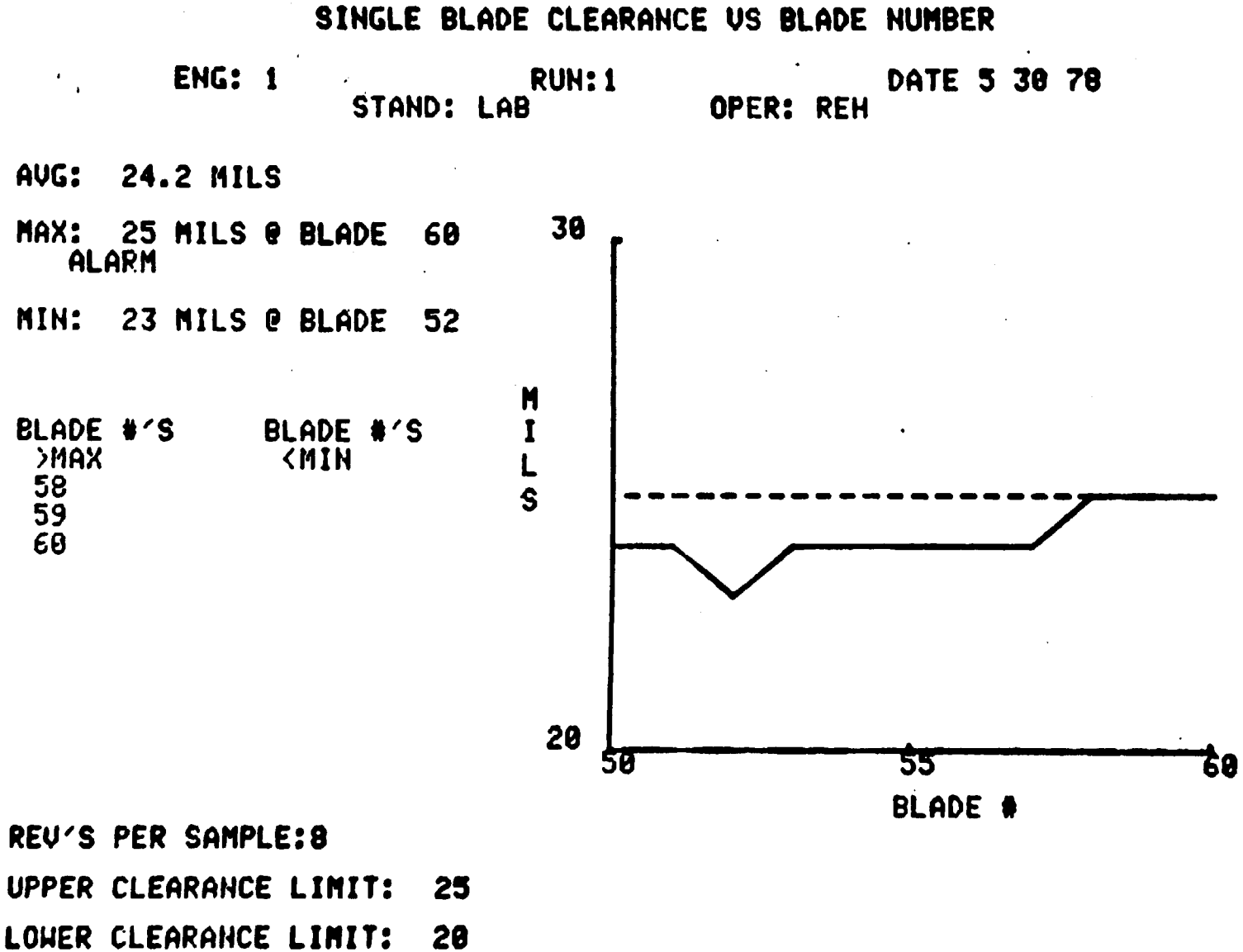


*Figure 13. Example Plot, ZOOM Presentation*

# VII. OPERATIONAL PERFORMANCE EVALUATION TESTS AND DISCUSSION OF RESULTS

## A. SUMMARY

A series of laboratory tests was conducted to determine the measurement system's operational performance characteristics. Results of these tests are presented. Evaluation of these tests results demonstrates that the measurement system performance characteristics meet overall program goals.

## B. SCOPE OF TEST

The operational performance evaluation test consisted of a static calibration to define measurement system accuracy and resolution, and a dynamic evaluation using a laboratory simulation of a rotating blade row to demonstrate blade tip clearance measurement capability. During these tests, all subsystems were checked to ensure proper operation, and documentation was generated where applicable.

## C. TEST RESULTS

### *Static Calibration*

A static calibration was performed with the system probe mounted in a micrometer calibration fixture. Calibration range was from 0.000 inches (0 mils) to 0.129 inches (129 mils) probe tip to micrometer face gap, and calibration increment was one diode site. Each calibration point was set by rotating the micrometer to obtain one diode increment change and then centering on the diode site by observing at least one hundred diode array scans on the Tektronix 4051 terminal display and verifying the desired diode site number presented at a 95% minimum occurrence rate. Repeatability data were also recorded for two cycles over the calibration range in increments of 25 diode sites upscale and downscale. The calibration data are presented in Table 4.

The 112 points (0-111 diode sites) of calibration data were fit to a third order polynomial equation using a least squares deviation method.

$$\text{Mils} = A_3 (DS)^3 + A_2 (DS)^2 + A_1 (DS) + A_0$$

where: Mils ~ Micrometer Gap (inches $\times 10^{-3}$)

(DS) ~ Diode Site

the curve coefficients of the equation were found to be

$A_3 = -0.00000281$
$A_2 = 0.00192680$
$A_1 = 0.97497589$
$A_0 = -0.11576363$

This equation defines the nonlinear characteristics of the system. The accuracy of the polynomial fit is the variability of the actual calibration data about the fit line. This value was calculated to be ±0.85 mils at the 95% confidence level. The maximum deviation about the fit line was 1.2 mils.

| Accuracy = ±0.85 mils (±0.022 mm) |
|---|

*Table 4. Static Calibration, Micrometer Gap (Mils) vs. Diode Site (DS)*

| DS | MILS | DS | MILS | DS | MILS | DS | MILS |
|---|---|---|---|---|---|---|---|
| 0 | 0 | 32 | 33.3 | 64 | 69.3 | 96 | 108.5 |
| 1 | 1.2 | 33 | 33.6 | 65 | 70.2 | 97 | 110.2 |
| 2 | 1.2 | 34 | 35.0 | 66 | 71.4 | 98 | 111.3 |
| 3 | 2.3 | 35 | 35.9 | 67 | 72.8 | 99 | 112.0 |
| 4 | 3.8 | 36 | 37.0 | 68 | 74.2 | 100 | 113.6 |
| 5 | 4.3 | 37 | 38.2 | 69 | 75.2 | 101 | 114.6 |
| 6 | 5.5 | 38 | 40.0 | 70 | 77.0 | 102 | 116.5 |
| 7 | 6.9 | 39 | 41.7 | 71 | 78.1 | 103 | 117.7 |
| 8 | 8 | 40 | 43.0 | 72 | 79.5 | 104 | 118.8 |
| 9 | 8.8 | 41 | 43.3 | 73 | 80.7 | 105 | 120.4 |
| 10 | 9.8 | 42 | 44.2 | 74 | 81.8 | 106 | 121.3 |
| 11 | 11.2 | 43 | 45.3 | 75 | 83.0 | 107 | 122.5 |
| 12 | 12.4 | 44 | 45.6 | 76 | 84.8 | 108 | 123.6 |
| 13 | 13.2 | 45 | 47.4 | 77 | 85.8 | 109 | 125.4 |
| 14 | 14.7 | 46 | 48.6 | 78 | 86.8 | 110 | 126.5 |
| 15 | 14.8 | 47 | 50.2 | 79 | 87.0 | 111 | 129.0 |
| 16 | 16.0 | 48 | 50.6 | 80 | 88.5 | | |
| 17 | 16.9 | 49 | 52.2 | 81 | 89.7 | 100 | 112.8 |
| 18 | 18.0 | 50 | 53.5 | 82 | 91.5 | 75 | 82.0 |
| 19 | 19.3 | 51 | 54.6 | 83 | 92.2 | 50 | 53.1 |
| 20 | 20.6 | 52 | 55.6 | 84 | 93.2 | 25 | 24.9 |
| 21 | 21.6 | 53 | 56.3 | 85 | 94.7 | 1 | 0 |
| 22 | 22.4 | 54 | 57.0 | 86 | 96.0 | 25 | 24.9 |
| 23 | 23.4 | 55 | 58.2 | 87 | 97.7 | 50 | 53.0 |
| 24 | 24.2 | 56 | 59.5 | 88 | 98.7 | 75 | 82.1 |
| 25 | 25.0 | 57 | 61.0 | 89 | 100.0 | 100 | 112.0 |
| 26 | 26.1 | 58 | 61.7 | 90 | 101.1 | 111 | 127.7 |
| 27 | 27.0 | 59 | 62.7 | 91 | 103.2 | 100 | 112.8 |
| 28 | 28.2 | 60 | 64.4 | 92 | 104.2 | 75 | 81.6 |
| 29 | 29.6 | 61 | 64.9 | 93 | 105.3 | 50 | 52.7 |
| 30 | 30.6 | 62 | 67.7 | 94 | 106.4 | 25 | 24.3 |
| 31 | 31.8 | 63 | 68.6 | 95 | 107.8 | 1 | 0.0 |

An upper limit on measurement system resolution was also obtained from the calibration data. Since the system has a nonlinear characteristic, the change in displacement corresponding to one diode site is not uniform. The maximum observed incremental change between diode sites was 2.8 mils, but 97% of the incremental changes were 1.8 mils or less. The 1.8 mil value was used in establishing the measurement system resolution which was considered to be equivalent to ±½ the incremental change observed between diode sites (i.e., a deviation in displacement equivalent to greater than ½ diode site would cause the adjacent site to indicate) at a minimum 95% confidence level.

Resolution = ±0.90 mils (±0.023 mm)

The repeatability calibration data were used to determine system repeatability. Displacements calculated from the diode site using the 3rd order polynomial were compared to measured displacements. The maximum deviation observed was −1.84 mils. The repeatability at the 95% confidence level was found to be ±1.73 mils.

Repeatability = ±1.73 mils (±0.044 mm)

***Dynamic Evaluation*** (Laboratory Simulation Test)

Demonstration of measurement system capability at design conditions was accomplished by using a laboratory simulation of a rotating blade row.

- Rotor Speed — 60,000 RPM

- Blade Tip Speed — 609.6 m/sec (2,000 ft/sec)
- Blade Tip Thickness — 0.79 mm (0.031 in.)
- Blade Tip Reflectivity — Test Blade No. 5 (least reflective of six contract test blades).
- Number of Blades — 120

The laboratory simulation setup is presented in Figure 14 and included the basic measurement system, plus

- Acousto-Optic Modulator inserted between Laser Attenuator Filter and Objective Lens Translator
- Signal Generator
- Acousto-Optic Modulator Driver
- 120:1 Frequency Divider
- Test Blade No. 5 mounted on X-Y Translator adjusted to simulate a tip clearance of 50 mils.

The acousto-optic modulator, controlled by the signal generator and acousto-optic modulator driver, was used to "chop" the laser beam, thus producing the simulated blade passing pulse train desired. The 120:1 frequency divider, fed by the 120 blade rotor simulation signal from the signal generator, provided the simulated one per revolution index pulse to the Electronic Subsystem. The signal generator was adjusted to provide the following input to the acousto-optic modulator driver:

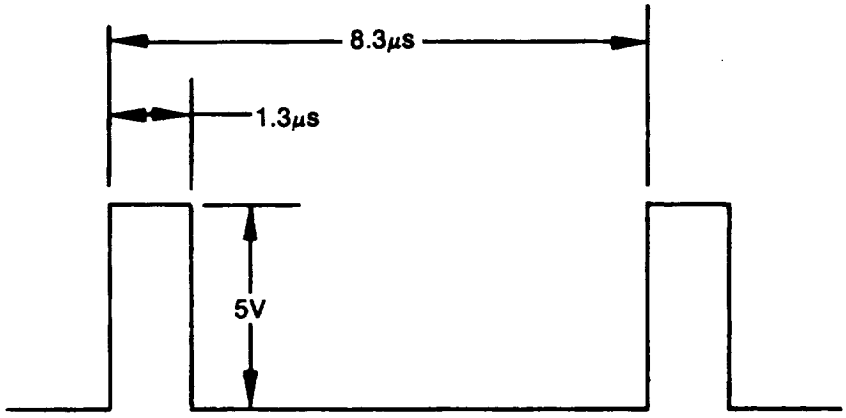


The light power output of the modulator was measured (using a Spectra-Physics Power Meter) to be as follows:

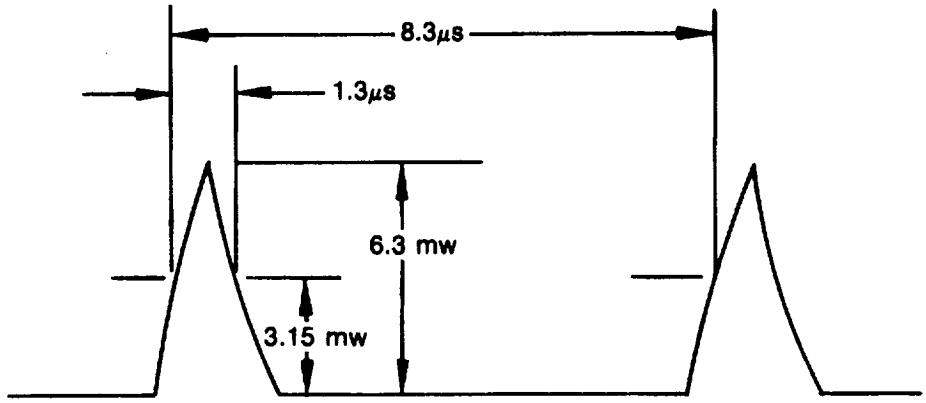


The resulting energy function provides the design condition duty cycle and repetition rate, but the energy available to the optical system using this simulation setup ($\approx 8 \times 10^{-9}$ watt-sec) was only 62% of the energy available to the optical system under "real-life" design conditions ($13 \times 10^{-9}$ watt-sec). This abnormal attenuation has a direct effect on the laboratory performance evaluation tests following, in that any situation requiring determination of a minimum "Revs per Sample" will produce a result which is greater than the realistic value by a factor of approximately 1.6. Any "Revs per Sample" value referred to in this section should therefore be reduced to 62% of that stated value to obtain a more realistic "Revs per Sample" value.

Figures 15, 16, and 17 demonstrate measurement system performance in the three basic modes of operation: SINGLE BLADE Mode-1 (sequence of blades), SINGLE BLADE Mode-2 (scan of one blade), and AVERAGE Mode. These data were obtained using the previously described laboratory dynamic simulation setup, and they essentially represent the overall measurement system dynamic performance capability. The minimum "Revs per Sample" required to obtain a usable LPA video output signal (0.4 V at peak diode with Image Intensifier tube microchannel plate gain at maximum) was 100.

Figures 18, 19, 20, and 21 demonstrate measurement system performance primarily in terms of maximum/minimum clearance limit alarm operation, "out of clearance limit" blade number identification, and "zoom" capability in the three basic modes of operation. These data were obtained using the laboratory dynamic simulation setup previously described with the exception of replacing the target test blade with a micrometer calibration fixture. This change permitted a more manageable variable gap (simulated clearance) technique.

Table 5 provides a map of measurement system performance with respect to the contract's six test blades. Using the laboratory dynamic simulation setup previously described and sequentially placing each of the test blades on the X-Y translator, the measurement system probe viewed three representatively reflective target locations on each of the blades. These target locations were arbitrarily assigned to be at 25%, 50%, and 75% chord length. The minimum "Revs per Sample" required to obtain a usable Reticon video output signal (0.4 V at peak diode with Image Intensifier tube microchannel plate gain at maximum) was determined for each target location. Clearance gap was maintained at approximately 50 mils for all tests, and the blade passing pulse train was verified to have adequate signal strength to achieve proper blade passing pulse electronic circuit operation for all tests.

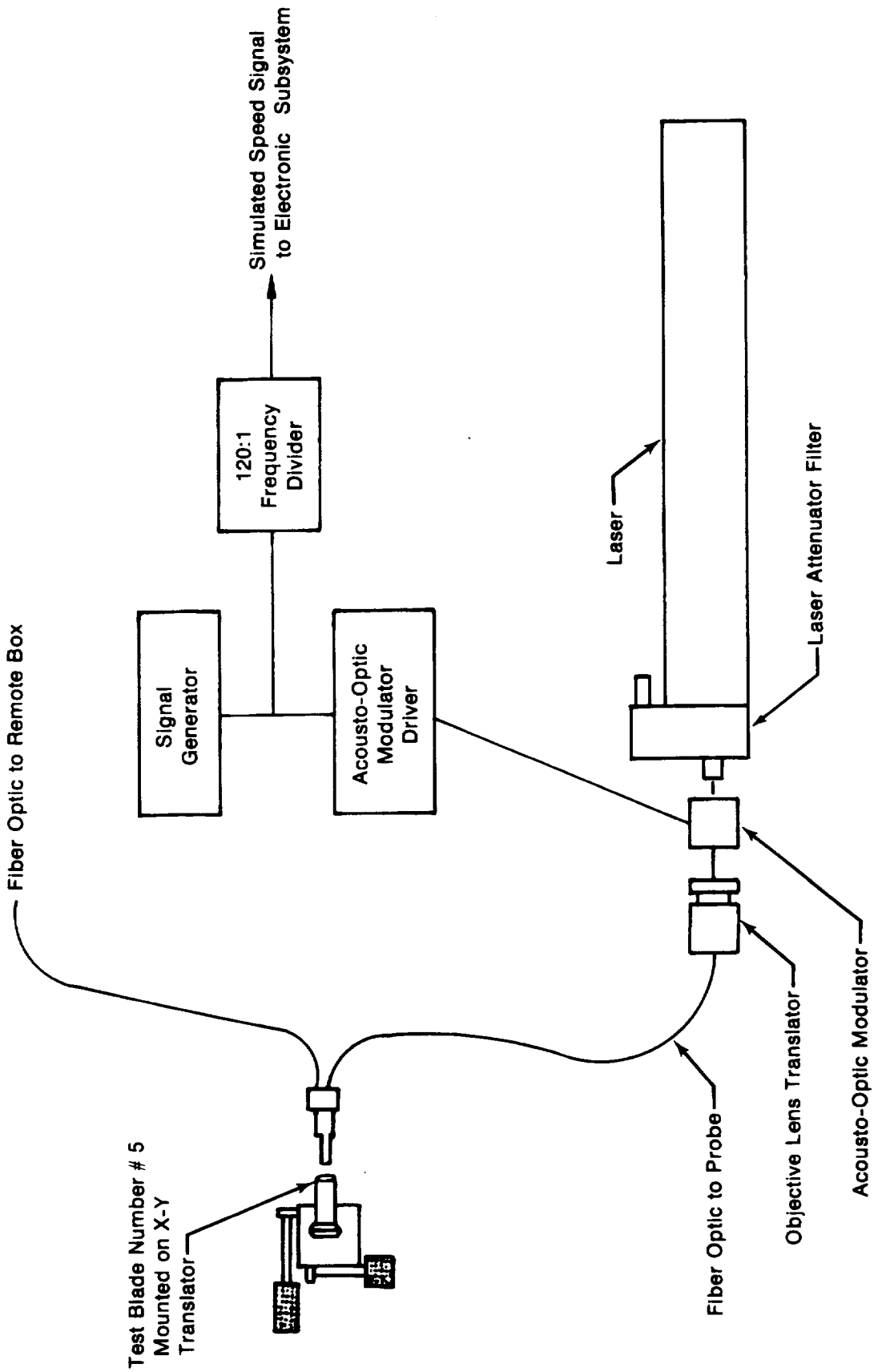


*Figure 14. Dynamic Evaluation Test Setup*

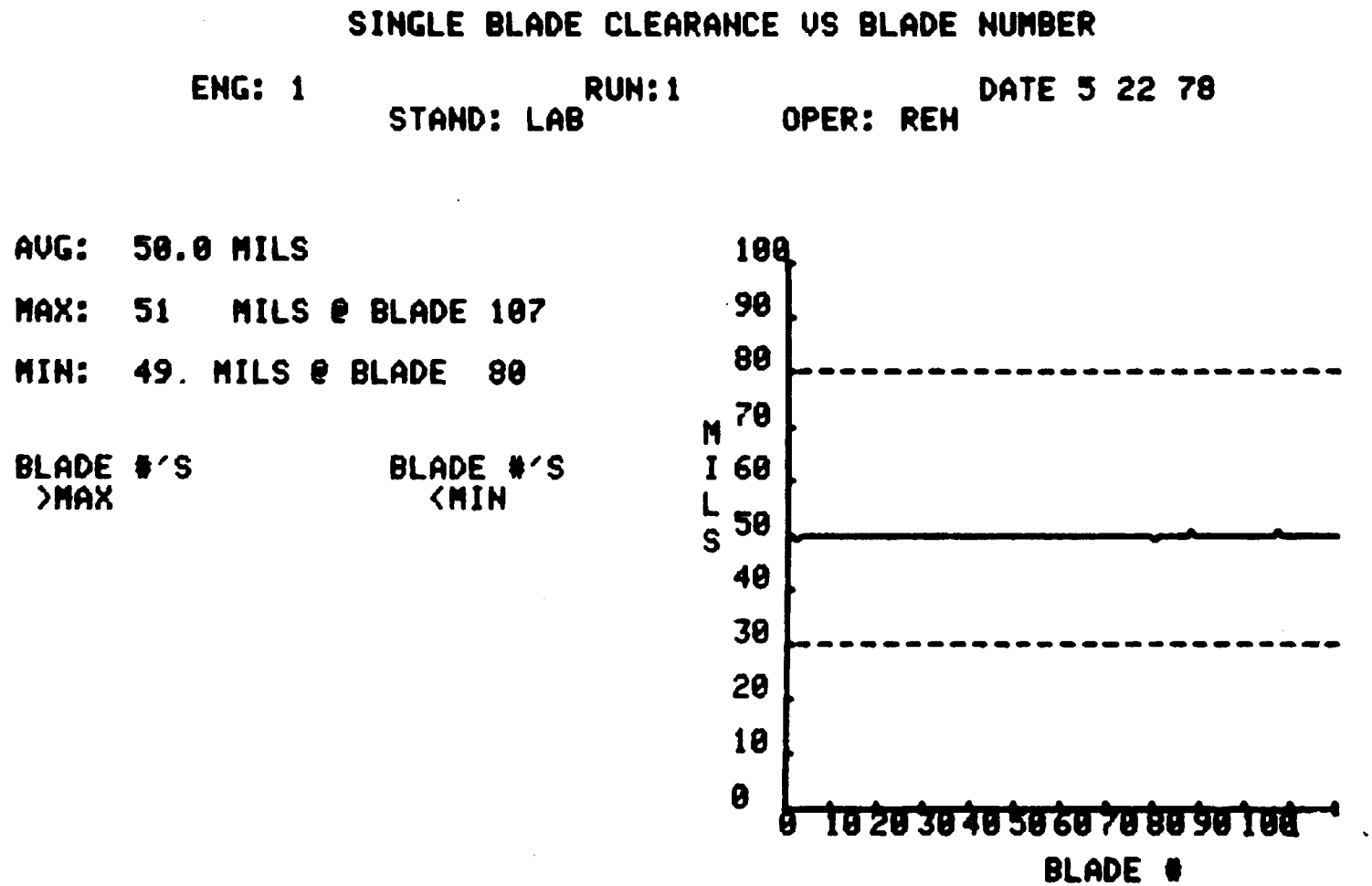


*Figure 15. Single Blade Mode-1 Dynamic Simulation*

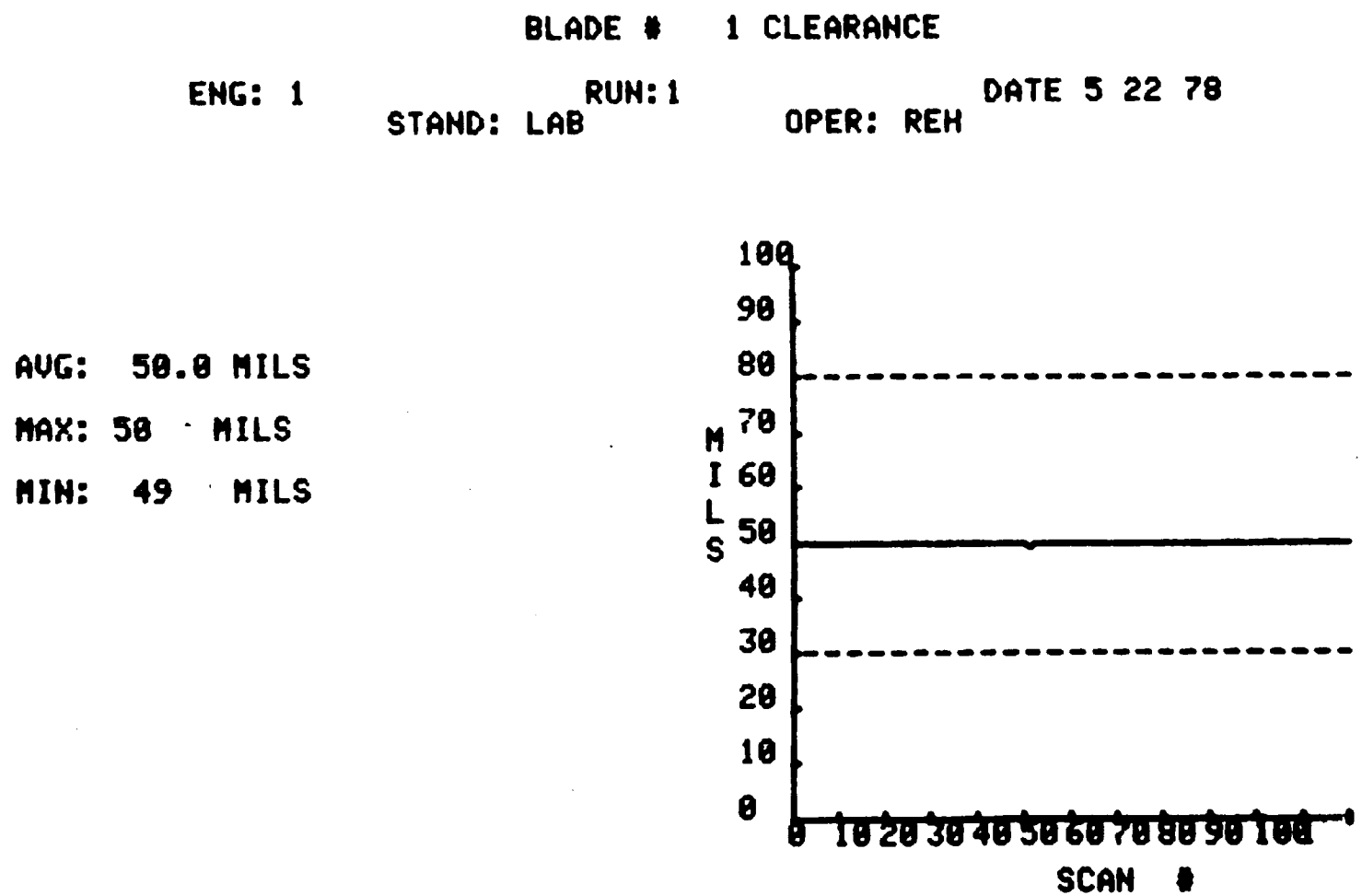


*Figure 16. Single Blade Mode-2 Dynamic Simulation*

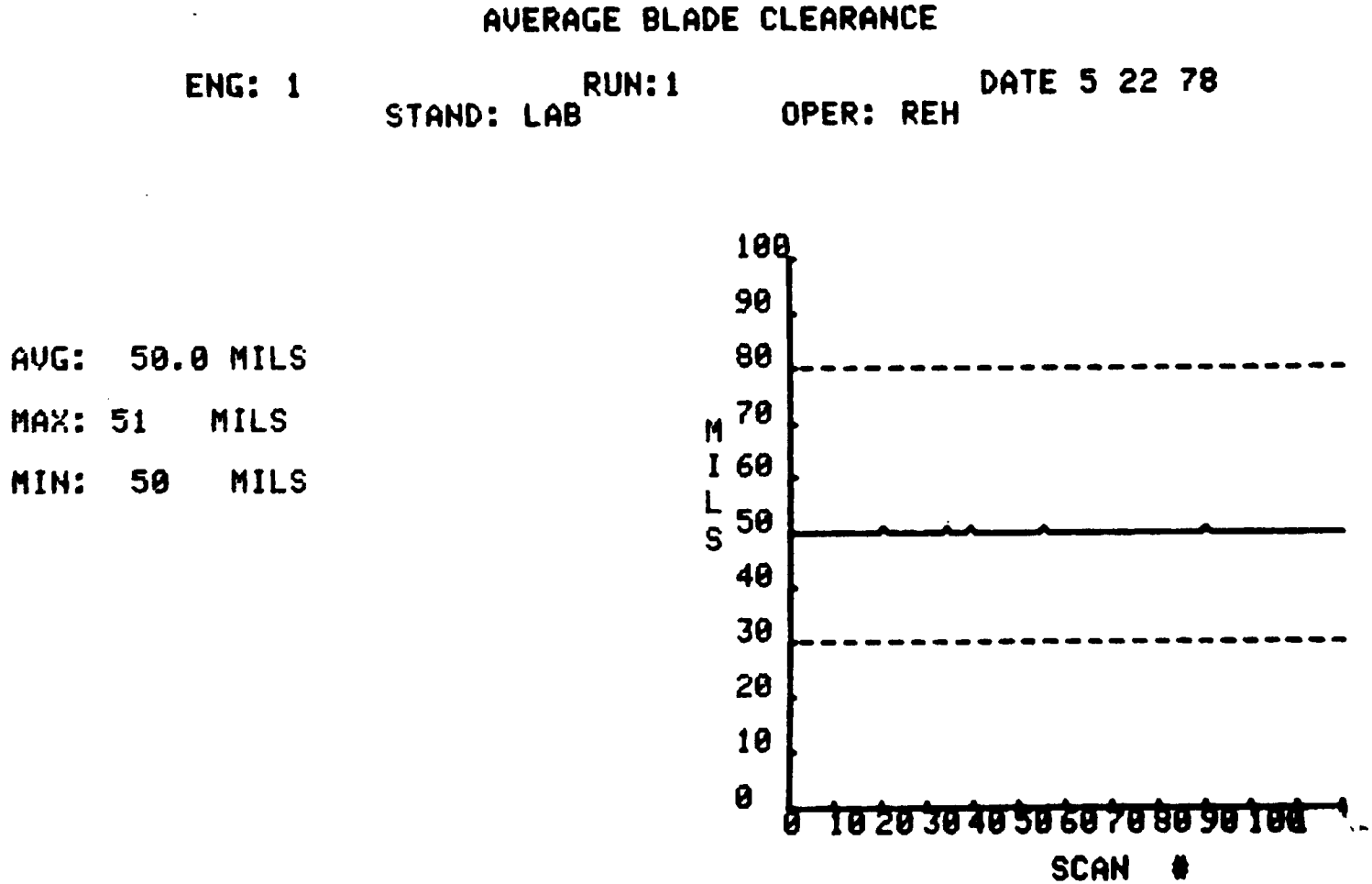


*Figure 17. Average Blade Mode Dynamic Simulation*

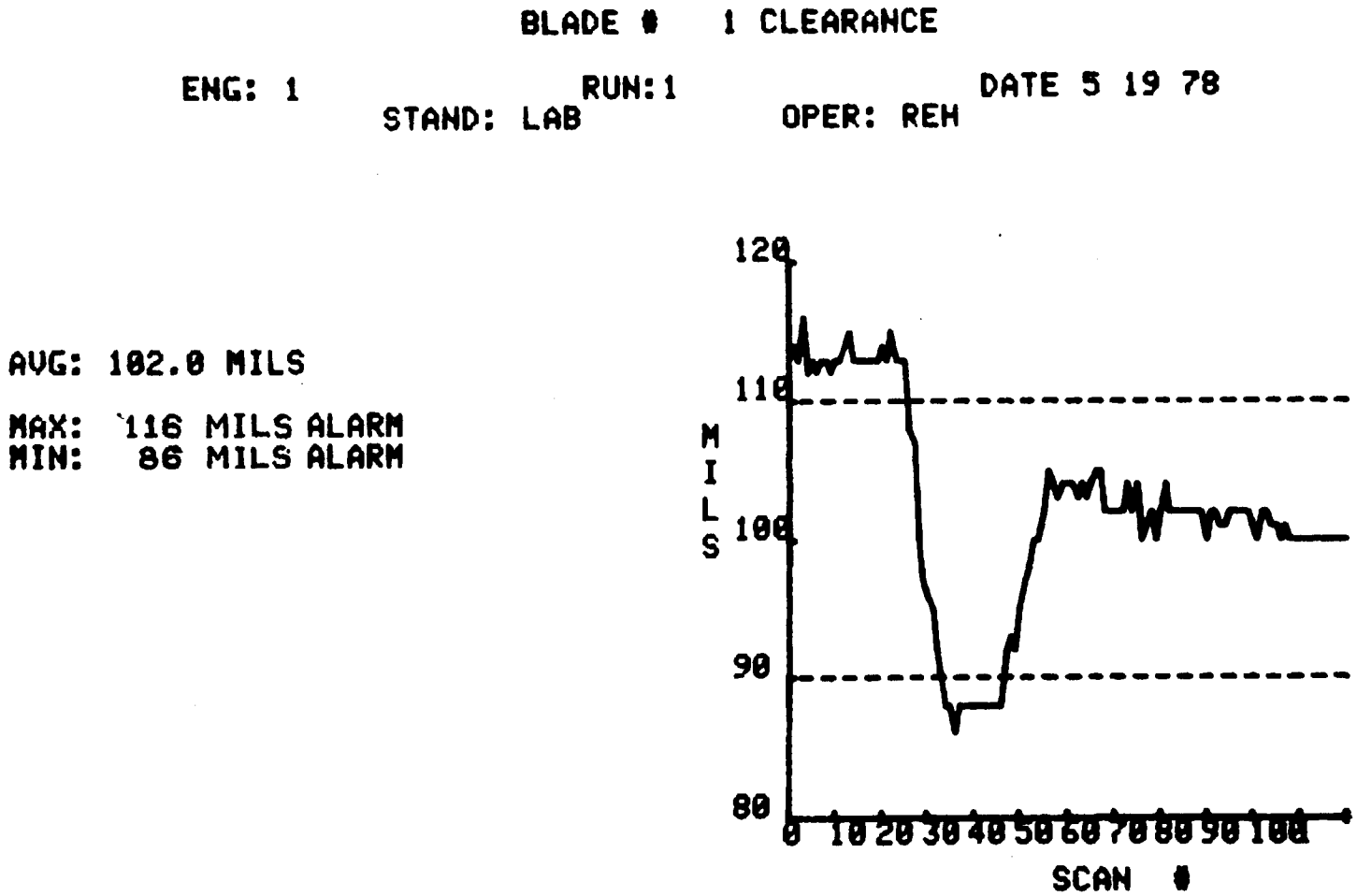


*Figure 18. Clearance Alarm Presentation*

SINGLE BLADE CLEARANCE VS BLADE NUMBER

ENG: 1 RUN:1 DATE 5 19 78

STAND: LAB OPER: REH

AVG: 99.5 MILS

MAX: 115 MILS @ BLADE 21
ALARM

MIN: 89 MILS @ BLADE 40
ALARM

| BLADE #'S >MAX | BLADE #'S <MIN |
|---|---|
| 18 | 35 |
| 19 | 36 |
| 20 | 37 |
| 21 | 38 |
| 22 | 39 |
| 23 | 40 |
| 24 | 41 |
| 25 | 43 |
| | 44 |


REV'S PER SAMPLE:9

UPPER CLEARANCE LIMIT: 110

LOWER CLEARANCE LIMIT: 90

*Figure 19. Blade "Out of Clearance Limit" Identification*

SINGLE BLADE CLEARANCE VS BLADE NUMBER

ENG: 1 RUN:1 DATE 5 19 78

STAND: LAB OPER: REH

AVG: 108.1 MILS

MAX: 115 MILS @ BLADE 21

ALARM

MIN: 97 MILS @ BLADE 30

| BLADE #'S >MAX | BLADE #'S <MIN |
|---|---|
| 18 | |
| 19 | |
| 20 | |
| 21 | |
| 22 | |
| 23 | |
| 24 | |
| 25 | |

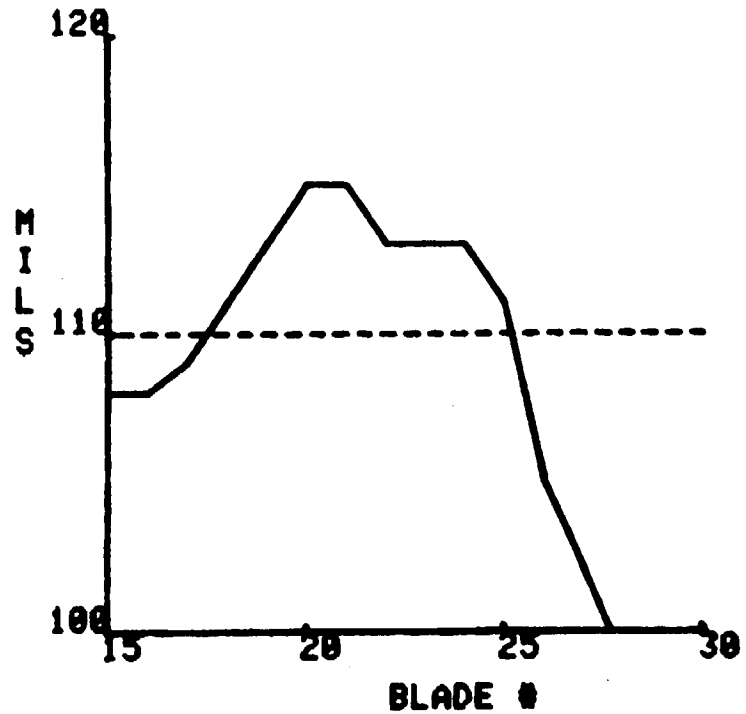


REV'S PER SAMPLE:9

UPPER CLEARANCE LIMIT: 110

LOWER CLEARANCE LIMIT: 90

*Figure 20. ZOOM Presentation*

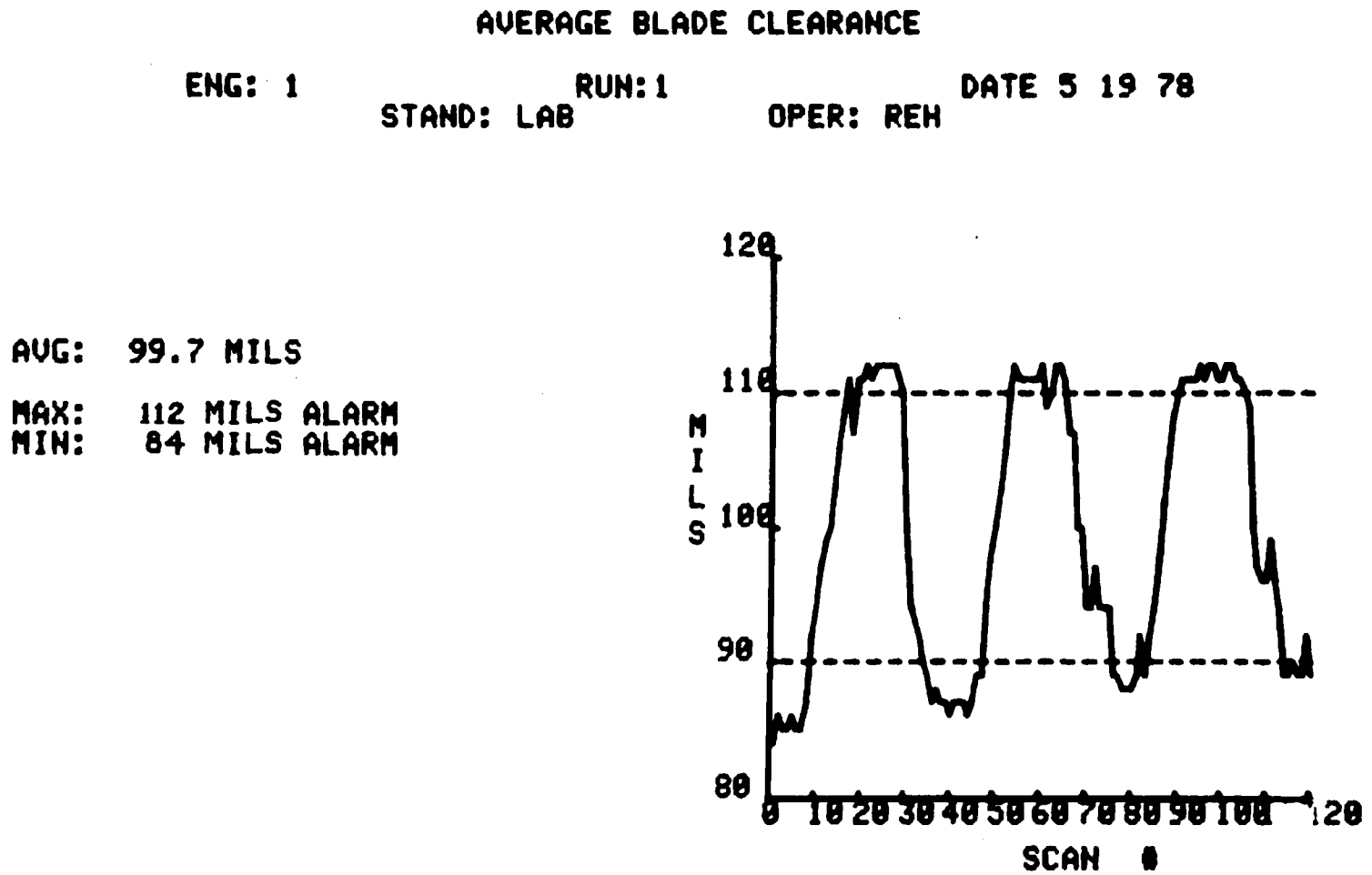


*Figure 21. Average Blade Mode Clearance Alarm Presentation*

*Table 5. Test Blade Sample Number Requirements*

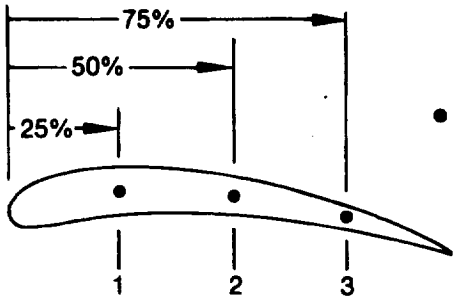


● Target Spot Location

| Test Blade | Revs Per Sample | | |
|---|---|---|---|
| | 1 | 2 | 3 |
| Blade No. 1 | 28 | 23 | 8 |
| Blade No. 2 | 15 | 40 | 70 |
| Blade No. 3 | 200 | 60 | 100 |
| Blade No. 4 | 75 | 22 | 16 |
| Blade No. 5 | 100 | * | * |
| Blade No. 6 | 100 | 150 | 50 |

* These Locations Required a Revs Per Sample Value Greater than 200. The Reticon LPA Dark Current Becomes Excessive With Integration Time >200 ms, or, in This Test Case, >200 Revs Per Sample. The Resulting LPA Video Signal Is Not Usable If Excessive Dark Current Buildup Is Present

## D. DISCUSSION OF TEST RESULTS

Results of the operational performance tests demonstrate that the measurement system performance capabilities meet the system design goals. The primary objective of the contract, to develop and demonstrate the technology required to measure the operating tip clearance of a selectable single blade, was successfully met. Some unanticipated system characteristics were encountered during the performance evaluation tests, notably a nonlinearity in the system calibration data and an apparent deterioration in Image Intensifier tube sensitivity and/or gain. Investigation and evaluation of these system characteristics was beyond the scope of this program; therefore, at this point they are simply noted and briefly discussed as possible items to be addressed in the future.

The accuracy analysis was based on a third order curve fit. Corrections can be made on a first, second, third, or whatever order is desired when it is decided what type of correction is to be applied. This correction will yield readings that are truly in mils instead of diode site labeled as mils.

The nonlinearity encountered in the system calibration data is associated with the system optics at some point prior to the Image Intensifier tube faceplate. Areas that should be investigated as the source of nonlinearity include the probe objective lens/light baffle interface and the relay lens assembly. The probe objective lens/light baffle interface arrangement does not allow the laser spot image to be projected through the principal axis of the lens. It is felt that the resulting optical magnification of the laser spot travel as seen at the input to the output fiber optic bundle, may be nonlinear with respect to a linear change in calibration gap. In addition, a misalignment could exist between the two lenses of the relay lens assembly or between the relay lens assembly and the Image Intensifier lens. It is felt that a very slight misalignment in this lens stack-up could result in nonlinear magnification of the laser spot travel.

A deterioration in Image Intensifier tube sensitivity/gain characteristics was observed during the course of the system performance evaluation tests which were conducted after the tube had been operated for approximately 50 hours. The loss in sensitivity/gain is suspected to have occurred over only a small area ($\approx$ 0.75 mm $\times$ 6 mm) of the available tube cross section; that is, the optical channel from the tube faceplate to the LPA. The Image Intensifier tube was designed to allow this problem to be corrected. The tube should eventually be returned to ITT to have the LPA relocated to another position on the tube output fiber optic coupler.

## VIII. ENVIRONMENTAL PERFORMANCE EVALUATION TESTS AND DISCUSSION OF RESULTS

### A. SUMMARY

The environmental evaluation tests subjected the measurement system probe to vibration, temperature, and pressure environments typically encountered in an operating gas turbine engine. Measurement system performance was monitored during these tests to verify no degradation in measurement capability.

### B. ENVIRONMENTAL TEST OBJECTIVES

The measurement system environmental test objectives are summarized as follows:

- To demonstrate that the measurement system probe is capable of operating without degradation in a typical gas turbine environment where probe adjacent wall temperatures reach 1311 K.

- To demonstrate that the measurement system probe is capable of operating without degradation in a typical gas turbine environment where gas path operating pressures reach 30 atmospheres.

- To demonstrate that the measurement system probe is capable of operating without degradation in a typical gas turbine environment where vibration levels encountered are as high as 12.7 mm/sec in the 50 Hz to 2500 Hz frequency range.

### C. ENVIRONMENTAL EVALUATION TEST METHODS AND RESULTS

#### Temperature Test

The objective of the environmental temperature test was to evaluate measurement system performance with the probe mounted in a configuration similar to that used in an actual gas turbine installation, where adjacent wall temperatures vary from near ambient to 1311 K. To achieve the required simulation, a test rig consisting basically of a 50 mm stainless steel pipe, 150 mm long, and support hardware for the probe was fabricated. One end of the pipe was inserted into a variable temperature tube furnace which provided the heat source. At the other end of the pipe, the probe was inserted perpendicular to the pipe axis and through the pipe wall such that the probe tip was flush with the pipe ID surface, thus providing the simulated installation. A hole was provided through the pipe wall 180° from the probe tip allowing calibration micrometer access. To establish the desired wall temperature simulation points, a thermocouple was attached to the pipe ID approximately 35 mm from the probe tip center and toward the heat source.

Measurement system performance data were obtained with simulated wall temperatures from approximately 367 K to 1311 K. At each data acquisition point, a gap of 50 mils was established by adjusting the micrometer to obtain a zero gap, recording the micrometer reading, and then

adjusting the micrometer to the zero reading plus 50 mils, thus minimizing any potential errors induced by thermal growth of the test rig. Measurement system determined gap was recorded at both the zero gap and the 50 mil gap for each point.

The results of the environmental temperature evaluation test are presented in Table 6, and they indicate that the measurement system performance is unaffected by adjacent wall temperatures up to 1311 K. In some cases, the zero and full scale values deviate slightly from the desired 0 mils and 50 mils values. These discrepancies are not believed to be associated with operation at elevated temperature, but a combined result of operator's inability to set desired values and the measurement system repeatability. It is noted that probe $GN_2$ coolant flowrates used in this test are not to be misconstrued as flowrates required for actual engine tests, as these environmental test flowrates are much lower. This lower required flowrate is due to the lower heat flux available from the tube furnace. Also, with reference to Table 6, it is noted that the coolant flowrate was decreased at the higher wall temperature simulation points. This lower flowrate was required to achieve the desired adjacent wall temperature.

*Table 6. Environmental Temperature Evaluation Test Results*

| *Wall Temperature (K)* | *Measurement Zero,* | *System Value (Mils) Zero+50 Mils* | *Probe Coolant Flow (lb/hr)* |
|---|---|---|---|
| 374 | 1, | 50 | 4.3 |
| 490 | 0, | 49 | 4.3 |
| 599 | 0, | 49 | 4.3 |
| 738 | 0, | 50 | 4.3 |
| 872 | 0, | 49 | 4.3 |
| 922 | 0, | 50 | 4.3 |
| 1033 | 0, | 50 | 4.3 |
| 1142 | 0, | 49 | 2.9 |
| 1253 | 0, | 50 | 2.9 |
| 1308 | 0, | 49 | 2.9 |

### Pressure Test

With the measurement system in the normal operating configuration, a fixed gap target adapter was coupled to the probe tip and adjusted to obtain a system measured gap (simulated clearance) of 50 mils. The probe body was then inserted into a pressurization adapter which allowed the probe assembly to be subjected to elevated pressure via the slot opening at the probe tip. In one atmosphere increments, the probe was pressurized with $GN_2$ from ambient to 30 atmospheres. The measurement system performance was monitored at each pressure setting. No degradation in performance was observed.

### Vibration Test

With the complete measurement system in the normal operating configuration, a fixed gap target adapter was coupled to the probe tip and adjusted to obtain a system measured gap (simulated clearance) of 50 mils. The probe body was then hard coupled by adapter fixtures to a vibration test shaker. The adapter fixtures allowed the probe to be excited in the three mutually perpendicular principal planes, one plane at a time. In each plane, the probe was subjected to a constant 12.7 mm/sec velocity excitation sweep from 50 Hz to 2500 Hz of approximately ten minutes duration. During each excitation sweep, the system measurement performance was continuously monitored. No degradation in measurement system performance was observed.

# IX. PHOTOGRAPHS OF SYSTEM


SYSTEM OPTICAL PROBE

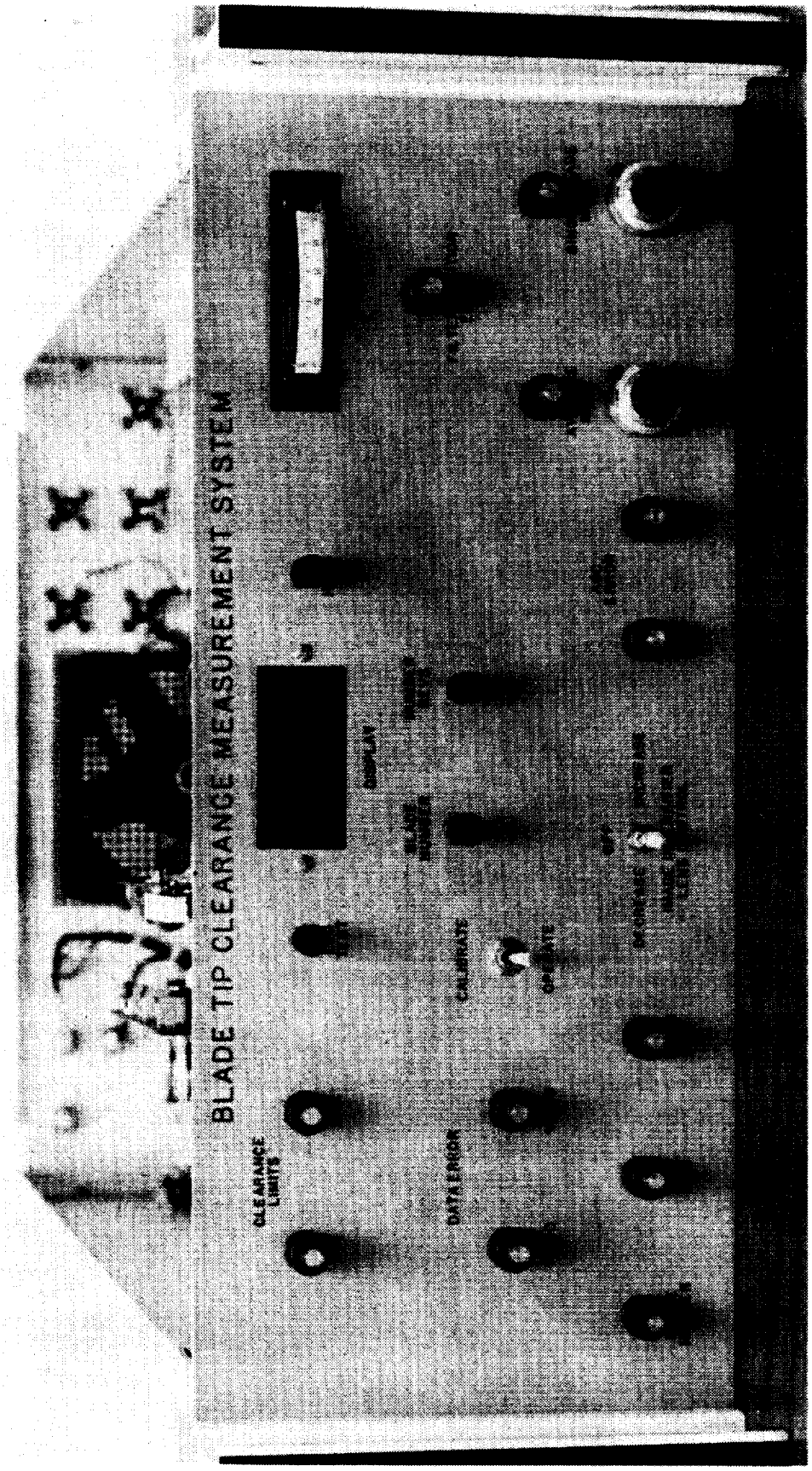


ELECTRONIC SUBSYSTEM

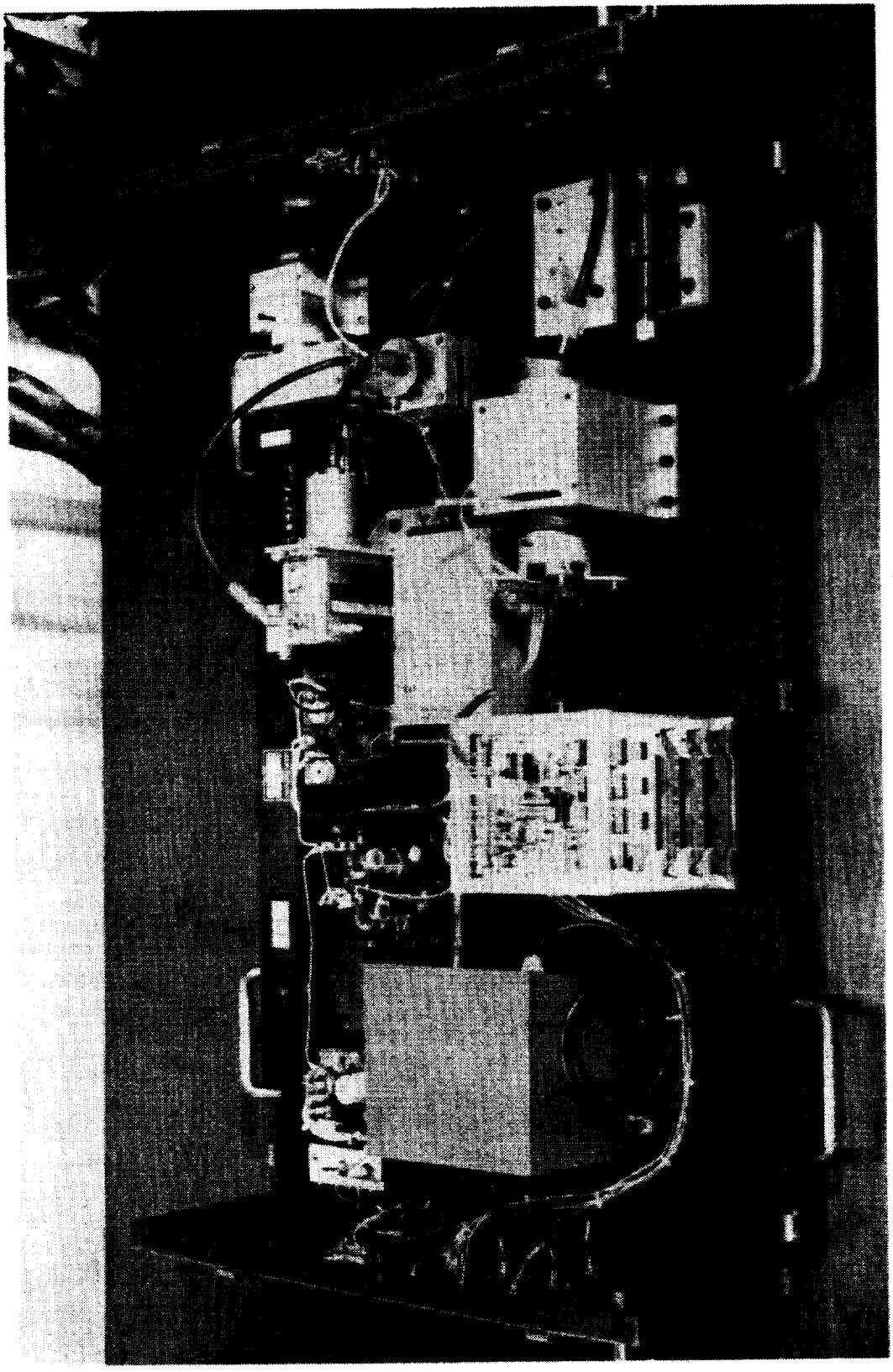

REMOTE SYSTEM

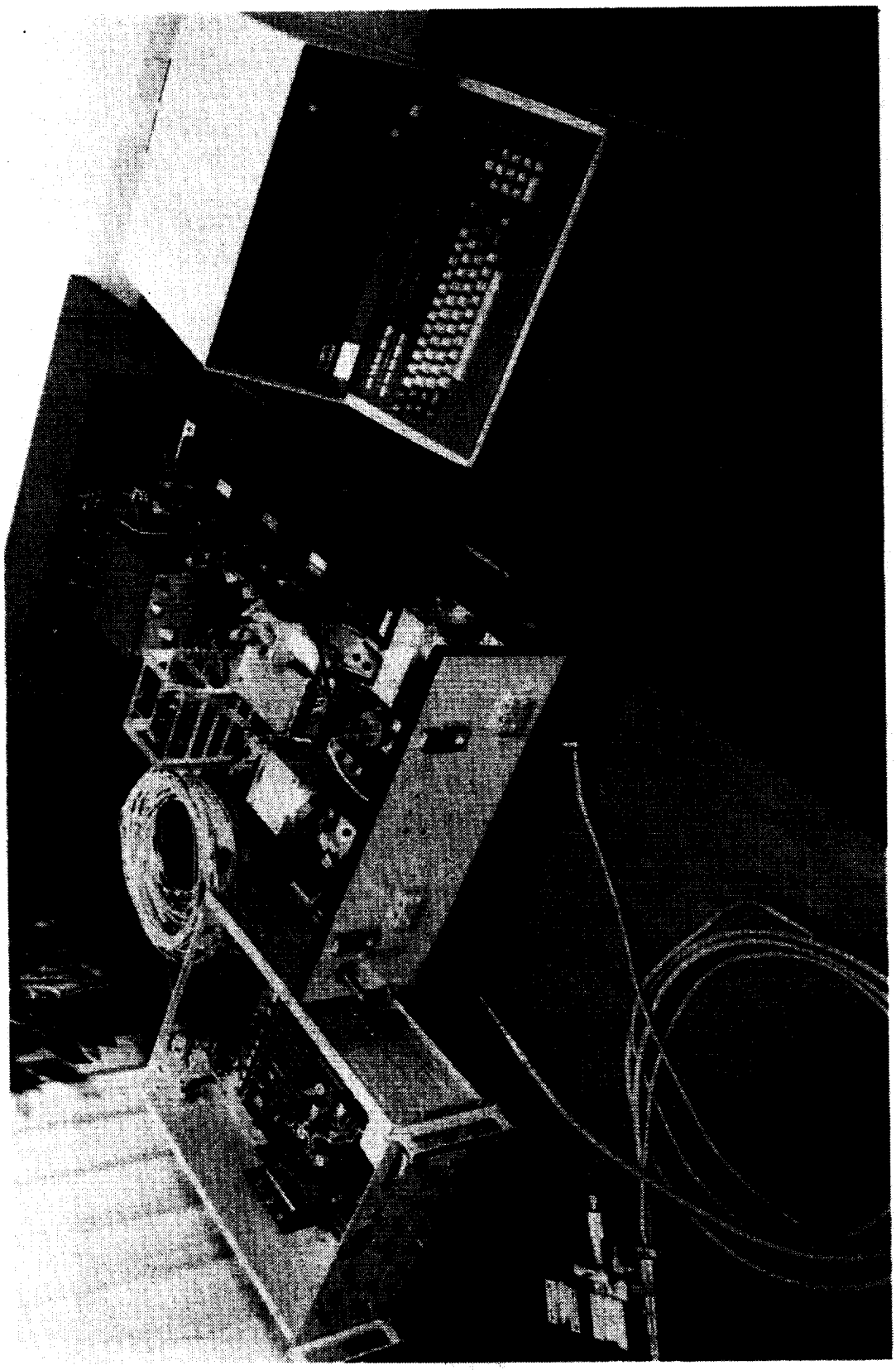

SYSTEM MAJOR HARDWARE

# CONCLUDING REMARKS

## A. SUMMARY

The performance evaluation test results demonstrate that the measurement system performance capabilities meet the system design goals; however, some characteristics were identified which could be improved in the future. It is suggested that these items be addressed and resolved in a follow-on effort. Improvement in overall system capability is also recommended.

## B. SUGGESTED PROGRAM FOLLOW-ON ITEMS

The suggested program follow-on effort includes the following items:

- *Measurement System Nonlinearity Investigation*

  This effort would locate the source of the nonlinearity present in the optical throughput path, provide the necessary design revisions and hardware changes to obtain a more linear throughput characteristic.

- *Image Intensifier Tube Sensitivity/Gain Deterioration Investigation*

  A very limited amount of basic research information is available on pulsed mode operating characteristics, including life expectancy, of microchannel plate (MCP) image intensifier tubes. This suggested effort would include a study and laboratory tests to better define the pulsed mode operating characteristics of the ITT F4111 Image Intensifier tube in terms of pulse duty cycle and repetition rate, tube faceplate spot flux density, MCP voltage, and sensitivity/gain deterioration rate. The results of this effort would provide the user with information necessary to establish system operating conditions for maximum tube performance and/or life expectancy.

- *Improvement in Overall System Capability*

  To improve the overall capability of the measurement system, an additional follow-on effort is suggested to develop a method for time-sharing up to six probes with the single Remote System, Electronic Subsystem, Tektronix terminal set-up. This capability would allow the user to economically monitor blade tip clearance at several rotor stages during the same test program. The feasibility of mechanically switching multiple optical paths while maintaining optical throughput integrity appears sound.

## REFERENCES

1. Hardy, H. D. : Use of Laser-Powered Optical Proximity Probe in Advanced Turbofan Engine Development. Instrumentation for Airbreathing Propulsion, Edited by A. E. Fuhs, MIT Press, Cambridge, Massachusetts, 1974, p. 317-323.

2. Drinkuth, W., Alwang, W. G., House, R. : Laser Proximity Probes for the Measurement of Turbine Blade Tip Running Clearances. Proceedings of the 20th International Instrumentation Symposium, 1974. ISA ASI 74228 (133-140).

## REPORT DISTRIBUTION LIST FOR NASA CR-159402

| | |
|---|---|
| Dr. John Barranger (30) | NASA Lewis Research Center<br>Attn: J. P. Barranger (MS 77-1)<br>21000 Brookpark Rd.<br>Cleveland, OH 44135 |
| Mr. Jan Lane (1) | Applied Technology Laboratories<br>Attn: Jan Lane DAVDL-EU-TAP<br>Fort Eustis, Virginia 23604 |
| Patent Counsel (1) | NASA Lewis Research Center<br>Attn: N. T. Musial (MS 500-311)<br>21000 Brookpark Rd.<br>Cleveland, OH 44135 |
| Technology Utilization (1) | NASA Lewis Research Center<br>Attn: P. E. Foster (MS 7-3)<br>2100 Brookpark Rd.<br>Cleveland, OH 44135 |
| NASA STIF (40 with DRA) | NASA Scientific and Technical<br>Information Facility<br>Attn: Accessioning Department<br>P. O. Box 8757<br>Balt/Wash International Airport<br>Maryland 21240 |
| Lewis Library (2) | NASA Lewis Research Center<br>Attn: Library (MS 60-3)<br>21000 Brookpark Rd.<br>Cleveland, OH 44135 |
| Lewis Management Services<br>Division (1) | NASA Lewis Research Center<br>Attn: Report Control Office (MS 5-5)<br>21000 Brookpark Rd.<br>Cleveland, OH 44135 |

# *Reproduced by NTIS*


U.S. DEPARTMENT OF COMMERCE
Technology Administration
National Technical Information Service
Springfield, VA 22161 (703) 605-6000